Doklady Physics, Vol. 45, No. 7, 2000, pp. 303–305. Translated from Doklady Akademii Nauk, Vol. 373, No. 1, 2000, pp. 33–35.

PHYSICS

Variational Description of Body Motion under the Action of an External Field in a Condensing Medium with Drag

A. S. Pleshanov

Presented by Academician G.S. Golitsyn October 5, 1999

Received October 7, 1999

It is shown that an allowance for the condensation of a medium occurring on the surface of a body moving in a gravitational field is equivalent, in particular, to both a new definition of the drag coefficient and an increase in its value. In the asymptotic mode, the condensation leads to uniformly accelerated motion, with the acceleration being smaller than that of the free fall by at least an order of magnitude or even more. A variational description of the problem is presented, and reasons and conditions making it possible to use this description for irreversible processes are discussed.

1. We assume that a body with a mass $m(t)$ moves in an external field having the potential $U(z)$ in a two-phase medium. The phase *1* consists of liquid droplets with the mass m_1, which condense on the surface of the body after the contact has occurred. The gaseous phase *2* causes the drag. Under the assumption that the Reynolds number $\mathrm{Re} = |v - v_1|d/\nu_2 \gg 1$, the equation describing the body motion in the direction of the external force ($-U_z > 0$) has the form

$$(mv)_t + U_z = m_t v_1 - \frac{\lambda}{2}\rho_2 (v - v_2)^2 S. \qquad (1)$$

Here, v, v_1, and v_2 are the velocities of the body, droplets, and gas, respectively; d is the equivalent body diameter; S is the area of the body cross section; ν_2 is the kinematic viscosity of the gas; ρ_2 is its density; and λ is the drag coefficient. The indices t and z denote differentiation with respect to the corresponding variables. In addition,

$$m = \rho^0 V, \quad m_1 = \rho_1^0 V_1,$$

where V and V_1 are volumes of the body and each droplet, respectively, and ρ^0 and ρ_1^0 represent their proper densities.

We use the law of condensation kinetics in the form

$$m_t = \mu\rho_1 |v - v_1| S, \qquad (2)$$

where $\mu < 1$ is the flow coefficient associated with the impact parameter. The modulus in (2) implies that for $v > v_1$, the condensation occurs at the frontal part of the body and at $v < v_1$, at its rear part. Furthermore, the natural situation $v > v_{1,2}$ is assumed to occur. Finally, the quantity $\rho_1 = m_1 n_1 = \rho_1^0 \varphi_1$ represents the density of the droplet substance smeared over the volume, where n_1 is the density of the droplet number and φ_1 is the droplet volume fraction. The body and the droplets are considered as balls.

For simplicity, only the capture of the droplets by the body is considered in (2), and their evaporation and subsequent condensation of the vapor on the body are not taken into account. We ignore also blowing off the liquid phase from the body, which is equivalent to a decrease in the flow coefficient μ. Here, we digress from the instability in the liquid film. An estimate of the most significant restriction, i.e., the instability of the film, is presented below.

Relations (1) and (2) yield

$$mv_t + U_z = -\mu\rho_1 (v - v_1)^2 S - \frac{1}{2}\lambda\rho_2 (v - v_2)^2 S < 0. \qquad (3)$$

Thus, the condensation increases the drag as it should be. According to (2) and the definition of m,

$$\frac{u}{v - v_1} = \frac{\mu}{4}\frac{\rho_1}{\rho^0} \equiv \varepsilon \ll 1, \qquad (4)$$

where it is accepted for simplicity that $\rho_1^0 = \rho^0$; $v = z_t$, and $u = r_t$ (r is the body radius). At $v_1 = \mathrm{const}$, this leads to the relation

$$r - r_0 = \varepsilon(z - z_0 - v_1 t). \qquad (5)$$

For $z_0 = 0$, taking into account the natural condition $v_0 \gg v_{1,2}$, we reduce relations (3)–(5) to the form

$$mv_t + U_z = -\frac{1}{2}\Lambda\rho_2 v^2 S; \qquad (6)$$

$$u = \varepsilon v, \quad r - r_0 = \varepsilon z. \qquad (7)$$

Krzhizhanovskiĭ Power Engineering Institute, Leninskiĭ pr. 19, Moscow, 117927 Russia

1028-3358/00/4507-0303$20.00

Here, the quantity

$$\Lambda = \lambda + 2\mu\rho_1/\rho_2 > \lambda$$

represents the newly defined drag coefficient.

Let, for definiteness, the body move in the gravity field $U = -mgz$. Then, substituting the definitions of m and S into (6), we arrive at the relation

$$r(v_t - g) + \frac{3}{8}\Lambda\frac{\rho_2}{\rho_0}v^2 = 0.$$

Passing according to (7) to the variable r instead of z, we have the equation

$$r\left(\frac{du^2}{dr} - 2\varepsilon g\right) + \nu u^2 = 0, \quad (8)$$

where

$$\nu = 3\left(2 + \frac{\lambda}{\mu}\frac{\rho_2}{\rho_1}\right).$$

For $\nu = \text{const}$ corresponding to $\lambda/\mu = \text{const}$, we write out the first and second integrals in equation (8) as

$$r^\nu\left(u^2 - \frac{2\varepsilon}{\nu+1}gr\right) = C_1 = r_0^\nu\left(u_0^2 - \frac{2\varepsilon}{\nu+1}gr_0\right) \quad (9)$$

and

$$\int_{r_0}^{r}\left(\frac{2\varepsilon}{\nu+1}gr' + \frac{C_1}{r'^\nu}\right)^{-1/2}dr' = t, \quad (10)$$

respectively. In the case of $t \gg r_0/u_0$ or $r \gg r_0$, we obtain

$$r \simeq \frac{1}{2}\frac{\varepsilon g}{\nu+1}t^2,$$

which yields

$$z \simeq \frac{1}{2}\frac{g}{\nu+1}t^2 \equiv \frac{1}{2}at^2, \quad (11)$$

where

$$\frac{a}{g} = \left(7 + 3\frac{\lambda}{\mu}\frac{\rho_2}{\rho_1}\right)^{-1} < \left(7 + 3\lambda\frac{\rho_2}{\rho_1}\right)^{-1} < \frac{1}{7}. \quad (12)$$

Thus, in contrast to a constant-mass body, whose velocity under the action of the gravity force and drag force tends to a constant value as $t \to \infty$, a body moving in the condensing medium has another asymptotic mode. In this mode, acceleration of the body is constant and smaller than the gravitational acceleration g approximately by an order of magnitude or even more. This difference occurs because both the integral gravity force and the drag force grow simultaneously, so that, as always, the volume effect caused by an increase in the body size (the gravity force) dominates the surface effect (the drag force).

Completing the analysis of the solution to the problem under consideration, we note the exceptionally strong dependence $m(t)$ occurring in the asymptotic mode:

$$m|_{t\to\infty} \sim r^3 \sim t^6. \quad (13)$$

The simpler problem that concerns motion of a body in the gravity field for the case of an ordinary medium causing drag results from the solution to the problem, which we have obtained as $\mu \to 0$.

The instability of a liquid film having viscosity η and surface tension α is estimated below. A liquid droplet moving in the gravity field in the linear (Stokes) flow mode becomes unstable at

$$\eta r v \sim \frac{\alpha}{r}r^2, \quad (14)$$

where v is estimated from the relation

$$\eta r v \sim \rho r^3 g. \quad (15)$$

According to these formulas, the critical size of the droplet has the order

$$r \sim a_* = \sqrt{\frac{2\alpha}{\rho g}}, \quad (16)$$

where a_* is the capillary constant. Estimate (16) is presented in [1]. In a more accurate form, relations (14) and (15) are written out as

$$6\pi\eta r v \sim \rho \times \frac{4}{3}\pi r^3 g \sim \frac{2\alpha}{r} \times 4\pi r^2,$$

which leads to the estimate

$$r \sim \sqrt{3}a_*. \quad (17)$$

In the case under consideration, expressions (14) and (15) are replaced by

$$\frac{1}{2}\Lambda\rho_2 v^2 \pi r^2 \sim \frac{2\alpha}{r} \times 4\pi r^2,$$

and

$$v^2 \sim \frac{2ar}{\varepsilon},$$

respectively. As a result, we obtain

$$r \sim a_*\sqrt{\theta}, \quad (18)$$

where

$$\theta = \left(7 + 3\frac{\lambda}{\mu}\frac{\rho_2}{\rho_1}\right)\left(2 + \frac{\lambda}{\mu}\frac{\rho_2}{\rho_1}\right)^{-1}.$$

Here, $\theta \in (3; 3.5)$, so that estimates (17) and (18) satisfactorily coincide with each other even with an accuracy of their numerical coefficients. Consequently, the critical dimension of the body is determined, as usual, by the capillary constant, which is, seemingly, the highest ($a_* \approx 11$ mm) for liquid beryllium. We note that, at

$\lambda \ll 1$, $\rho_2^0/\rho_1^0 \ll 1$, and arbitrary $\mu < 1$, the quantity $\lambda\rho_2/(\mu\rho_1)$ can have an arbitrary value because $\varphi_1 \ll 1$.

2. The problem under discussion admits variational description. Indeed, equation (8), written as

$$2rr_{tt} + \nu r_t^2 - 2\varepsilon g r = 0 \quad (19)$$

has the Lagrangian

$$\mathcal{L} = r^\nu\left(r_t^2 + \frac{2\varepsilon}{\nu+1}gr\right), \quad (20)$$

whose variation is written out as

$$\delta\mathcal{L} = 2(r^\nu r_t \delta r)_t - r^{\nu-1}(2rr_{tt} + \nu r_t^2 - 2\varepsilon g r)\delta r, \quad (21)$$

which leads to (19). The possibility of variationally describing irreversible processes (here, we deal with an absolutely inelastic interaction in the processes of condensation and friction) is of certain interest.

The fact is that there exists a standpoint proposed even by Lagrange and clearly formulated by Planck (see two of his papers referred to in [2]), which is directly related to the problem being analyzed. According to this standpoint, irreversible processes proceeding with the energy change cannot be described by variational methods. In mechanics, this implies that these processes cannot be described in the framework of the so-called principle of least action [2].

The contradiction arising in this consideration is removed as discussed below. Both original equation (19) and Lagrangian (20) do not explicitly depend on the argument t. According to the general theory (see, for example, [3]), this leads to the integral

$$H = r_t\mathcal{L}_{r_t} - \mathcal{L} = \text{const}, \quad (22)$$

which, as can be easily shown, coincides with integral (9). In mechanics, with the given least action of Lagrangian

$$L = \frac{1}{2}mv^2 - U, \quad (23)$$

where m = const and U depends only on coordinates, the quantity H has an additional meaning and corresponds to the energy. Here, H is already not the energy. It conserves its general meaning as the invariance condition $\mathcal{L}$ with respect to the time shift and reflects the absence of an explicit dependence of the original functional on t. Therefore, when the energy is not conserved, the principle of least action in its conventional formulation (23) is actually ill-posed. Nevertheless, as is shown here, the variational description of irreversible processes is possible when the condition H = const has only its basic sense. Evidently, the concept of the absence of an explicit time dependence for the functional is more general than that of the energy conservation. It should be kept in mind that the absence of the explicit dependence of an original equation on an argument represents the necessary (but not sufficient) condition for this property of the functional, provided that it exists.

ACKNOWLEDGMENTS

The author is grateful to A.P. Kuznetsov for fruitful discussions and to N.A. Sheveleva for her help in the process of this work.

REFERENCES

1. L. D. Landau and E. M. Lifshitz, *Hydrodynamics* (Nauka, Moscow, 1986).
2. *Variational Principles of Mechanics*, Ed. by L. S. Polak (Fizmatgiz, Moscow, 1959).
3. I. M. Gel'fand and S. V. Fomin, *Calculus of Variations* (Gostekhizdat, Moscow, 1960; Prentice-Hall, Englewood Cliffs, N. J., 1963).

Translated by Yu. Verevochkin

Doklady Physics, Vol. 45, No. 7, 2000, pp. 306–307. Translated from Doklady Akademii Nauk, Vol. 373, No. 2, 2000, pp. 178–180.

PHYSICS

Main Indications of the Changes in Microcontact Spectra Induced by Dislocations

V. N. Nikiforenko and F. F. Lavrent'ev

Presented by Academician V.E. Panin October 22, 1999

Received November 1, 1999

The effect of dislocations on microcontact spectra (MCS) was first reported in [1]. In this paper, it was shown that the MCS for zinc single crystals changed with an increase in dislocation density revealed by the method of selective chemical etching. However, this result should be considered as preliminary. Electron microscopy data were needed to find out the effect of dislocation on quasiparticle generation in the vicinity of the point contact. Only further studies [2–4] employing transmission electron microscopy established the qualitatively new level of these experiments.

The goal of this paper is to study the main features of MCS in zinc single crystals related to the dislocation network in the system $(0001)\langle 11\bar{2}0\rangle$ formed in the contact region.

The experimental problem was solved by measuring the MCS method of single crystal zinc electrodes. The electrode axis was strictly parallel to the [0001] direction to prevent the effect of easy dislocation glide in the basal system at the moment when electrodes were put into contact. The basis plane (0001) was used as the ground for the formation of point contacts at 1.5 K. The method of forming hexagonal dislocation networks and the MCS measuring technique is described in [2, 5]. It employs the dependence of the second derivative of the I–V curves $V_2(E)$ on the bias energy at the contact. Microcontact spectra were obtained as a result of more than 20 reproducible experiments. The initial structural state of single-crystalline electrodes was characterized by the density of basal $N_b = 10^8$ m^{-2} and pyramidal $N_p = 3 \times 10^6$ m^{-2} dislocations.

The effect of basal dislocations upon the behavior of $V_2(E)$ curves is illustrated in Fig. 1. It is clear that the formation of the network of basal dislocations results in a fundamental change in the behavior of $V_2(E)$ curves in comparison to spectra (curve *1*) typical of the initial structural state. The main differences of spectra related to dislocations are as follows: the anomalies at $E > kT$, $E = h\nu_0$ ($\nu_0 = 0.36$ THz), the shift of the main MCS peak toward higher energies, and a strong increase of the background level. All these new features arise alongside the disappearance of the spectral features characteristic of the initial structural state.

The anomalies at energy $E = 1.5$ meV arising independent of the contact resistance (Fig. 2) are typical of type-*2* spectra in the athermal region. Consequently, the value $E = h\nu_0$ is one of the main parameters, characterizing a hexagon in the basal dislocation network surrounding the point contact. This result demonstrates that the dislocations form a monochromatic microwave source. According to data [6], phonons do not penetrate the region of the dislocation core. Meeting in their path the dislocation scattering source, electrons and phonons emitted by the contact and interacting with the segments of basal dislocations seem to affect their linear tension. In its turn, the changed linear tension of a

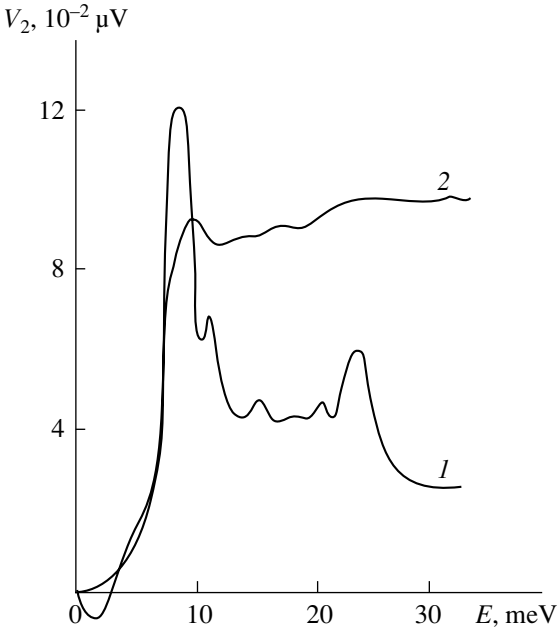

Fig. 1. Microcontact spectra of zinc single crystal related to the initial structural state (*1*) and to the network of basal dislocations (*2*).

Verkin Institute of Low Temperature Physics and Technology, National Academy of Sciences of Ukraine, pr. Lenina 47, Kharkov, 310164 Ukraine

1028-3358/00/4507-0306$20.00

dislocation can affect the reflectivity of quasiparticles returning to the region of point contact and change the behavior of $V_2(E)$.

The expression for a linear tension per unit dislocation length has the form

$$\Phi = \alpha G b^2, \quad (1)$$

where α is the coefficient characterizing interaction between dislocations, G is the shear modulus, and b is the Burgers vector. The force necessary to bend a dislocation down to radius r_k is given by the relation

$$F_c = \frac{\Phi}{r_k}. \quad (2)$$

If one assumes that F_c is proportional to the force of dynamic drag, which depends on the vibration rate of dislocations V_d, the measure of energy dissipation in this motion can be characterized by the effective viscosity

$$B = \frac{\Phi}{r_k V_d}. \quad (3)$$

The increase in energy supplied to the contact will probably favor the change of both F_c and the effective vibration motion velocity of dislocation segments near the equilibrium state. The available experimental data allow us to consider the possible mechanisms of energy dissipation related to the vibrational motion of the basal dislocation network in the field of microcontact.

We denote the value of V_2 at the extremum through U_d, and the value of E corresponding to it as E_0. The anomalies in the region of starting segments of MCS arise owing to the network of basal dislocations, and the change in the potential U_d is completely determined by the dislocations; hence, U_d is nothing but the dislocation potential. Taking into account the results of [7], we can write out in the first approximation the following expression for the dislocation potential,

$$U_d = \frac{\alpha G b^2 B \nu}{n m V_e i}, \quad (4)$$

where n is the density of electrons, m is the electron mass, V_e is the electron velocity, and i is the current in the vicinity of the point contact.

Taking into account the experimental value U_d = 10 nV, α = 0.24 [8], $i = 6 \times 10^{-3}$ A, we determine the coefficient of viscous friction $B = 0.65 \times 10^{-12}$ MPa s. According to theory [9], the main mechanism of the dislocation drag in normal metals at low temperatures is the electron viscosity, which is independent of the temperature. The value of the electron-induced friction coefficient calculated in [9] varies in the range $B = 10^{-13}$–10^{-11} MPa s, depending on the value of deformation potential. A satisfactory agreement of experimental estimates with theoretical results allows us to assume that the segments of basal dislocations in the athermal region of the spectrum transfer the energy to the various excitation branches of crystal lattice owing to the electron drag mechanism.

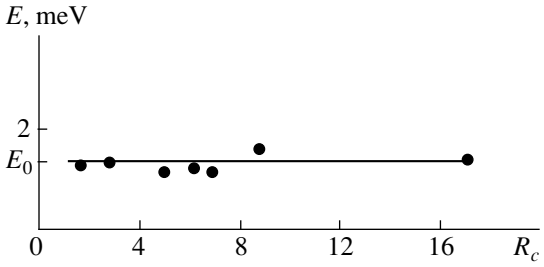

Fig. 2. Energy E versus the contact resistance R_c for the initial part of MCS.

Thus, the main features determining the MCS behavior are related to the changes in the dislocation potential. These changes are caused by the interaction of dislocations with quasiparticles emitted by the point contact. The basal dislocations, which can be present as high-frequency wave packets in the teraherz frequency range, are the main source of quasiparticle drag. The results of this paper suggest that the dislocations exhibit soliton properties probably stemming from the features of atomic interactions in the dislocation core. The dislocation energy $E = h\nu_0$ in the initial part of the spectrum is independent of temperature (Fig. 2); hence, the dislocation can participate in the vibrational motion at $T \longrightarrow 0$. The latter fact suggests the possibility of undamped soliton-like vibrations existing in a vibrational system formed by the hexagonal network of basal dislocations and the microcontact.

REFERENCES

1. A. G. Batrak, F. F. Lavren'ev, V. N. Nikiforenko, and I. K. Yanson, Fiz. Nizk. Temp. **6**, 1146 (1980) [Sov. J. Low Temp. Phys. **6**, 556 (1980)].
2. V. N. Nikiforenko and F. F. Lavrent'ev, Izv. Vyssh. Uchebn. Zaved. Fiz., No. 12, 65 (1989).
3. V. N. Nikiforenko, Fiz. Nizk. Temp. **18**, 1198 (1992) [Sov. J. Low Temp. Phys. **18**, 963 (1992)].
4. V. N. Nikiforenko, Inzh.-Fiz. Zh., No. 1, 23 (1997).
5. F. F. Lavrent'ev, V. N. Nikiforenko, and I. V. Tret'yak, Dokl. Akad. Nauk SSSR **291**, 599 (1986) [Sov. Phys.–Dokl. **31**, 915 (1986)].
6. I. M. Dubrovskiĭ and A. S. Kovalev, Fiz. Nizk. Temp. **2**, 1483 (1976) [Sov. J. Low Temp. Phys. **2**, 726 (1976)].
7. E. E. Vdovin and A. Yu. Kasumov, Fiz. Tverd. Tela (Leningrad) **30**, 311 (1988) [Sov. Phys. Solid State **30**, 180 (1988)].
8. F. F. Lavrent'ev, O. P. Salita, and P. D. Shutyaev, Fiz. Met. Metalloved. **48**, 1025 (1979).
9. M. I. Kaganov, V. Ya. Kravchenko, and V. D. Natsik, Usp. Fiz. Nauk **111**, 655 (1973) [Sov. Phys. Usp. **16**, 878 (1973)].

Translated by T. Galkina

Doklady Physics, Vol. 45, No. 7, 2000, pp. 308–310. Translated from Doklady Akademii Nauk, Vol. 373, No. 3, 2000, pp. 320–322.

PHYSICS

Equations for the Envelope of a Curvilinear Charged-Particle Beam

N. D. Naumov

Presented by Academician V.V. Osiko September 9, 1999

Received October 18, 1999

The necessity of developing self-consistent models for the motion of charged-particle flows in external electromagnetic fields is caused by practical problems of beam and electron-ring formation and transport. Employing the equations of an envelope is one of methods for taking into account the effect of the self-field on the beam transverse dynamics. These equations are known for rectilinear and circular beams of charged particles [1–3]. In the present paper, a method for constructing equations of the envelope for a curvilinear charged-particle beam propagating in a nonuniform magnetic field is proposed. A specific example for the occurrence of such a configuration is provided by the electron-beam injection at a certain angle to the geomagnetic field. Such a statement of the problem is of practical significance in the context of employing the electron beam for studying the ionosphere [4].

An analytical solution to the problem of constructing a self-consistent model for a curvilinear charged-particle beam can be found for a pencil beam, when the ratios of the beam transverse size to both the radius of curvature and the radius of torsion are small quantities. In this case, there exists an approximate solution to the Euler equation for charged-particle gas in an external magnetic field, which happens to be correct to first-order terms with respect to the specified small parameter. Here, we imply self-similar solutions to gas-dynamic equations related to the class of gas motions for charged-particles, velocities of which are proportional to the distance to the center of symmetry [5].

Particle motion at the beam axis depends solely on an external field. Therefore, the position of the beam axis is determined by the trajectory $\mathbf{Y}(s)$ of the axial particle, where s is the trajectory length measured from the beam injection point. Substituting the expression for the velocity, $\mathbf{v} = u\mathbf{t}$, into the equation of particle motion in an external magnetic field, we obtain the curvature of the trajectory $\mathbf{Y}(s)$:

$$k_1 = -\frac{e\mathbf{b}\mathbf{B}_0}{mcu\gamma}.$$

Here,

$$\mathbf{B}_0 = \mathbf{B}_{\text{ext}}(\mathbf{Y}), \quad \gamma = \left(1 - \frac{u^2}{c^2}\right)^{-1/2},$$

and $\mathbf{t}$, $\mathbf{n}$, and $\mathbf{b}$ are the vectors of the Frénet trihedron associated with the curve $\mathbf{Y}(s)$.

For weak-current charged-particle beams (i.e., when the beam current is substantially lower than the ultimate Alfven current), only the lengthwise motion of particles is relativistic. In this case, the Euler equation for charged-particle gas in an external magnetic field is of the form [6]

$$\frac{\partial \mathbf{V}}{\partial t} + (\mathbf{V}\nabla)\mathbf{V} + \frac{1}{mn\gamma}\nabla p = \frac{e}{m\gamma}\left(\mathbf{E} + \frac{1}{c}[\mathbf{V}(\mathbf{B} + \mathbf{B}_{\text{ext}})]\right). \quad (1)$$

Here, e and m are the charge and mass of a particle, respectively; p is the gas pressure determined by the beam emittance; and $\mathbf{E}$, $\mathbf{B}$ are the beam electromagnetic self-field strengths.

The beam transverse dynamics is conveniently considered in the curvilinear coordinate system q_1, q_2, and s:

$$\mathbf{x} = \mathbf{Y}(s) + q_1\mathbf{n} + q_2\mathbf{b}.$$

We represent the beam gas-dynamic velocity in the form

$$\mathbf{V} = V_1\mathbf{n} + V_2\mathbf{b} + U\mathbf{t}$$

and find from (1) the following equation for the

Central Physics Engineering Institute, Sergiev Posad, Moscow oblast, Russia

1028-3358/00/4507-0308$20.00

function U:

$$\frac{\partial U}{\partial t} + \frac{U}{\sigma}\left(\frac{\partial U}{ds} - k_1 V_1\right) + \left(V_1 + k_2 q_2 \frac{U}{\sigma}\right)\frac{\partial U}{\partial q_1} + \left(V_2 - k_2 q_1 \frac{U}{\sigma}\right)\frac{\partial U}{\partial q_2} = -k_1 u V_1, \quad (2)$$

where $\sigma = 1 - k_1 q_1$ and k_2 is the torsion of the curve $\mathbf{Y}(s)$.

It is easy to verify that only second-order terms remain after substitution of the function $U = u(\sigma + 1/\sigma)/2$ into equation (2). Thus, being accurate to terms of the first order of smallness, a possible steady-state solution to equation (2) has the form $U = u$, where u is the particle velocity at the beam axis. Writing out the external field in the vicinity of the beam axis as $\mathbf{B}_{ext} = \mathbf{B}_0 + \mathbf{B}_1$ and ignoring the second-order terms, we find from equation (1) the following equations for the function V_i:

$$LV_1 = (k_2 - k_3)V_2 - u^2 k_1^2 q_1 - \frac{eu}{mc\gamma}\mathbf{b}\mathbf{B}_1 + F_n, \quad (3)$$

$$LV_2 = (k_3 - k_2)V_1 + \frac{eu}{mc\gamma}\mathbf{n}\mathbf{B}_1 + F_b. \quad (4)$$

Here,

$$k_3 = -\frac{e\mathbf{t}\mathbf{B}_0}{mcu\gamma},$$

$$L = \frac{\partial}{\partial t} + u\frac{\partial}{\partial s} + (V_1 + uk_2 q_2)\frac{\partial}{\partial q_1} + (V_2 - uk_2 q_1)\frac{\partial}{\partial q_2},$$

and the terms F_n and F_b are determined by the self-field and emittance of the beam, respectively.

The beam self-field can be approximated by the electromagnetic field of the uniform beam with an elliptic cross section,

$$n(\mathbf{x}, t) = \frac{I}{\pi abu|e|}H(1 - \xi^2 - \eta^2). \quad (5)$$

In this equation, I is the beam current; a and b are the semiaxes of the beam cross section; $H(x)$ is the Heaviside step-function; $\xi = x_1/a$; and $\eta = x_2/b$. Here, a new system of transverse coordinates x_1, x_2 associated with the axes of symmetry for the beam cross section is employed. It is worth noting that expression (5) satisfies the continuity equation if the first-order terms are ignored. As in the case of a circular beam [3], corrections to the beam self-field with allowance for the beam curvature and nonuniformity of particle density have the second order of smallness. As a result, in the coordinate system related to the symmetry axes of the beam cross section, the functions F_1 and F_2 have the form [7]:

$$F_1 = x_1 u^2\left(\frac{g}{a^4} + \frac{h}{a(a+b)}\right),$$

$$F_2 = x_2 u^2\left(\frac{g}{b^4} + \frac{h}{b(a+b)}\right).$$

Here, the following notation is used: $g = E/u$, $h = 4Ic^2/I_A u^2\gamma^2$, E and $I_A = \gamma umc^2/e_0$ being the beam emittance and the Alfven current, respectively.

Since the orientation of the beam cross section varies as the beam propagates, the axes of the coordinate system x_1, x_2 will be turned through an angle ψ with respect to the unit vectors $\mathbf{n}$, $\mathbf{b}$:

$$x_1 = q_1\cos\psi + q_2\sin\psi, \quad x_2 = q_2\cos\psi - q_1\sin\psi.$$

Correspondingly, V_i should be represented in terms of the components Λ_i of the gas velocity in the new coordinate system:

$$V_1 = \Lambda_1\cos\psi - \Lambda_2\sin\psi - q_2\Omega,$$
$$V_2 = \Lambda_2\cos\psi + \Lambda_1\sin\psi + q_1\Omega.$$

Here, $\Omega = u\dot{\psi}$ is the angular velocity for the rotation of the beam as a whole with respect to the Frénet trihedron. Hereafter, for brevity, differentiation with respect to s is symbolized by a dot.

If the variable $\tau = t - s/u$ is introduced instead of t, the derivative with respect to τ disappears from equations (3) and (4). Therefore, the τ-dependence of the beam characteristics has a parametric nature and is determined by the initial conditions for the injection of the beam with the cross section under consideration. As a result, from equations (3) and (4), we obtain the following equations for the functions Λ_i:

$$N\Lambda_1 + k_4\Lambda_2 - x_2\dot{\Omega} + \lambda x_1 + uk_1^2\left(x_1\cos^2\psi - \frac{x_2}{2}\sin 2\psi\right) = \frac{e}{mc\gamma}(\mathbf{n}\mathbf{B}_1\sin\psi - \mathbf{b}\mathbf{B}_1\cos\psi) + \frac{1}{u}F_1, \quad (6)$$

$$N\Lambda_2 - k_4\Lambda_1 + x_1\dot{\Omega} + \lambda x_2 + uk_1^2\left(x_2\sin^2\psi - \frac{x_1}{2}\sin 2\psi\right) = \frac{e}{mc\gamma}(\mathbf{n}\mathbf{B}_1\cos\psi + \mathbf{b}\mathbf{B}_1\sin\psi) + \frac{1}{u}F_2, \quad (7)$$

where

$$k_4 = k_3 - k_2 - 2\dot{\psi}, \quad \lambda = \Omega(k_3 - \dot{\psi}),$$

and

$$N = \frac{\partial}{\partial s} + \left(\frac{\Lambda_1}{u} + k_2 x_2\right)\frac{\partial}{\partial x_1} + \left(\frac{\Lambda_2}{u} - k_2 x_1\right)\frac{\partial}{\partial x_2}.$$

An internal transverse gas motion of the rotational type can arise along with variation of the beam sizes in the x_1,x_2-coordinate system while propagating the beam in an external field. Therefore, one should pro-

ceed from the following expressions for Λ_i in terms of the previously introduced self-similar variables ξ, η:

$$\Lambda_1 = u(\dot{a}\xi - \kappa a\eta), \quad \Lambda_2 = u(\dot{b}\eta + \kappa b\xi). \tag{8}$$

Here, $\kappa(s)$ is a function characterizing internal displacements of the charged-particle gas with elliptic streamlines.

Substitution of expressions (8) into equations (6) and (7) makes it possible to receive a system of ordinary differential equations for the functions a, b, ψ, and κ. In particular, for a beam in a slightly nonuniform magnetic field, under condition of applicability for the drift approximation, the equations for the envelope are of the form

$$\ddot{a} + \left(\mu + \kappa k_2\frac{a}{b} + k_1^2\cos^2\psi\right)a + \kappa k_4 b = \frac{h}{a+b} + \frac{g}{a^3}, \tag{9}$$

$$\ddot{b} + \left(\mu + \kappa k_2\frac{b}{a} + k_1^2\sin^2\psi\right)b + \kappa k_4 a = \frac{h}{a+b} + \frac{g}{b^3}, \tag{10}$$

$$\ddot{\psi} + \left(\dot{\psi} - \frac{k_3}{2}\right)\left(\frac{\dot{a}}{a} + \frac{\dot{b}}{b}\right) + \frac{1}{2ab}\frac{d}{ds}\kappa(a^2 + b^2) = 0, \tag{11}$$

$$\frac{d}{ds}\kappa(a^2 - b^2) + (k_4 - k_2)(b\dot{a} - a\dot{b}) + k_1^2 ab\sin 2\psi = 0, \tag{12}$$

where $\mu = \dot{\psi}(k_3 - \dot{\psi}) - \kappa^2$.

Equations (9)–(12) can be slightly simplified for a beam in a uniform magnetic field when the beam axis is a helical line. In this case, the curvature and torsion of the beam axial line are s-independent:

$$k_1 = |k|\sin\alpha, \quad k_2 = k\cos\alpha = k_3.$$

Here, $k = -eB_{\text{ext}}/mcu\gamma$, and α is the angle between the direction of the magnetic field and that of the beam injection. For a helical beam, we can find from equation (11) a relation between the rotation of the beam as a whole with respect to the Frénet trihedron and the internal charged-particle gas motion:

$$\dot{\psi} = \frac{1}{2ab}\left[2a_0b_0\left(\dot{\psi}_0 - \frac{k_2}{2}\right) + \kappa_0(a_0^2 + b_0^2) - \kappa(a^2 + b^2)\right] + \frac{k_2}{2}.$$

Terms caused by the external-field gradient are absent in equations (9)–(12) since their contribution is of the second order of smallness. Indeed, from the condition of applicability for the drift approximation $|\nabla\mathbf{B}_{\text{ext}}|/k_1B_{\text{ext}} \sim \varepsilon$, it follows that

$$|\mathbf{B}_1| \sim r|\nabla\mathbf{B}_{\text{ext}}| \sim \varepsilon k_1 r B_{\text{ext}},$$

where r is the characteristic beam transverse size. For a nonuniform magnetic field of the focusing type, the terms indicated appear in equations for the envelope. For example, the magnetic field in a double-threaded stellatron can be represented in the form [8]

$$\mathbf{B}_0 = C_1\mathbf{b} + C_2\mathbf{t}, \quad \mathbf{B}_1 = C_3(\rho\sin\beta + \zeta\cos\beta)\mathbf{n} + C_3(\rho\cos\beta - \zeta\sin\beta)\mathbf{b} + C_2\rho\mathbf{t},$$

where $\rho = k_1q_1$, $\zeta = k_1q_2$, $\beta = nk_1s$; n is an integer; and C_i are constants. In this case, employing the proposed method allows us to find equations for the envelope of a corrugated circular beam.

REFERENCES

1. I. M. Kapchinskiĭ, *Particle Dynamics in Linear Resonant Accelerators* (Atomizdat, Moscow, 1966).
2. E. P. Lee and R. K. Cooper, Part. Accel. **7**, 83 (1976).
3. V. P. Sarantsev and É. A. Perel'shteĭn, *Collective Acceleration of Ions by Electron Rings* (Atomizdat, Moscow, 1979).
4. *Artificial Particle Beams in Space Plasma Studies*, Ed. by B. Grandal (Plenum, New York, 1982; Mir, Moscow, 1985).
5. N. D. Naumov, Dokl. Akad. Nauk **346**, 468 (1996) [Phys.–Dokl. **41**, 50 (1996)].
6. R. C. Davidson, *Theory of Nonneutral Plasmas* (Benjamin, New York, 1974; Mir, Moscow, 1978).
7. J. D. Lawson, *The Physics of Charged-Particle Beams* (Clarendon Press, Oxford, 1977; Mir, Moscow, 1980).
8. C. W. Robertson, A. Mondelli, and D. Chernin, Phys. Rev. Lett. **50**, 507 (1983).

Translated by V. Tsarev

Doklady Physics, Vol. 45, No. 7, 2000, pp. 311–316. Translated from Doklady Akademii Nauk, Vol. 373, No. 3, 2000, pp. 323–328.

PHYSICS

Entropy of bcc → L, fcc → L, and fcc → bcc Phase Transitions of Elemental Substances as Function of Transition Temperature

A. L. Udovskiĭ

Presented by Academician I.I. Novikov October 20, 1999

Received October 20, 1999

In the last two-three decades, the thermodynamic calculations of phase diagrams for both binary and multicomponent systems have been in general use (see, e.g., [1–3]). For most systems, a thermodynamic description of virtual phase transitions for pure components entering a system is necessary for performing these calculations. Thus, e.g., for calculating the Ni–Cr phase diagram, it is necessary to know the enthalpies and entropies of phase transitions for Ni and Cr both in the case of the actual phase transitions [fcc ⟶ liquid melt (L) for Ni and bcc ⟶ L for Cr] and virtual phase transitions of metastable phases of pure Ni (bcc phase) and Cr (fcc phase) to the liquid phase.

Studies on the relative stability of various phases for pure components have a rather long history. Trawton, and then Nernst and other researchers (see [4]), assumed the entropy of evaporation to be constant under atmospheric pressure for thermodynamically similar substances. Later on, this hypothesis was generalized by Krompton [4], who assumed the melting entropy jumps to be equal for all chemical elements with similar crystal structures (the "generalized Trawton rule") [5]. Later, Kaufman [5] calculated the differences in enthalpy and entropy between hcp and bcc phases, as well as between hcp and fcc phases of transition metals, as the functions on the number of the group in the Mendeleev periodic table of elements. They suggested that the elements of the same group in the periodic table have similar values for the phase transition entropy if the transition occurs between phases of the same type. In particular, the entropy of melting for bcc phases of elemental Zr, Hf, Nb, Ta, Mo, and W has the same value of 2 cal/(g atom K). Comparison of these values with recent thermodynamic experimental data [6] shows that both the generalized Trawton rule and the assumptions of [5] do not agree well with experiment. In [7], plots of the melting entropy for bcc, fcc, and hcp phases of metals as functions of melting temperature are presented. However, an attempt to graphically extrapolate experimental data on the entropies of phase transitions to zero temperature results in a finite value of the entropy difference between the various phases. This contradicts the third law of thermodynamics (the vanishing of the entropy at zero temperature).

The goal of this paper is using physical models for phases to construct the dependence of melting entropies on the phase-transition temperature for both bcc and fcc phases of most chemical elements of the periodic table, which could be free of the contradictions mentioned above.

The temperature dependence of the Gibbs free energy for any phase of a pure component can be described by the following formula (see, e.g., [8]):

$$G(T) = H(0) - \int_0^T S(T)dT, \tag{1}$$

where $H(0)$ is the enthalpy at 0 K; $S(T)$ is the temperature dependence for the entropy. Then, the difference in the Gibbs free energies between α- and β-phases of the component as a function of T has the form

$$\Delta G^{\alpha \longrightarrow \beta}(T) \equiv G^{\beta}(T) - G^{\alpha}(T)$$
$$= \Delta H^{\alpha \longrightarrow \beta}(0) - \int_0^T \Delta S^{\alpha \longrightarrow \beta}(T)dT. \tag{2}$$

Since, at the temperature of the phase transitions α ⟶ β, the Gibbs free energies for α- and β-phases are equal, we find from (2)

$$\Delta H^{\alpha \longrightarrow \beta}(0) = \int_0^{T^{\alpha \longrightarrow \beta}} \Delta S^{\alpha \longrightarrow \beta}(T)dT; \tag{3}$$

i.e., the difference between the enthalpies of α- and β-phases of the pure component at zero temperature is

Baĭkov Institute of Metallurgy and Materials Science, Russian Academy of Sciences, Leninskiĭ pr. 49, Moscow, 117334 Russia

1028-3358/00/4507-0311$20.00

equal to the area bounded by the $\Delta S^{\alpha \longrightarrow \beta}(T)$ curve at temperatures ranging from zero to the temperature $\alpha \longrightarrow \beta$-phase transition point $T^{\alpha \longrightarrow \beta}$. Dividing the integration range in the right-hand side of (2) into two parts, from zero to $T^{\alpha \longrightarrow \beta}$ and $T^{\alpha \longrightarrow \beta}$ to T, and then substituting (3) into (2), we find

$$\Delta G^{\alpha \longrightarrow \beta}(T) = \int_{T}^{T^{\alpha \longrightarrow \beta}} \Delta S^{\alpha \longrightarrow \beta}(T)dT. \quad (4)$$

Using the definition of specific heat, relationship (4) can be presented in the form

$$\Delta G^{\alpha \longrightarrow \beta}(T) = \int_{T}^{T^{\alpha \longrightarrow \beta}} dT' \int_{0}^{T'} \Delta C_P^{\alpha \longrightarrow \beta}(T'')dT''/T''. \quad (5)$$

All relationships (1)–(5) are exact. Then, we use conventional models to describe the temperature dependence of the specific heat for the phases under study, e.g., for the α-phase,

$$C_P^{\alpha}(T) = C_V^{\alpha}(T)(1 + \alpha_V^{\alpha}(T)\gamma_G^{\alpha}(T)T) + \gamma^{\alpha}(T)T. \quad (6)$$

In (6), the specific heat is considered as a sum of the lattice contribution (with the anharmonism taken into account) and the electronic contribution (with the renormalized electron–phonon coupling constant), α_V^{α} is the temperature-dependent volume coefficient of the thermal expansion for the α-phase, and $\gamma_G^{\alpha}(T)$ is the temperature-dependent Grüneisen parameter of the α-phase, which can be written in the form [9]

$$\gamma_G^{\alpha}(T) = \gamma_G^{\alpha}(T)_{LT} - \frac{2\exp(-\theta_D^{\alpha}/3T)}{3[1 + \exp(-\theta_D^{\alpha}/3T)]}, \quad (7)$$

where $\gamma_G^{\alpha}(T)_{LT}$ is the Grüneisen parameter at low temperatures and θ_D^{α} is the Debye temperature for the α-phase. For solid phases, $C_V^{\alpha}(T)$ is described by the Debye model.

We consider the temperature range in which $T > \max(\theta_D^{\alpha}, \theta_D^{\beta})$. The anharmonism will be described within the framework of the quasi-harmonic theory; i.e., we describe the lattice contribution of the specific heat by the Debye temperature depending on the volume. The latter, in its turn, depends on temperature as well {see formulas (67.5) and (67.6) in [10]}. It is well known that the difference $C_P - C_V$ at high temperatures is proportional to the first power in T, and we have $C_P - C_V \ll C$ [10, p. 226] for each phase. However, when we analyze the difference between specific heats of α- and β-phases of the pure component as a function of temperature, the value of $C_P - C_V$ at the temperature of the phase transition can be comparable with the entropy jump at this temperature. For example, according to the experimental data [6], we have for the fcc $\longrightarrow$ bcc phase transition in Ca that $\mathrm{mod}(C_P^{\mathrm{bcc}} - C_P^{\mathrm{fcc}})/\Delta S^{\mathrm{fcc} \longrightarrow \mathrm{bcc}} = \mathrm{mod}(-1.2332/1.2973) = 0.95$; in the case of Hf, $\mathrm{mod}(C_P^{\mathrm{bcc}} - C_P^{\mathrm{fcc}})/\Delta S^{\mathrm{fcc} \longrightarrow \mathrm{bcc}} = \mathrm{mod}(-6.6207/2.9069) = 2.28$; for the fcc $\longrightarrow$ bcc phase transition in Th, this ratio is equal to 2.63. The characteristics considered here are presented in the table for fcc $\longrightarrow$ bcc and hcp $\longrightarrow$ bcc phase transitions for 19 elements, among which the ratio of the difference of the specific heats in various phases to the entropy of the phase transition is on the order of unity for 17 elements. These facts confirm our previous statement. Thus, to describe the differences between thermodynamic functions of different phases in a sufficiently wide temperature range around the phase transition, we should take into account the difference in the specific heats of the various phases of the elements themselves. In this case, the entropy of the α-phase as function of temperature at $T > \theta_D^{\alpha}$ has the following form:

$$S^{\alpha}(T) = 3(R\ln(T/\theta_D^{\alpha}(T))) + 4R + \gamma^{\alpha}T, \quad (8)$$

where

$$\theta_D^{\alpha}(T) \approx \theta_D^{\alpha}(0)(1 - \bar{\alpha}_V^{\alpha}\gamma_G^{\alpha}T), \quad (9)$$

$$\bar{\alpha}_V^{\alpha} = 1/T^{\alpha \longrightarrow \beta} \int_{0}^{T^{\alpha \longrightarrow \beta}} \alpha_V^{\alpha}(T)dT, \quad (10)$$

$\bar{\alpha}_V^{\alpha}$ is the mean volume coefficient of thermal expansion and

$$\gamma_G^{\alpha} = (\gamma_G^{\alpha})_{LT} + 1/3 \quad (11)$$

is the Grüneisen parameter in the high-temperature limit, which is obtained from relationship (7) under condition $\theta_D^{\alpha}/3T \ll 1$. In this case, the difference between entropies of the α- and β-phases for the pure component as a function of temperature takes the form

$$\Delta S^{\alpha \longrightarrow \beta}(T) = 3R\ln(\theta_D^{\alpha}(0)/\theta_D^{\beta}(0)) + \{3R(\bar{\alpha}_V^{\alpha}\gamma_G^{\alpha} - \bar{\alpha}_V^{\beta}\gamma_G^{\beta}) + (\gamma^{\beta} - \gamma^{\alpha})\}T. \quad (12)$$

Thus, for the temperature range, whose lower limit exceeds the maximum Debye temperature of α- and β-phases of the pure component, the temperature dependence of the entropy difference between α- and β-phases of the pure component has a linear form. Since only nine elements have the fcc $\longrightarrow$ bcc phase transition (at atmospheric pressure), the sampling for finding the entropy jump at the fcc $\longrightarrow$ bcc phase transition is not sufficiently representative. However, the following approach can be used. We can also take into consideration two phase transitions bcc $\longrightarrow$ L and

Parameter of nonlinearity entering into the temperature dependence for the difference in the Gibbs free energy between fcc (hcp) and bcc phases for pure elements

Element	Phase transition	$T^{\alpha \to \beta}$, K [6]	$\Delta S^{\alpha \to \beta}(T^{\alpha \to \beta})$, J/(mol K) [6]	$[C_P^{\alpha \to \beta}]_{T^{\alpha \to \beta}}$, J/(mol K) [6]	$[C_P^{\alpha \to \beta}]_{T^{\alpha \to \beta}}/\Delta S^{\alpha \to \beta}$
Am	fcc ⟶ bcc	1350	4.3422	1.2898	0.297
Be	hcp ⟶ bcc	1527	4.4853	–1.852	–0.413
Ca	fcc ⟶ bcc	716	1.2973	–1.2332	–0.951
Ce	fcc ⟶ bcc	1000	2.9916	–0.1165	0.039
Fe	fcc ⟶ bcc	1667.5	0.4953	2.1830	4.407
Gd	hcp ⟶ bcc	1535	2.3959	–1.0745	–0.448
Hf	hcp ⟶ bcc	2016	2.9069	–6.6207	–2.278
Ho	hcp ⟶ bcc	1703	2.5084	–4.0963	–1.633
La	fcc ⟶ bcc	1134	2.7524	4.515	1.640
Mn	fcc ⟶ bcc	1411	1.3525	3.2561	2.407
Sc	hcp ⟶ bcc	1608	2.4927	4.1361	1.659
Sr	fcc ⟶ bcc	820	1.0207	–2.361	–2.313
Tb	hcp ⟶ bcc	1562	2.8045	–0.3401	–0.1213
Th	fcc ⟶ bcc	1633.2	2.2034	–5.7949	–2.630
Ti	hcp ⟶ bcc	1155	3.6104	–5.0272	–1.392
Tl	hcp ⟶ bcc	507	0.7097	2.0997	2.959
Y	hcp ⟶ bcc	1752	2.8490	–2.453	–0.861
Yb	fcc ⟶ bcc	1033	1.693	4.059	2.398
Zr	hcp ⟶ bcc	1139.45	3.6011	–6.3138	–1.753

fcc ⟶ L for pure elements, since the bcc ⟶ L phase transition occurs for 39 elements, and the fcc ⟶ L phase transition is observed for 13 elements. Then, on the one hand, according to (7), the difference in enthalpies at 0 K between fcc and bcc phases is expressed in the form

$$\Delta H^{\text{fcc} \to \text{bcc}}(0) = \int_0^{T^{\text{fcc} \to \text{bcc}}} \Delta S^{\text{fcc} \to \text{bcc}}(T)dT, \qquad (13)$$

and, on the other hand, it can be expressed as the combination bcc ⟶ L and fcc ⟶ L phase transition

$$\Delta H^{\text{fcc} \to \text{bcc}}(0) = \Delta H^{\text{fcc} \to \text{L}}(0) - \Delta H^{\text{bcc} \to \text{L}}(0)$$
$$= \int_0^{T^{\text{fcc} \to \text{L}}} \Delta S^{\text{fcc} \to \text{L}}(T)dT - \int_0^{T^{\text{bcc} \to \text{L}}} \Delta S^{\text{bcc} \to \text{L}}(T)dT. \qquad (14)$$

Thus, on one hand, the difference of enthalpies at 0 K between fcc and bcc phases of the pure component can be expressed through the integral of the difference of entropies for the corresponding phases, which is defined within the range from zero temperature up to the fcc ⟶ bcc phase transition, whereas the difference of enthalpies at 0 K between the fcc and bcc phases of the pure component can be expressed through the difference of two integrals. The first one is defined through the entropy difference between the liquid and fcc phases of the component, and the second integral is calculated through the difference of entropies between the liquid and bcc phases of the pure component within the range from 0 K to the melting temperature for the bcc phase of this component.

For describing the vibration contribution to the entropy of the liquid phase for the pure component, we can use the Einstein model. The anharmonism can be introduced with the help of the Grüneisen parameter for a liquid phase, similarly to the quasi-harmonic

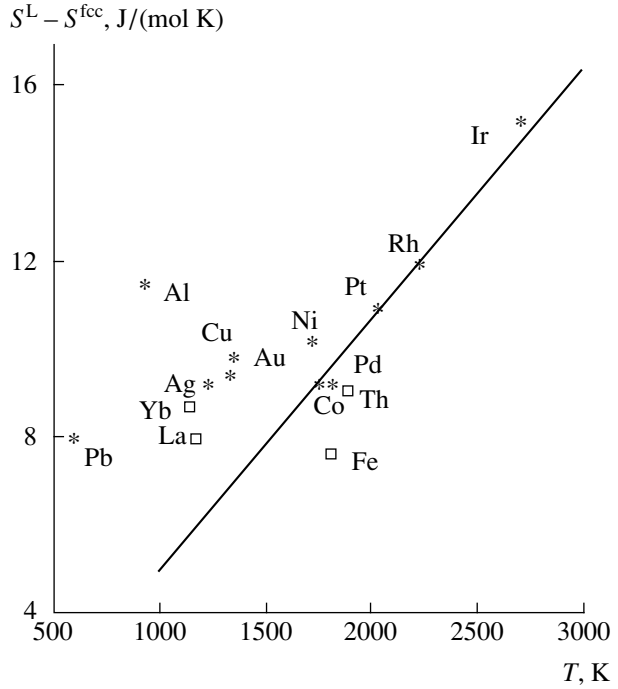

Fig. 1. Comparison of the melting entropy jump for pure components with the fcc structure as a function of melting temperature [relationship (20)] with the corresponding experimental data [6].

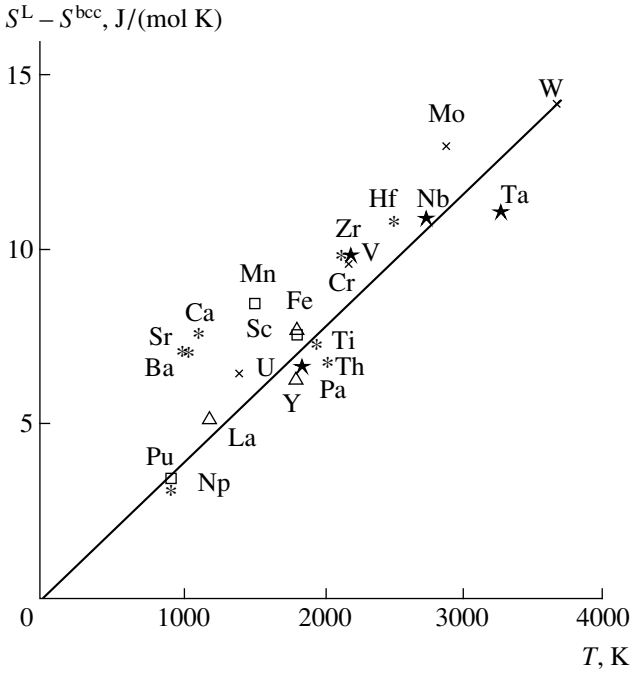

Fig. 2. Comparison of the calculating melting-entropy jump for pure components with bcc structure as a function of melting temperature [relationship (21)] and the relevant experimental data [6].

approach for solids. The Grüneisen parameter can be defined as

$$\gamma_{GE}^{L} = -\frac{\partial \ln \theta_E^L}{\partial \ln V}.$$

In this case, the entropy of the liquid phase for the component depends on temperature (for the case $T > \theta_E^L$) and can be presented in the form

$$S^L(T) = 3R\ln(T/\theta_E^L(T)) + 3R + \gamma^L T, \qquad (15)$$

where the temperature dependence of the Einstein temperature has the form

$$\theta_E^L(T) = \theta_E^L(0)(1 - \bar{\alpha}_V^L \gamma_{GE}^L T), \qquad (16)$$

and $\bar{\alpha}_V^L$ and γ^L are, respectively, the mean volume coefficient of thermal expansion and the coefficient characterizing the electron specific heat for the liquid phase of the pure component. In this case, the difference between the entropies of solid, e.g., α-phase, and the liquid phase of the pure component as a function of temperature is written as:

$$\Delta S^{\alpha \to L}(T) = 3R\ln(\theta_D^\alpha(0)/\theta_E^L(0)) + \{3R(\bar{\alpha}_V^\alpha \gamma_G^\alpha - \bar{\alpha}_V^L \gamma_{GE}^L) - R + (\gamma^L - \gamma^\alpha)\}T. \qquad (17)$$

Thus, according to relationship (17), the temperature dependence for the difference between the entropies of liquid and solid phases, e.g., of the bcc phase, also has a linear form, however, with a different free term and a temperature slope compared to the temperature dependence of the entropy difference between solid phases. As a rule, the Einstein temperature, the Grüneisen parameter, and the coefficient of the electronic specific heat for the liquid phase of pure components are unknown. We present dependence (17) for bcc $\longrightarrow$ L and fcc $\longrightarrow$ L phase transitions only in a functional form as relationships (18) and (19) with unknown coefficients, which we determine based on the experimental data:

$$\Delta S^{bcc \to L}(T) = a^{bcc \to L} + b^{bcc \to L} T, \qquad (18)$$

$$\Delta S^{fcc \to L}(T) = a^{fcc \to L} + b^{fcc \to L} T. \qquad (19)$$

Using the available reference data on the thermal properties for all bcc metals undergoing the bcc $\longrightarrow$ L phase transitions [6], we calculate the coefficients in dependence (19), employing the χ^2 criterion (the generalized least-squares method) [11]. As a result, we get

$$\Delta S^{fcc \to L}(T) = -0.685 + (5.655 \times 10^{-3})T, \ \text{J/(mol K)}. \qquad (20)$$

The calculated dependence (20) is compared in Fig. 1 with the experimental data for bcc $\longrightarrow$ L phase transi-

tions in 13 pure elements. Using a similar procedure, we processed the experimental data on fcc ⟶ L phase transitions in all 39 elements [6]. The results are presented in the form of the following relationship,

$$\Delta S^{\mathrm{bcc}\longrightarrow\mathrm{L}}(T) = -0.03 + (3.8403\times10^{-3})T,\ \ \mathrm{J/(mol\ K)}, \tag{21}$$

and are compared with the experimental data in Fig. 2. The accuracy of relationships (20) and (21) can be verified by comparing the calculated difference of the entropies for phase transitions between bcc and fcc phases as a function of the bcc ⟶ fcc phase-transition temperature of the elements,

$$\Delta S^{\mathrm{fcc}\longrightarrow\mathrm{bcc}}(T) = S^{\mathrm{L}}(T) - S^{\mathrm{fcc}}(T) - (S^{\mathrm{L}}(T) - S^{\mathrm{bcc}}(T)) \equiv \Delta S^{\mathrm{fcc}\longrightarrow\mathrm{L}}(T) - \Delta S^{\mathrm{bcc}\longrightarrow\mathrm{L}}(T) \tag{22}$$

with the corresponding experimental data.

Substituting the derived relationships (20) and (21) into (22), we obtain

$$\Delta S^{\mathrm{fcc}\longrightarrow\mathrm{bcc}}(T) \equiv S^{\mathrm{bcc}}(T) - S^{\mathrm{fcc}}(T) = a^{\mathrm{fcc}\longrightarrow\mathrm{bcc}} + b^{\mathrm{fcc}\longrightarrow\mathrm{bcc}}T = -0.682 + (1.8147\times10^{-3})T. \tag{23}$$

In Fig. 3, the results of calculation based on (23) are compared with the experimental data of [6] for the fcc ⟶ bcc phase transition in pure elements Ca, Ce, La, Mn, Sr, Th, and Yb. The phase transition in Fe is not included since the bcc ⟶ fcc transition here occurs twice due to the effect of ferromagnetism on the bcc phase. Figure 3 demonstrates satisfactory agreement of the experimental data with a fit made according to (23). When the temperature tends to zero, the entropy difference between the solid phases below the Debye temperature also tends to zero as

$$S^{\mathrm{bcc}} - S^{\mathrm{fcc}} = 3R\{(T/\theta^{\mathrm{bcc}})^3 - (T/\theta^{\mathrm{fcc}})^3\} = 18R(T/\theta_{\mathrm{av}})^3(\Delta\theta/\theta_{\mathrm{av}}), \tag{24}$$

where $\theta_{\mathrm{av}} = (\theta^{\mathrm{bcc}} + \theta^{\mathrm{fcc}})/2$ is the mean Debye temperature and $\Delta\theta = (\theta^{\mathrm{fcc}} - \theta^{\mathrm{bcc}})/2$. Therefore, in the first approximation the temperature dependence of the entropy difference between the bcc and fcc phases can be written as

$$\Delta S^{\mathrm{fcc}\longrightarrow\mathrm{bcc}}(T) = S^{\mathrm{bcc}}(T) - S^{\mathrm{fcc}}(T) = \begin{cases} 0, & 0 < T < \theta_{\mathrm{av}} \\ \mathrm{const}\times(T - \theta_{\mathrm{av}}), & T > \theta_{\mathrm{av}}, \end{cases} \tag{25}$$

i.e., within the temperature range from zero up to the mean Debye temperature, this difference $\Delta S^{\mathrm{fcc}\longrightarrow\mathrm{bcc}}(T)$ is approximately taken to be zero [see (24)], and above θ_{av}, it is taken in the form of a linear dependence according to relationship (12). It follows from (23) and (25) that the ratio $a^{\mathrm{fcc}\longrightarrow\mathrm{bcc}}/b^{\mathrm{fcc}\longrightarrow\mathrm{bcc}} = \theta_{\mathrm{av}}$. Thus, as it follows from (25), $\Delta S^{\mathrm{fcc}\longrightarrow\mathrm{bcc}}(T) = 0$ at $T = \theta_{\mathrm{av}}$. Using the values of coefficients in (23), we find that $\theta_{\mathrm{av}} = 375.8$ K. Relationships (14), (20), and (21) obtained in this paper allow us, in particular, to evaluate the melting entropy for the metastable bcc phase of Ni [it equals 5.032 J/(mol K)] and the energy difference at 0 K between the fcc and bcc phases of Ni (3200 J/mol), if we take into account that, according to [6], $T_{\mathrm{Ni}}^{\mathrm{bcc}\longrightarrow\mathrm{L}} = 1318$ K. These results agree well with *ab initio* calculations [12], according to which $\Delta H_{\mathrm{Ni}}^{\mathrm{bcc}\longrightarrow\mathrm{fcc}}(0\ \mathrm{K}) = 3$ kJ/mol, and also with the value of 3536 J/mol reported in [6] without details of the estimation method.

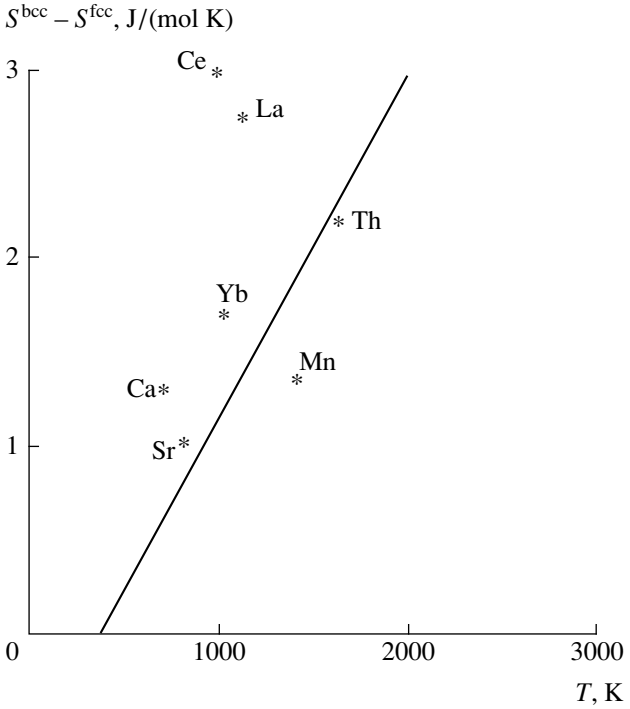

Fig. 3. Comparison of the calculated entropy jump at fcc ⟶ bcc phase transition for pure components with the fcc structure as a function of phase transition temperature [relationship (23)] and the relevant experimental data [6].

ACKNOWLEDGMENTS

This work was supported in part by the Russian Federal Program "Intergratsiya," projects nos. K0573 and A0075.

REFERENCES

1. L. Kaufman and H. Bernstein, *Computer Calculation of Phase Diagrams* (Academic, New York, 1970; Mir, Moscow, 1972).

2. G. Cacciamani, Y. A. Chang, G. Grimvall, *et al.*, CALPHAD: Comput. Coupling Phase Diagrams Thermochem. **21**, 220 (1997).
3. P. Liang, H. L. Lukas, H. J. Seifert, and F. Aldinger, in *Proceedings of the Final Workshop "COST 507, Definition of Thermochemical and Thermophysical Properties to Provide a Database for the Development of New Light Alloys," Vaals, 1997* (Office Official Publ. Eur. Communities, Luxembourg, 1998), Vol. 1, pp. 114–127.
4. K. A. Putilov, *Thermodynamics* (Nauka, Moscow, 1971), pp. 278-292.
5. L. Kaufman, in *Phase Stability in Metals and Alloys*, Ed. by A. Rudman, J. Stringer, *et al.* (New York, 1967; Mir, Moscow, 1970).
6. A. Dinsdale, CALPHAD: Comput. Coupling Phase Diagrams Thermochem. **15**, 317 (1991).
7. N. Saunders, P. Miodovnik, and A. Dinsdale, CALPHAD: Comput. Coupling Phase Diagrams Thermochem. **12**, 351 (1988).
8. A. L. Udovskiĭ, in *Alloys for Nucleonics* (Nauka, Moscow, 1979), pp. 56–70.
9. V. L. Moruzzi, J. F. Janak, and K. Schwartz, Phys. Rev. B: Condens. Matter. **37**, 790 (1988).
10. L. D. Landau and E. M. Lifshitz, *Statistical Physics* (Nauka, Moscow, 1976; Pergamon, Oxford, 1980), Part 1.
11. D. Hudson, *Statistics. Lectures on Elementary Statistics and Probability* (Geneva, 1964; Mir, Moscow, 1970).
12. H. L. Skriver, Phys. Rev. B: Condens. Matter. **31**, 1309 (1985).

Translated by T. Galkina

Doklady Physics, Vol. 45, No. 7, 2000, pp. 317–319. Translated from Doklady Akademii Nauk, Vol. 373, No. 1, 2000, pp. 36–38.

TECHNICAL PHYSICS

The Use of a Singular Integral Equation in the Design of a Thin Electric Dipole

V. A. Neganov and I. V. Matveev

Presented by Academician V.P. Shorin September 8, 1999

Received October 13, 1999

1. The essence of the problem. Thin electric dipoles have been widely applied both as antennas in their own right and as components of complex antenna systems. As a rule, the design of a thin electric dipole is based on solving an integral equation describing the current distribution in the dipole. By now, the Pocklington and Harrington integrodifferential equations and also the Hullen integral equation are known [1–4]. The kernels of these equations are of the Fredholm type, and the form of these kernels stems from using the integral relations for the vector electrodynamic potential. The kernel in the formula for the latter is the Green's function for an inhomogeneous Helmholtz equation written in a spherical coordinate system. Most often, integral equations are solved by the method of moments [1–3]. In essence, this method reduces to transforming of the aforementioned equations into a system of linear algebraic equations for N unknowns. Typically, the latter are the coefficients in the expansion for current in a certain appropriate system of basis functions. Depending on the choice of the basis and weighting functions, there exists a fairly great diversity of specific implementations for the integral-equation method: the Galerkin method, sewing at discrete points, matching the responses, etc. In our opinion, the main drawback of such an approach consists in the fact that the aforementioned integral equations with the Fredholm kernel belong to the integral equations of the first kind; finding a solution to these equations is an ill-posed problem [5]. As a result, the question of how to check whether the solution is proper and establish its adequacy to the physical problem under consideration remains open.

2. Integral equation of the first kind. In this paper, we consider an approach to the analysis of a thin electric dipole. This approach is unconventional from the standpoint of antenna-related problems (Fig. 1). The first special feature consists in rejecting the use of vector electrodynamic potentials. Consideration is directly based on the use of Maxwell equations written out in a cylindrical coordinate system which makes it possible to obtain an integral equation. In contrast, the use of vector potentials results in integrodifferential equations (the Pocklington and Harrington equations). The second feature is related to using the mathematical tools of the theory of singular integral equations. These tools were developed for strip–slot structures for microwave and extremely high frequencies [6, 7].

We consider a thin conductor with a length of $2l$ and a radius of a, which is excited by a high-frequency generator at the discontinuity point l_0 (Fig. 1). In deriving a system of algebraic equations, we use the generally accepted model of a thin dipole ($a \ll l, \lambda$) [1–4]. According to this model, the electric-current density along with the equivalent magnetic-current density in the gap are replaced by the longitudinal electric-current density $\eta_z(z)$ at the surface of a cylinder with a radius a. This current is considered to be continuous in the gap

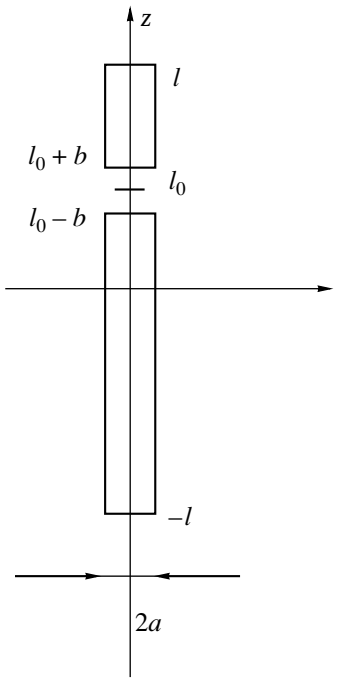

Fig. 1. Schematic representation of an electric dipole.

Near-Volga Institute of Computer Science, Radio Engineering, and Communications, ul. Tolstogo 23, Samara, 443010 Russia

1028-3358/00/4507-0317$20.00

region and vanishes at the dipole ends. The ends' currents are not taken into account. The electric-field vector component E_z generated by the current line vanishes at the cylinder surface $\rho = a(z \in [-l, l])$ everywhere except for the gap region $2b$, where it is made equal to the extraneous field $E^{\text{ext}}(z)$.

In the context of the adopted physical model, the Maxwell equations and the boundary conditions at the dipole surface were used to derive the integral equation of the first kind

$$i\omega\varepsilon_0\varepsilon E^{\text{ext}}(z) = \int_{-l}^{l} \eta_z'(z')G(z', z)dz', \tag{1}$$

where

$$G(z', z) = \frac{i}{2\pi}\int_{-\infty}^{\infty} e^{ih(z'-z)}g(h)dh,$$
$$g(h) = \frac{\sqrt{\gamma^2 - h^2}H_0^{(2)}(a\sqrt{\gamma^2 - h^2})}{hH_1^{(2)}(a\sqrt{\gamma^2 - h^2})}, \tag{2}$$

for the unknown function $\eta_z' = \dfrac{d\eta_z}{dz}$. In formulas (1) and (2), we introduce the following notation: $H_0^{(2)}(x)$ and $H_1^{(2)}(x)$ are the Hankel functions of the second kind of the zero and first orders, respectively; $\gamma^2 = k^2\varepsilon_0\varepsilon\mu$; $k = \omega/c$ is the wave number; ε and μ are the relative permittivity and permeability, respectively; and ε_0 is the permittivity of free space.

3. Singular integral equation. We now find the asymptotic behavior of the function $g(h)$ for $|h| \longrightarrow \infty$. In view of the properties of the Hankel functions of imaginary argument and the known relation [8]

$$\int_{-\infty}^{\infty} e^{-ih(z'-z)}\text{sgn}(h)dh = \frac{2i}{z'-z}, \tag{3}$$

where

$$\text{sgn}(h) = \begin{cases} 1 & \text{for } h > 0 \\ -1 & \text{for } h < 0, \end{cases}$$

it is easy to verify that

$$G\left((z', z) \longrightarrow \frac{1}{\pi(z'-z)} \text{ for } |h| \to \infty.\right) \tag{4}$$

Thus, the kernel $G(z', z)$ in integral equation (1) contains implicitly a singularity of the Cauchy type; therefore, equation (1) is singular.

We now isolate the singularity in equation (1). To this end, we add and subtract the term $\text{sgn}(h)e^{ih(z'-z)}$ in integral expression (2) for the kernel $G(z', z)$. On performing simple transformations, we obtain the following singular integral equation:

$$i\omega\varepsilon_0\varepsilon E^{\text{ext}}(z) = \frac{1}{\pi}\int_{-l}^{l}\frac{\eta_z'(z')}{z'-z}dz' + \int_{-l}^{l}\eta_z'(z')K(z', z)dz'. \tag{5}$$

Here,

$$K(z', z) = \frac{i}{2\pi}\int_{-\infty}^{\infty} e^{ih(z'-z)}\Delta g(h)dh,$$
$$\Delta g(h) = \frac{\sqrt{\gamma^2 - h^2}H_0^{(2)}(a\sqrt{\gamma^2 - h^2})}{hH_1^{(2)}(a\sqrt{\gamma^2 - h^2})} + \text{sgn}(h). \tag{6}$$

Formula (5) represents a singular integral equation of the first kind. It can be used to determine the unknown current density η_z and has no analogues in available publications. Solving the singular integral equation of the first kind relates to the class of well-posed problems [9] (in contrast to the Fredholm integral equations of the first kind). The integrand in the kernel $K(z', z)$ tends to zero $\Delta g(h) \longrightarrow 0$ as $|h| \longrightarrow \infty$.

4. Solution of singular integral equation. Numerical results. In the course of numerical simulation, we considered a symmetric dipole with $l_0 = 0$. While solving the system of singular integral equations (5), we performed a passage to the new variables u and v as $z = lu$ and $z' = lv$ and transformed kernel (6) to the form

$$K(u, v) = \sum_{n=1, m=0}^{\infty} \alpha_{n,m}T_m(v)U_{n-1}(u), \tag{7}$$

where $T_m(v)$ and $U_{n-1}(u)$ are the Chebyshev polynomials of the first and the second kinds, respectively, $\alpha_{n,m}$ being rather cumbersome constant coefficients. When writing the kernel $K(u,v)$ in the form given by (7), we used the known expansions in series of an exponential in terms of the Chebyshev polynomials [10]

$$e^{i\alpha u} = \frac{2}{\alpha}\sum_{n=1}^{\infty} i^{n+1}nJ_n(\alpha)U_{n-1}(u),$$
$$e^{-i\alpha v} = 2\sum_{m=0}^{\infty}\frac{(-i)^m J_m(\alpha)T_m(v)}{1 + \delta_{m,0}}. \tag{8}$$

Here, $J_m(\alpha)$ are the Bessel functions, and $\delta_{m,0}$ is the Kronecker delta.

Since the coefficients in the expansion given by (7) decrease rather rapidly ($\alpha_{n,m} \sim 1/n^3$, $\sim 1/m^3$), we may truncate the series for a certain number N. As can be easily seen, the result of this operation is that kernel (7) of singular integral equation (5) becomes degenerate. Searching for a solution to a singular integral equation with a degenerate kernel presents no special problems [9].

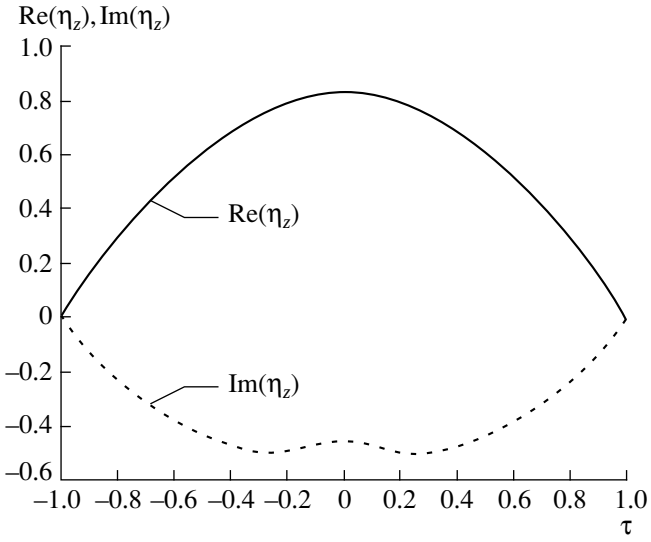

Fig. 2. Real and imaginary components of the surface current for $l/\lambda = 1/4$, $a/\lambda = 1/400$, and $b/\lambda = 1/100$.

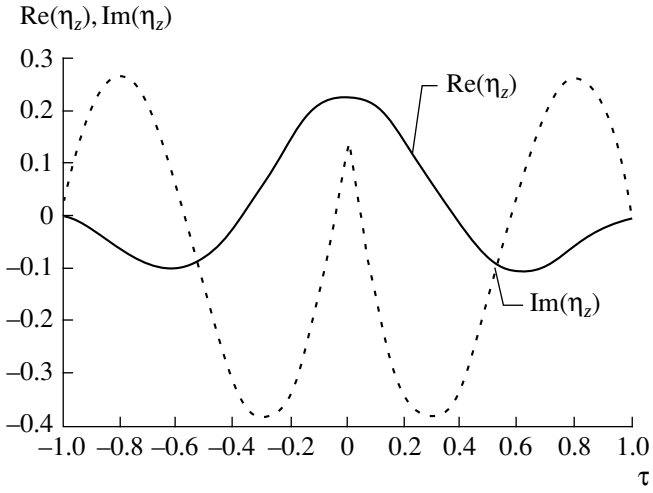

Fig. 3. Real and imaginary components of the surface current for $l/\lambda = 1$, $a/\lambda = 1/40$, and $b/\lambda = 1/100$.

The method suggested was used to calculate the surface current density for various dipole lengths l. Figures 2 and 3 show the representative plots of distributions for the real [$\mathrm{Re}(\eta_z)$] and imaginary [$\mathrm{Im}(\eta_z)$] components of the surface current. The calculation results were in good agreement with the data reported in [4]. Studies of the intrinsic convergence of numerical results showed that the method features rather rapid convergence and high exactness. In expansion (7), it is sufficient to restrict the consideration to $N = 10$ in order to attain a relative error of less than 1%.

5. Thus, the suggested approach based on abandoning the conventional use of the vector electrodynamic potentials and on using the tools of the theory of singular integral equations made it possible to approach in the mathematically correct form the analysis of a thin electric dipole. The obtained singular integral equation for determining the unknown current density in the dipole has no analogues in scientific literature. It is not difficult to generalize the suggested approach to the case of coupled vibrators in free space as well as to the case of vibrators above the conducting surfaces.

REFERENCES

1. *Computational Methods in Electrodynamics*, Ed. by É. P. Burshteĭn (Radio i Svyaz', Moscow, 1996).
2. D. M. Sazonov, *Antennas and Antenna Devices: Textbook for Radio Engineering High Schools* (Vysshaya Shkola, Moscow, 1988).
3. G. A. Erokhin, O. V. Chernyshev, N. D. Kozyrev, and V. G. Kocherzhevskiĭ, *Antenna–Feeder Devices and Radiowave Propagation: Textbook for High Schools*, Ed. by G. A. Erokhin (Radio i Svyaz', Moscow, 1996).
4. S. I. Eminov, *Radiotekh. Elektron.* **38**, 2160 (1993).
5. A. N. Tikhonov and V. Ya. Arsenin, *Solutions to Ill-Posed Problems* (Nauka, Moscow, 1986; Halsted Press, New York, 1977).
6. V. A. Neganov, E. I. Nefedov, and G. P. Yarovoĭ, *Strip Lines and Slot Lines for Microwave and Extremely High Frequencies* (Nauka, Moscow, 1996).
7. V. A. Neganov and E. I. Nefedov, Dokl. Akad. Nauk SSSR **299**, 1124 (1988) [Sov. Phys.–Dokl. **33**, 277 (1988)].
8. F. D. Gakhov and Yu. I. Cherskiĭ, *Convolutional Equations* (Nauka, Moscow, 1978).
9. F. D. Gakhov, *Boundary Value Problems* (Nauka, Moscow, 1977, 3rd ed.; Addison-Wesley, Reading, Mass., 1966).
10. *Mathematical Analysis: Functions, Limits, Series, Chain Fractions*, Ed. by L. A. Lyusternik and A. R. Yanpol'skiĭ (Fizmatlit, Moscow, 1961).

Translated by A. Spitsyn

Doklady Physics, Vol. 45, No. 7, 2000, pp. 320–323. Translated from Doklady Akademii Nauk, Vol. 373, No. 2, 2000, pp. 181–184.

TECHNICAL PHYSICS

An Inductance–Capacitance Model for Heart Electrogenesis

A. N. Volobuev*, V. A. Neganov, and P. I. Romanchuk*****

Presented by Academician V.P. Shorin September 8, 1999

Received September 22, 1999

As was shown in [1–4], biological tissue in its excited state features not only capacitance, but sizable inductance as well.

The goal of the present study is to elucidate the role of the inductance in simulating an equivalent electric generator for the heart in its norm and to solve a direct diagnostic problem under these conditions.

The current-dipole model is traditionally used as an electric model for myocardium excitation. Therefore, we consider the operation of a heart equivalent dipole electric generator (HEDEG) during an electric systole. The heart is considered to have the resistance R, the inductance L, and the capacitance C. Variations in projections of a heart integral electric vector (IEV) (i.e., the dipole moment of the electric-current dipole) onto certain planes are routinely studied in heart diagnostics [5]. Therefore, three mutually perpendicular circuits located in the frontal, horizontal, and sagittal planes are considered as a model for the HEDEG (see Fig. 1). Electric-current sources with the electromotive force E are identical for all the circuits. The variation of the currents for these sources accounts for pacemaker operation. For ventricles, the atrioventricular node is the immediate pacemaker.

We now analyze the operation of a particular circuit. To simplify the notation, indices at the electric characteristics are omitted. The Kirchhoff equation for instantaneous values of the voltage in a circuit has the form

$$U_R + U_L + U_C = E. \tag{1}$$

Here, on the left-hand side of the equation, there is the sum of voltages across the corresponding resistances. Employing the well-known relations between these voltages and the electric current i, we find

$$iR + \frac{d(Li)}{dt} + \int\frac{idt}{C} = E. \tag{2}$$

The active resistance of myocardium is determined primarily by the resistance of cytoplasm and intercellular liquid. Therefore, it can be considered to be a constant in the course of a cardiac cycle. The inductance of the excitable membrane exists only during the time of its excitation and is associated with the spiral motion of ions along ionic channels [4]. Therefore, it is difficult to assume that the active-regulation mechanism for the inductance could be formed evolutionary. The heart inductance is considered to be constant as well.

After a simple transformation of (2), we have

$$\frac{d^2i}{dt^2} + \frac{R}{L}\frac{di}{dt} + \omega_0^2 i = \frac{1}{L}\frac{dE}{dt}, \tag{3}$$

where $\omega_0 = 1/(LC)^{1/2}$ is the natural frequency of the current oscillations in the HEDEG.

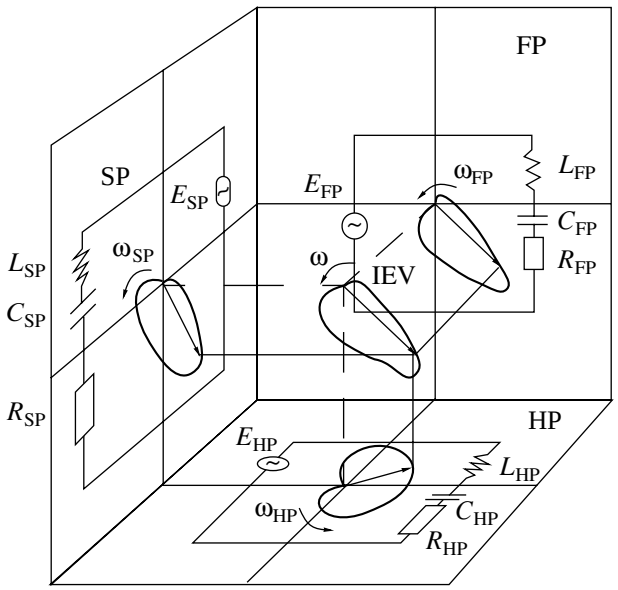

Fig. 1. Electric model for the heart equivalent electric dipole generator.

* *Samara State Medical University, Samara, Russia*

** *Povolzhskiĭ Institute of Information Science, Radio Electronics, and Communication, Samara, Russia*

*** *Center of Arterial Hypertension, Samara, Russia*

1028-3358/00/4507-0320$20.00 © 2000 MAIK “Nauka/Interperiodica”

Equation (3) describes parametric oscillations of an oscillator [6], since the natural frequency of the heart oscillations can vary with changing its capacitance C.

We seek the solution to equation (3) by multiplying it by a function $f(t)$, which must obey the condition [7]

$$f(t)\frac{d^2i}{dt^2} + f(t)\frac{R}{L}\frac{di}{dt} = \frac{d}{dt}\left(f(t)\frac{di}{dt}\right). \quad (4)$$

We introduce a new variable according to the formula

$$d\theta = \frac{dt}{f(t)}. \quad (5)$$

The function $f(t)$ has the dimension of the reciprocal cyclic frequency. Therefore, we denote it by $f(t) = 1/\omega_d$.

We multiply equation (3) by the value of the distance between the source and the sink of the HEDEG and rewrite it in the new notation:

$$\frac{1}{\omega_d}\frac{d}{dt}\left(\frac{l}{\omega_d}\frac{dD}{dt}\right) + \left(\frac{\omega_0}{\omega_d}\right)^2 D = \frac{l}{\omega_d^2 L}\frac{dE}{dt}. \quad (6)$$

Here, $D = il$ is the dipole moment of the integral electric vector. The function θ, in accordance with (5), is the rotation angle for the HEDEG vector rotating with the cyclic frequency ω_d.

In line with (4) and taking into consideration that R and L are constants, we have the following form for the time dependence of ω_d:

$$\omega_d = \omega_{t_0}\exp\left[-\frac{R(t-t_0)}{L}\right], \quad (7)$$

where ω_{t_0} is the cyclic rotation frequency for the HEDEG vector at the time moment t_0. Dependence (7) is supported by the observation that the ratio of the ventricle polarization and depolarization cycles falls between 1.3 and 2.7 [5]. This indicates a decrease of the angular velocity for the HEDEG-vector rotation.

The time dependence for the vector-rotation angle can be found from the formula

$$\theta = \int_{t_0}^{t}\omega_d dt - \varphi = Q_0\left[1 - \exp\left(-\frac{R(t-t_0)}{L}\right)\right] - \varphi. \quad (8)$$

Here, $Q_0 = \omega_{t_0} L/R$ is the equivalent-circuit Q-factor at the time moment t_0 and φ is the angle at which the principal axis of the *QRS* loop (electric axis of the heart; see, below, Fig. 3) is directed.

According to [5], the drop in the potential of the pacemaker (consisting of atypical myocardial fibers) and, consequently, in $\frac{dE}{dt}$ within the Q–T interval follows the exponential law. Therefore, we can assume the left-hand side of (6) to be nearly constant. We denote it by C_1 and also take into account that $d\theta = \omega_d dt$.

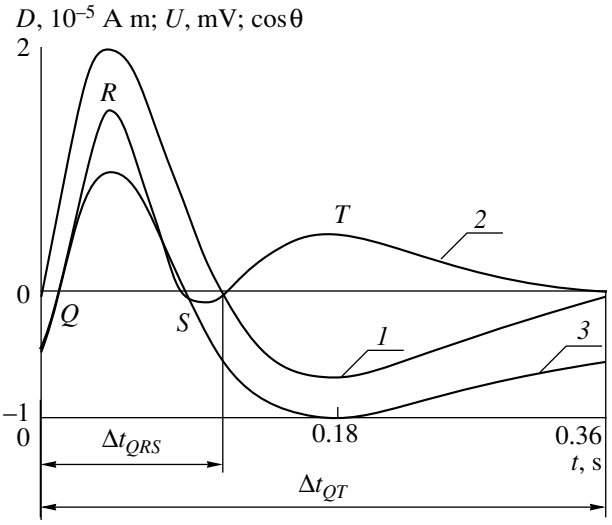

Fig. 2. Analysis of *QRST*-complex formation in the electrocardiogram. (*1*) Dipole moment of the heart integral electric vector D; (*2*) the potential U in the model electrocardiogram; (*3*) $\cos\theta$.

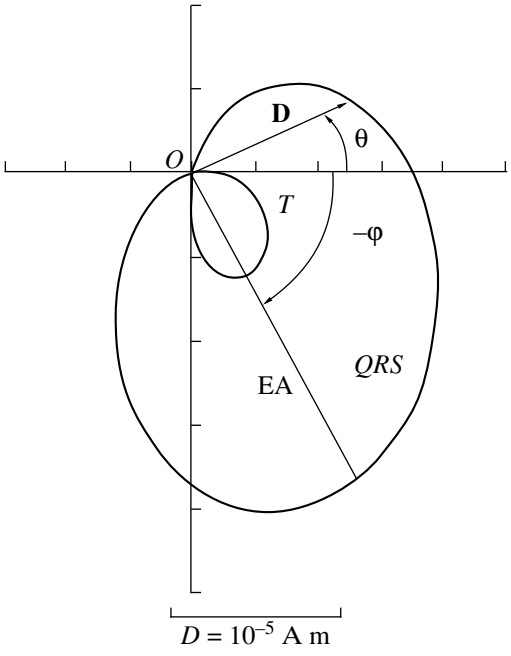

Fig. 3. Vector-electrocardiogram for the *QRST* complex constructed in polar coordinates $D(\theta)$. EA is the electric axis.

Furthermore, it is natural to assume that in the course of evolution, myocardium electric parameters had been developed in such a manner that the natural frequency ω_0 became equal to the rotation frequency ω_d for the dipole-moment vector D of the HEDEG. Then, equation (6) takes the form

$$\frac{d^2D}{d\theta^2} + D = C_1. \quad (9)$$

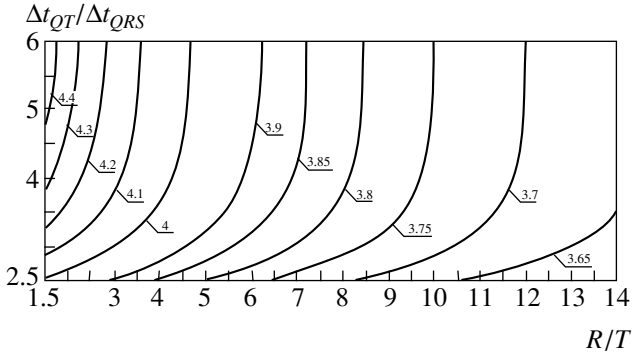

Fig. 4. Diagram for determining the *Q*-factor (Q_0) of the heart dipole equivalent electric generator in the course of ventricle depolarization according to the parameters of the patient electrocardiogram.

The solution to this equation yields the dependence of the dipole-moment vector D on the rotation angle and time. This solution can be conveniently expressed in the form

$$D = \frac{A\sin^2(\theta + \varphi)}{2} + \frac{B\cos^2(\theta + \varphi)}{2}, \qquad (10)$$

where A and B are integration constants, so that $C_1 = (A + B)/2$.

A linear electrocardiogram can be constructed from the formula

$$U = kD\cos\theta = \left(R\frac{\cos^2(\theta + \varphi)/2}{\cos\varphi} - T\frac{\sin^2(\theta + \varphi)/2}{\cos\varphi}\right)\cos\theta, \qquad (11)$$

where R and T are the amplitudes of electrocardiogram spikes and k is a constant.

The time dependences for the dipole moment D, $\cos\theta$, and the linear electrocardiogram constructed from formulas (8), (10), and (11) for R = 1.5 mV, T = 0.5 mV, Q_0 = 4.4, and R/L = 9 s^{-1} are shown in Fig. 2. $\varphi = 0$ was also taken (i.e., the heart electric axis coincides with the abduction line, which is the most typical for the norm of second standard abduction). As is seen from the curves, positive values of R and T for the spikes are determined by the identical signs of D and $\cos\theta$, whereas their different signs correspond to the negative values of Q and S for the spikes. The parameters were fitted in such a way that the electrocardiogram corresponds to the norm. Since for $t = t_0$, $\theta = -\varphi$ in accordance with (8), we have from (11) that $U = R$. Consequently, t_0 is the time for which the maximum R of the spike is attained.

Figure 3 shows the projection of the *QRS* and *T* loops onto a certain plane constructed for $B = 2.0 \times 10^{-5}$ A m [5], $A = \dfrac{B}{R/T} = 0.67 \times 10^{-5}$ A m, and $\varphi = -2.3$ rad (B and A are the principal axes of the loops).

Determining electrocardiogram interval characteristics independent of the angle φ of the heart electric axis is of interest. As our analysis has shown, there are two such characteristics, namely, the duration $QRS\Delta t_{QRS}$ of the *QRS*-complex and duration Δt_{QT} of an electric systole.

Equalizing D in (10) [or the bracketed expression in (11)] to zero and separately finding the initial and final instants for the *QRS* complex, we obtain after certain transformations

$$\Delta t_{QRS} = 2\frac{L}{R}\operatorname{arctanh}\left(\frac{2\arctan(R/T)^{1/2}}{Q_0}\right). \qquad (12)$$

The duration of the electric systole is

$$\Delta t_{QT} = \frac{L}{R} \times \ln\left|\left(1 + \frac{2\arctan(R/T)^{1/2}}{Q_0}\right)\Big/\left(1 + \frac{2\arctan(R/T)^{1/2}}{Q_0} - \frac{2\pi}{Q_0}\right)\right|. \qquad (13)$$

The ratio $\Delta t_{QT}/\Delta t_{QRS}$ is independent of the value of L/R and, as was already mentioned, of the direction of the heart electric axis. Thus, the ratio R/T of the intervals and amplitudes of the corresponding spikes, which are easily measured according to an electrocardiogram, allows one to find the value of the electric *Q*-factor for a heart at the maximum of the R spike.

In Fig. 4, the plots for $\Delta t_{QT}/\Delta t_{QRS}$ versus the ratio R/T for the amplitudes of the corresponding spikes are shown for various values of Q_0. In the norm, the *Q*-factor varies within the range from 3.9 to 4.4.

Clinical experience shows that, frequently, a pathological process that has gone too far is not reflected in the monitored parameters of an electrocardiogram, whereas the value of the heart *Q*-factor can change in this case, because it is a cumulative parameter depending on basic heart characteristics: capacitance, inductance, and resistance. Therefore, by monitoring the tendency of the variation in the heart *Q*-factor with time and detecting, e.g., its decline based on Fig. 4, we can infer the development of a pathological process, even though the other parameters of the electrocardiogram remain within the normal range.

The ratio R/L can also be estimated from the corresponding electrocardiogram. Both the terminal Q and initial S points of the spike (see Fig. 2) correspond to $\cos\theta = 0$. Therefore, between these points of the electrocardiogram, the turning angle of the integral electric vector is equal to π. Consequently, $\omega_{t_0} = \pi/\Delta t_R$, where

Δt_R is the time separation between the points indicated, which is measured in the electrocardiogram. Taking into account the relation $Q_0 = \omega_{t_0} L/R$, we find that $R/L = \pi/(\Delta t_R Q_0)$. The value Q_0 of the Q-factor can be found from the plot in Fig. 4 or, to be more precise, can be calculated from the ratio $\Delta t_{QT}/\Delta t_{QRS}$ on the basis of formulas (12) and (13).

We can consider the circular frequencies for the three mutually perpendicular circuits as vectors directed perpendicular to these circuits (Fig. 1), which vary in the course of a cardiac cycle. If we add up these vectors in space, then a three-dimensional analysis for heart electric genesis can be performed employing a position of the spatial oscillation circuit, which varies in the course of an electric systole.

REFERENCES

1. K. S. Cole and R. F. Baker, J. Gen. Physiol. **24**, 771 (1941).
2. A. N. Volobuev, V. N. Gridin, V. A. Neganov, and E. I. Nefedov, Dokl. Akad. Nauk **359**, 185 (1998) [Dokl. Phys. **43**, 165 (1998)].
3. A. N. Volobuev, V. N. Gridin, V. A. Neganov, and E. I. Nefedov, Dokl. Akad. Nauk **366**, 549 (1999).
4. A. N. Volobuev, *Biophysics* (Samara, Samar. Dom Pechati, 1999).
5. V. O. Samoĭlov, *Medical Biophysics* (Leningrad, 1982), p. 327.
6. K. Magnus, *Schwingungen* (Teubner, Stuttgart, 1961; Mir, Moscow, 1982).
7. D. S. Kuznetsov, *Special Functions* (Vysshaya Shkola, Moscow, 1995), p. 71.

Translated by V. Tsarev

Doklady Physics, Vol. 45, No. 7, 2000, pp. 324–326. Translated from Doklady Akademii Nauk, Vol. 373, No. 2, 2000, pp. 185–187.

TECHNICAL PHYSICS

"Subsolidus" Superplasticity

R. O. Kaĭbyshev and F. F. Musin

Presented by Academician I.N. Frindlyander August 10, 1999

Received September 9, 1999

It is well known that aluminum alloys exhibit very high values of relative extension in the course of their superplastic deformation (SPD) at temperatures close to those of the solidus [1, 2]. In available publications, we cannot find a consistent explanation for the mechanical behavior of aluminum alloys at premelting temperatures. This is associated with the fact that there are only a few studies of the mechanism concerning "subsolidus" superplasticity.

The goal of this paper is to investigate the phenomenology and mechanisms of subsolidus superplasticity in the 5083 alloy with a modified chemical composition (Al–4.7%Mg–1.6%Mn–0.2%Zr).

A uniform microstructure with a grain mean size of 6.2 μm was formed by a special thermomechanical processing of this alloy. An elevated specific volume of secondary phases Al_6Mn, Al_3Cr, and Al_3Zn, whose size was ranged from 20 nm to 0.3 μm, provided a high stability of the microstructure at subsolidus temperatures.

The study of mechanical behavior of the 5083 alloy in the temperature range 500–580°C shows that the SPD optimum-rate range extends toward lower deformation rates almost by two orders of magnitude (Figs. 1 and 2) at subsolidus temperatures. For example, the SPD optimum range is located within 1.6×10^{-3}–4×10^{-2} s^{-1} at 550°C and within 2.8×10^{-5}–1.6×10^{-2} s^{-1} at 570°C. The highest value (1150%) of relative extension is attained at $T = 570$°C and at a deformation rate of 2.8×10^{-3} s^{-1}. The coefficient m of the rate sensitivity increases up to 0.61.

Such unusual mechanical behavior of the 5083 alloy is caused by the absence of threshold stresses at subsolidus temperatures. Figure 3 shows the dependence of threshold stresses on deformation temperature. The threshold stresses were found by the graphical method proposed in [3]. In the temperature range 500–550°C, the values of threshold stresses clearly decrease almost linearly with the increase in the deformation temperature. At $T = 570$°C, the threshold stresses vanish. For SPD, the values of threshold stresses are specified by a binding force between the grain-boundary dislocations and by the doping-element atoms [4]. Therefore, we can assume that an increase in temperature from 550 to 570°C leads to expelling the grain-boundary dislocations from the doping-atom atmospheres. The dislocation acquires the ability to move at arbitrary applied stresses. This fact results in the threshold stresses, the disappearance of which is the cause of the SPD optimum rate range spreading toward low deformation rates.

The values of true activation energy Q_c of deformation are presented in Table 1. The analysis of obtained results show that the Q_c value increases with the SPD temperature. Within the temperature range $T = 500$–525°C, the Q_c value is close to the activation energy of the grain-boundary diffusion in aluminum (84 kJ/mol). In the temperature region $T = 525$–570°C, the Q_c values rise linearly with a decrease in the applied stresses and become close to the activation energy (142 kJ/mol) of

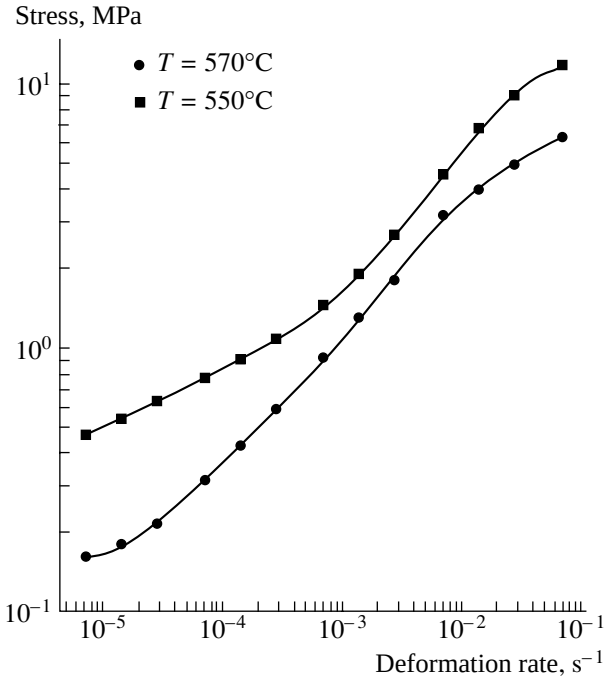

Fig. 1. Yield stress of the 5083 alloy as a function of the deformation rate.

Institute of Problems of Metal Superplasticity, Russian Academy of Sciences, ul. Khalturina 39, Ufa, Bashkortostan, 450001 Russia

1028-3358/00/4507-0324$20.00

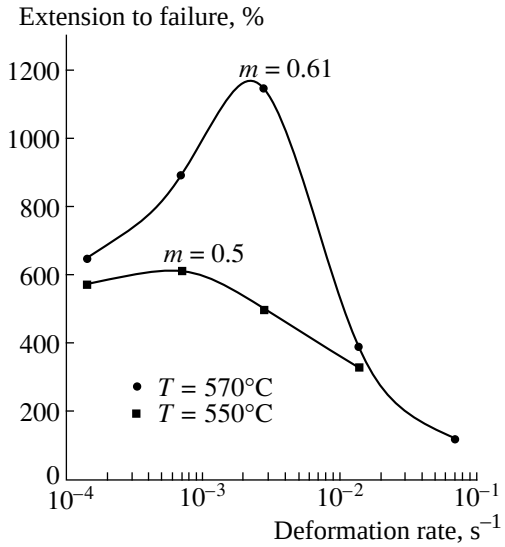

Fig. 2. Extension to failure as a function of the deformation rate for the 5083 alloy.

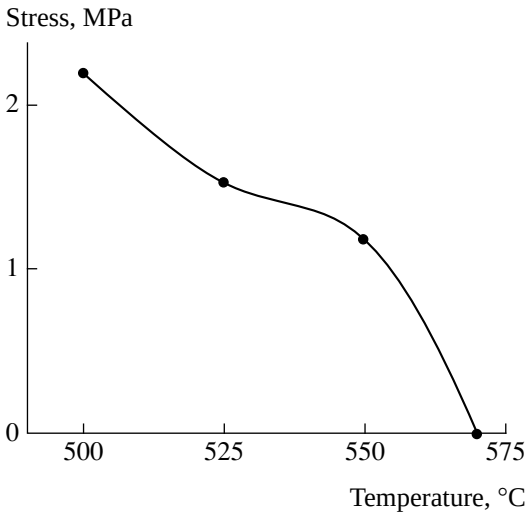

Fig. 3. Threshold stresses in the 5083 alloy as a function of deformation temperature.

diffusion for magnesium atoms in aluminum at T = 550–570°C. Thus, the SPD at subsolidus temperatures are not controlled by the grain-boundary diffusion, and its rate is governed by the viscous sliding rate of lattice dislocations. This statement agrees well with the results of [5], in which it was shown that, for an AMg4 alloy with a composition approximately similar to that of the 5083 alloy, the intragrain dislocation sliding provides a significant contribution to the total strain for subsolidus temperatures.

A special feature of the subsolidus SPD mechanism is an intense grain-boundary slip between individual grains. At $T \le 550$°C, the cooperative grain-boundary slip of large groups of grains prevails in the slip observed for the conventional SPD [6, 7]. At 570°C, we observe the relative rotations of individual grains (Fig. 4).

An increase in the uniformity of grain-boundary sliding facilitates the strain accommodation owing to the intragrain dislocation sliding. This fact leads to a considerable decrease in pore formation at $T \ge 550$°C (Table 2).

Summing up, we can conclude that a specific subsolidus SPD is observed in the 5083 alloy at premelting temperatures higher than 550°C.

We can indicate three characteristic features of the subsolidus SPD in the 5083 alloy:

(1) The absence of threshold stresses;

(2) The broadening of the optimum range of SPD up to the region of lower diffusion rates;

(3) The values of the activation energies for the subsolidus SPD and for the viscous sliding of dislocations being close to each other.

This type of superplasticity differs from the conventional SPD by the mechanisms of deformation acting at both the mesoscopic and microscopic level. The key feature of the microscopic mechanism underlying the subsolidus SPD is the detachment of the grain-boundary diffusion from the atmospheres of impurities and, as a consequence, the acceleration of the grain-bound-

Table 1. Dependence of the true activation energy Q_c for deformation of the 5083 alloy on deformation temperature

T, °C	500	525	550	570	580
Q_c, kJ/mol	82	114	141	151	186

Table 2. Porosity of the 5083 alloy after SPD and before fracture at various temperatures (at a deformation rate equal to 2.8×10^{-3} s^{-1})

T, °C	Porosity, %	Degree of deformation, %
500	1.8/1.5	200
525	2.1/1.7	290
550	6.5/5.0	500
570	3.0/1.8	1150
580	0.5/0.5	280

Note: We indicate the values measured along the deformation axis in the numerator and those measured across the deformation axis in the denominator.

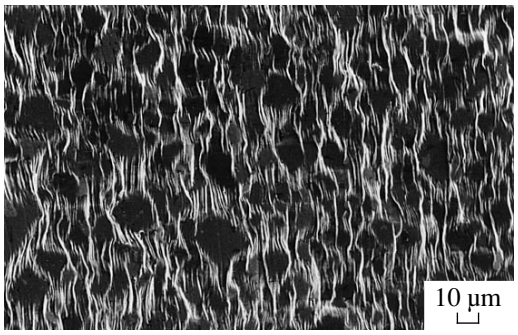

Fig. 4. Microstructure of the 5083 alloy after 100% deformation at temperature of 570°C and for the deformation rate of 2.8×10^{-3} s^{-1}.

ary sliding. The viscous sliding of lattice dislocations becomes the slowest deformation process that controls the subsolidus SPD rate in the 5083 alloy. The special feature of the subsolidus SPD mesoscopic mechanism is the transition from the cooperative grain-boundary sliding to the sliding between the individual grains. This is the cause of a negligible pore formation in the process of the subsolidus SPD.

ACKNOWLEDGMENTS

We are grateful to I.N. Sabirov for his help in performing the mechanical tests.

REFERENCES

1. K. Higashi, Mater. Sci. Forum **170/172**, 131 (1994).
2. I. I. Novikov, V. K. Portnoy, V. S. Levchenko, and A. O. Nikiforov, Mater. Sci. Forum **243/245**, 463 (1997).
3. F. A. Mohamed, K. T. Park, and E. J. Lavernia, Mater. Sci. Eng. A **150**, 21 (1992).
4. S. Yan, C. Eartman, and F. Mohamed, Philos. Mag. A **69**, 1039 (1994).
5. I. I. Novikov, A. O. Nikiforov, V. I. Pol'kin, and V. S. Levchenko, Izv. Vyssh. Uchebn. Zaved., Tsvetn. Metall., No. 1, 43 (1996).
6. V. V. Astanin, O. A. Kaibyshev, and S. N. Faizova, Acta Metall. Mater. **42**, 2617 (1994).
7. O. A. Kaibyshev, A. I. Pshenichniuk, and V. V. Astanin, Acta Mater. **46**, 4911 (1998).

Translated by V. Bukhanov

Doklady Physics, Vol. 45, No. 7, 2000, pp. 327–329. Translated from Doklady Akademii Nauk, Vol. 373, No. 2, 2000, pp. 188–190.

TECHNICAL PHYSICS

Exchange Enhancement of Magnetoelastic Vibrations in an $YBa_2Cu_3O_6$ Crystal

I. R. Kyzyrgulov and M. Kh. Kharrasov

Presented by Academician V.V.Osiko November 23, 1999

Received October 5, 1999

1. We study the interaction of spin waves and elastic waves in a $YBa_2Cu_3O_6$ crystal taken in the tetragonal phase and having an antiferromagnetic long-range order. In the absence of an external magnetic field, the ground state of the antiferromagnetic subsystem for the crystal under consideration is determined by eight compensated magnetic sublattices. Therefore, taking into account the crystal structure of the compound, we can consider a magnetic cluster to be composed of two physically equivalent subclusters, each being formed by four sublattices.

We start from the Hamiltonian involving the energies H_M and H_U of the magnetic and elastic subsystems, respectively, as well as of their interaction (H_{MU}):

$$H = H_M + H_U + H_{MU}, \tag{1}$$

$$H_M = \frac{1}{2}\int d\mathbf{x}\left\{\chi_{jm}^{\alpha\beta}M_j^\alpha M_m^\beta + \alpha_{ijmn}^{\alpha\beta}\frac{\partial M_i^\alpha}{\partial x_j}\frac{\partial M_m^\beta}{\partial x_n} - 2\sum_\alpha(\mathbf{H}_0, \mathbf{M}^\alpha)\right\}, \tag{1.1}$$

$$H_U = \frac{1}{2}\int d\mathbf{x}\{\rho\dot{\mathbf{u}}^2 + \Lambda_{ijmn}u_{ij}u_{mn}\}, \tag{1.2}$$

$$H_{MU} = \int d\mathbf{x}\{\lambda_{ijmn}^{\alpha\beta}M_i^\alpha M_j^\beta u_{mn}\}, \tag{1.3}$$

$$\chi_{jm}^{\alpha\beta} = I_{jm}^{\alpha\beta} + \beta_{jm}^{\alpha\beta}.$$

Here, $I_{jm}^{\alpha\beta}$ and $\alpha_{ijmn}^{\alpha\beta}$ are the tensors of the homogeneous and inhomogeneous exchange interactions, respectively; $\beta_{jm}^{\alpha\beta}$ is the anisotropy tensor; Λ_{ijmn} is the elasticity tensor; $\lambda_{ijmn}^{\alpha\beta}$ is the magnetostriction tensor; u_{mn} is the deformation tensor; $\mathbf{M}^\alpha$ is the lattice magnetization; $\alpha, \beta = 1, \ldots, 8$; and $i, j, m, n = x, y, z$.

Experiments on inelastic neutron scattering yield the following values for the constants of the intraplane and interplane exchange interactions: $I = (120 \pm 20)$ meV and $\sigma' = 8$ meV, respectively. In addition, $\sigma'' = (0.04 \pm 0.01)$ meV [1, 2].

2. We write out Hamiltonian (1) in the secondary-quantization representation and consider the magnetic subsystem. The sublattice magnetizations $\mathbf{M}^\alpha$ can be expressed in terms of the Holstein–Primakoff operators as

$$\mathbf{M}^\alpha = (M_0 - \mu a_\alpha^+ a_\alpha)\mathbf{e}_3^\alpha + \sqrt{\mu M_0}(\mathbf{e}_\perp^\alpha a_\alpha + \mathbf{e}_\perp^{\alpha *} a_\alpha^+),$$

$$\mathbf{e}_3^\alpha = \frac{\mathbf{M}_0^\alpha}{M_0},\ \mathbf{e}_\perp^\alpha = \frac{1}{\sqrt{2}}(\mathbf{e}_1^\alpha + i\mathbf{e}_2^\alpha), \tag{2}$$

$$\mathbf{e}_1^\alpha \perp_s (\mathbf{M}_0, \mathbf{H}_0),\ \mathbf{e}_2^\alpha = [\mathbf{e}_3^\alpha, \mathbf{e}_1^\alpha],$$

where $\mathbf{M}_0^\alpha$ is the equilibrium magnetization of the αth sublattice; $\mu = g\mu_B$ (g is the Landé factor), and $\mu_B = e\hbar/(2m_e c)$ is the Bohr magneton.

Substituting (2) into (1.1) and passing to the Fourier representation for operators, we obtain

$$H_M = \frac{1}{2}\sum_{\alpha\beta k}\{A_k^{\alpha\beta}a_{k\alpha}^+ a_{k\beta} + B_k^{\alpha\beta}a_{k\alpha}^+ a_{-k\beta}^+\} + \text{h.c.}, \tag{3}$$

$$A_k^{\alpha\beta} = \mu M_0\left[(\chi_{jm}^{\alpha\beta}e_{\perp j}^{\alpha *} + \alpha_{ijmn}^{\alpha\beta}k_j k_n e_{\perp i}^{\alpha *})e_{\perp m}^\beta - \delta^{\alpha\beta}\left(\sum_{\beta jm}\chi_{jm}^{\alpha\beta}e_{3j}^\alpha e_{3m}^\beta - \frac{1}{M_0}(\mathbf{H}_0, \mathbf{e}_3)\right)\right],$$

$$B_k^{\alpha\beta} = \mu M_0[\chi_{jm}^{\alpha\beta}e_{\perp j}^{\alpha *} + \alpha_{ijmn}^{\alpha\beta}k_j k_n e_{\perp i}^{\alpha *}]e_{\perp m}^{\beta *}.$$

Let the external magnetic homogeneous field $\mathbf{H}_0$ be directed along the second-order axis OZ. In the absence of the field, magnetic moments are aligned within the

Bashkortostan State University, ul. Frunze 39, Ufa, Bashkortostan, 450074 Russia
e-mail: Kizirgulov IR@ic.bashedu.ru

1028-3358/00/4507-0327$20.00 © 2000 MAIK "Nauka/Interperiodica"

XOY basis plane of the tetragonal elementary cell. In the fields $H_0 < H_\delta$ applied, all the moments turn through the angle of $\pi/2 - \theta_\alpha$, with $\cos\theta_\alpha = H_0/H_\delta$. When $H_0 = H_\delta$, the sublattices collapse.

Using the canonical Bogolyubov u,v transformation, we can rewrite Hamiltonian (3) in terms of the magnon operators $c_{k\gamma} = c^+_{k\gamma}$, $\gamma = 1, \ldots, 8$. The diagonalized operator has the standard form

$$H_M = \sum_{k\gamma} \varepsilon^M_{k\gamma} c^+_{k\gamma} c_{k\gamma}, \tag{4}$$

where $\varepsilon^M_{k\gamma} = [C^2_\gamma - D^2_\gamma]^{1/2}$ is the spin-wave spectrum,

$$\begin{aligned}
C_{1,2} &= A^{11} \pm A^{12} + A^{13} \pm A^{14} \\
&\quad + A^{15} \pm A^{16} + A^{17} \pm A^{18}, \\
C_{3,4} &= A^{11} \pm A^{12} - A^{13} \mp A^{14} \\
&\quad + A^{15} \pm A^{16} - A^{17} \mp A^{18}, \\
C_{5,6} &= A^{11} \pm A^{12} + A^{13} \pm A^{14} \\
&\quad - A^{15} \mp A^{16} - A^{17} \mp A^{18}, \\
C_{7,8} &= A^{11} \pm A^{12} - A^{13} \mp A^{14} \\
&\quad - A^{15} \mp A^{16} + A^{17} \pm A^{18}.
\end{aligned}$$

D_γ are expressed in a similar manner in terms of the *B*-matrix components.

3. We now consider the elastic subsystem. The elastic-displacement vector for atoms can be represented in the form [3]

$$\mathbf{u} = \frac{1}{\sqrt{2\rho V}} \sum_{ks} \frac{\mathbf{e}^s_k}{\sqrt{\varepsilon^U_{ks}}} (b_{ks} e^{ikx} + b^+_{ks} e^{-ikx}), \tag{5}$$

where b^+_{ks} and b_{ks} are, respectively, the creation and destruction operators for phonons having the momentum $\mathbf{k}$ and polarization $s = (l, t_1, t_2)$, with l and t_1, t_2 being the longitudinal and transverse polarizations, respectively; ε^U_{ks} and $\mathbf{e}^s_k$ are the energy and the unit polarization vector for phonons, respectively.

Then, substituting (5) into (1.2), we obtain

$$H_U = \sum_{ks} \varepsilon^U_{ks} b^+_{ks} b_{ks}. \tag{6}$$

Similarly, taking into account (2) and (5), we can rewrite Hamiltonian (1.3) in the form

$$\begin{aligned}
H_{MU} = i\left(\frac{2\mu M_0^3}{\rho}\right)^{1/2} \sum_{ks\alpha\beta} \frac{e^s_{km} k_n}{\sqrt{\varepsilon^U_{ks}}} \lambda^{\alpha\beta}_{ijmn} [b_{-ks} - b^+_{ks}] \\
\times [e^\alpha_{3i} e^\beta_{\perp j} a_{k\beta} + e^\beta_{3j} e^\alpha_{\perp i} a_{k\alpha} + e^{\alpha}_{3i} e^{\beta *}_{\perp j} a^+_{-k\beta} + e^\beta_{3j} e^{\alpha *}_{\perp i} a^+_{-k\alpha}].
\end{aligned} \tag{7}$$

Applying the Bogolyubov u,v-transformation to the Hamiltonian (7), we arrive at the conclusion that, within the approximation used, only two spin-wave branches do interact with sound waves,

$$H_{MU} = \sum_{ks,\,\gamma = 1,2} \Psi_{k\gamma s} c_{k\gamma} (b_{-ks} - b^+_{ks}) + \text{h.c.}, \tag{8}$$

with the magnetoelastic-interaction parameter being given in the form

$$\begin{aligned}
\Psi_{k\gamma s} &= 4\left(\frac{2\mu M_0^3}{\rho \varepsilon^U_{ks}}\right)^{1/2} \\
&\times [-L^{(1)}_{k\gamma s}(u_{k\gamma} - v_{k\gamma}) + iL^{(2)}_{k\gamma s}(u_{k\gamma} + v_{k\gamma})], \\
u_{k\gamma} &= \frac{\sqrt{C_\gamma + D_\gamma} + \sqrt{C_\gamma - D_\gamma}}{2\sqrt{\varepsilon^M_{k\gamma}}}, \\
v_{k\gamma} &= -\frac{\sqrt{C_\gamma + D_\gamma} - \sqrt{C_\gamma - D_\gamma}}{2\sqrt{\varepsilon^M_{k\gamma}}}, \\
L^{(1)}_{k1s} &= \sin 2\theta [(\lambda_1 + \lambda_2) e^s_{kx} k_x \\
&+ (\lambda_3 + \lambda_4) e^s_{ky} k_y + (\lambda_5 + \lambda_6) e^s_{kz} k_z], \\
L^{(1)}_{k2s} &= \lambda_7 \cos 2\theta (e^s_{kx} k_z + e^s_{kz} k_x), \\
L^{(2)}_{k1s} &= \lambda_8 \sin\theta (e^s_{kx} k_y + e^s_{ky} k_x), \\
L^{(2)}_{k2s} &= \lambda_9 \cos\theta (e^s_{kz} k_y + e^s_{ky} k_z).
\end{aligned}$$

The magnetostriction constants have the form

$$\begin{aligned}
&\lambda_1 = \lambda^{11}_{xxxx} - \lambda^{12}_{xxxx}, \ \lambda_2 = \lambda^{11}_{zzxx} + 3\lambda^{12}_{zzxx} + 4\lambda^{15}_{zzxx}, \\
&\lambda_3 = \lambda^{11}_{xxyy} - \lambda^{12}_{xxyy}, \ \lambda_4 = \lambda^{11}_{zzyy} + 3\lambda^{12}_{zzyy} + 4\lambda^{15}_{zzyy}, \\
&\lambda_5 = \lambda^{11}_{xxzz} - \lambda^{12}_{xxzz}, \ \lambda_6 = \lambda^{11}_{zzzz} + 3\lambda^{12}_{zzzz} + 4\lambda^{15}_{zzzz}, \\
&\lambda_7 = \lambda^{11}_{xzxz} - \lambda^{12}_{xzxz}, \ \lambda_8 = \lambda^{11}_{xyxy} - \lambda^{12}_{xyxy}, \\
&\lambda_9 = \lambda^{11}_{yzyz} - \lambda^{12}_{yzyz}.
\end{aligned}$$

We now find the spectrum of the coupled magnetoelastic waves.

In order to diagonalize total Hamiltonian (4), (6)–(8), we apply the Bogolyubov u,v-transformation. This provides the following dispersion equation that governs the spectrum E of coupled magnetoelastic vibrations:

$$\begin{aligned}
&\prod_{\gamma s} (E^2 - \varepsilon^2_{k\gamma})(E^2 - \varepsilon^2_{ks}) - 4\sum_{\gamma s} |\Psi_{\gamma s}|^2 \varepsilon_{k\gamma} \varepsilon_{ks} \\
&\times \prod_{\substack{\gamma' \neq \gamma \\ s' \neq s}} (E^2 - \varepsilon^2_{k\gamma'})(E^2 - \varepsilon^2_{ks'}) = 0, \\
&\varepsilon_{k\gamma} \equiv \varepsilon^M_{k\gamma}, \ \varepsilon_{ks} \equiv \varepsilon^U_{ks}, \ \Psi_{\gamma s} \equiv \Psi_{k\gamma s}.
\end{aligned}$$

The spectrum of coupled magnetoelastic waves in the vicinity of the corresponding resonances exhibits the form

$$E_{k\gamma,\,ks} = \frac{1}{2}[\varepsilon_{k\gamma} + \varepsilon_{ks} \pm \sqrt{[\varepsilon_{k\gamma} - \varepsilon_{ks}]^2 + 16|\Psi_{k\gamma s}|^2\varepsilon_{k\gamma}\varepsilon_{ks}}].$$

The interaction between the magnetic and elastic subsystems affects the spectrum of those branches that have the nonzero coupling coefficient.

4. We assume that the phonon-polarization unit vectors $\mathbf{e}_l$, $\mathbf{e}_{t_1}$, $\mathbf{e}_{t_2}$ represent the right-hand triplet. Next, we consider the parameters of the magnetoelastic interaction for various directions of the coupled-wave propagation. Here, the zero-coupling (within our approximation) parameters are omitted.

(i) $\mathbf{k} \parallel \mathbf{Z}_0$,

$$\Psi_{k1l} = 4\gamma_s\sqrt{C_1 + D_1}\sin 2\theta(\lambda_5 + \lambda_6)k_z/\sqrt{\varepsilon_{k1}},$$

$$\Psi_{k2t_1} = 4\gamma_s\sqrt{C_2 + D_2}\cos\theta\lambda_7 k_z/\sqrt{\varepsilon_{k_2}},$$

$$\Psi_{2kt_2} = 4i\gamma_s\sqrt{C_2 - D_2}\cos\theta\lambda_9 k_z/\sqrt{\varepsilon_{k2}},$$

$$\cos\theta = \frac{H_0}{H_\delta},\ \gamma_s = 4\left(\frac{2\mu M_0^3}{\rho\varepsilon_{ks}^U}\right)^{1/2},\ s = l, t.$$

The coupling of the second spin branch with the first transverse-phonon branch is enhanced by a factor of $I^{1/2}$ owing to the existence of the exchange interaction. This effect has been observed for the first time in [4], while studying a two-sublattice single-axis antiferromagnetic substance (see also [5, 6]).

(ii) $\mathbf{k} \parallel \mathbf{Y}_0$,

$$\Psi_{k1l} = 4\gamma_s\sqrt{C_1 + D_1}\sin 2\theta(\lambda_3 + \lambda_4)k_y/\sqrt{\varepsilon_{k1}},$$

$$\Psi_{k1t_2} = 4i\gamma_s\sqrt{C_1 - D_1}\sin\theta\lambda_8 k_y/\sqrt{\varepsilon_{k1}},$$

$$\Psi_{k2t_1} = 4i\gamma_s\sqrt{C_2 - D_2}\cos\theta\lambda_9 k_y/\sqrt{\varepsilon_{k2}}.$$

Here, the exchange amplification affects the coefficient of the first spin-branch coupling with the second transverse phonon branch.

(iii) $\mathbf{k} \parallel \mathbf{X}_0$,

$$\Psi_{k1l} = 4\gamma_s\sqrt{C_1 + D_1}\sin 2\theta(\lambda_1 + \lambda_2)k_x/\sqrt{\varepsilon_{k1}},$$

$$\Psi_{k1t_1} = 4\gamma_s\sqrt{C_1 - D_1}\sin\theta\lambda_8 k_x/\sqrt{\varepsilon_{k1}},$$

$$\Psi_{k2t_2} = 4i\gamma_s\sqrt{C_2 + D_2}\cos 2\theta\lambda_7 k_x/\sqrt{\varepsilon_{k2}}.$$

In this case, the exchange enhances the coupling of the first and the second spin branches with the t_1 and t_2 transverse phonon branches, respectively.

Thus, in the crystal under study, which is taken in the phase featuring the antiferromagnetic long-range order, there exist new quasi-particles, i.e., strongly coupled phonons and magnons. The enhanced coupling of certain spin and phonon modes is caused by the exchange interaction between the localized magnetic moments of the antiferromagnetic sublattices.

REFERENCES

1. S. Shamoto, M. Sato, J. M. Tranquada, *et al*., Phys. Rev. D **48**, 13817 (1993).
2. J. M. Tranquada, G. Shirana, B. Keimer, *et al.*, Phys. Rev. D **40**, 4503 (1989).
3. N. N. Bogolyubov, Jr., B. I. Sadovnikov, and A. S. Shumovskiĭ, *Mathematical Methods of Statistic Mechanics for Model Systems* (Nauka, Moscow, 1989).
4. M. A. Savchenko, Fiz. Tverd. Tela (Leningrad) **6**, 864 (1964) [Sov. Phys. Solid State **6**, 666 (1964)].
5. V. I. Ozhogin and M. A. Savchenko, Usp. Fiz. Nauk **143**, 676 (1984) [Sov. Phys. Usp. **27**, 643 (1984)].
6. M. Kh. Kharrasov, Dokl. Akad. Nauk **335**, 175 (1994) [Phys.–Dokl. **39**, 169 (1994)].

Translated by O. Chernavskaya

Doklady Physics, Vol. 45, No. 7, 2000, pp. 330–332. Translated from Doklady Akademii Nauk, Vol. 373, No. 1, 2000, pp. 39–41.

MECHANICS

On Features of Relations for a General Two-Dimensional Problem in the Ideal-Plasticity Theory

D. D. Ivlev and L. A. Maksimova

Presented by Academician A.Yu. Ishlinskiĭ September 9, 1999

Received October 8, 1999

Relations of the ideal-plasticity theory under the condition of complete plasticity were considered in [1, 2]. In what follows, statically definable relations of this theory are examined in the case when all stress components σ_{ij} depend on two coordinates x, y. A two-dimensional strain is the particular case of the relations under discussion.

We consider the condition of complete plasticity

$$\sigma_1 = \sigma_2, \quad \sigma_3 = \sigma_1 + 2\kappa, \quad \kappa = \text{const}, \tag{1}$$

where σ_i are the components of the principal stresses and κ is the shear yield stress.

With constraints (1), we can write out

$$\begin{aligned}
\sigma_x &= \sigma - \frac{2\kappa}{3} + 2\kappa n_1^2, \quad \tau_{xy} = 2\kappa n_1 n_2,\\
\sigma_y &= \sigma - \frac{2\kappa}{3} + 2\kappa n_2^2, \quad \tau_{yz} = 2\kappa n_2 n_3,\\
\sigma_z &= \sigma - \frac{2\kappa}{3} + 2\kappa n_3^2, \quad \tau_{xz} = 2\kappa n_1 n_3,\\
\sigma &= \frac{1}{3}(\sigma_x + \sigma_y + \sigma_z).
\end{aligned} \tag{2}$$

Here, σ_x, τ_{xy}, … are the components of the stress in the Cartesian coordinate system xyz, $n_1 = \cos\varphi_1$, $n_2 = \cos\varphi_2$, and $n_3 = \cos\varphi_3$ are the direction cosines defining the orientation of the third principal stress σ_3 in the xyz-coordinate system.

The following relation holds true:

$$n_1^2 + n_2^2 + n_3^2 = 1. \tag{3}$$

It follows from formulas (2) and (3) that

$$\sigma_x = \sigma - \frac{2\kappa}{3} + \frac{\tau_{xy}\tau_{xz}}{\tau_{yz}},$$

$$\sigma_y = \sigma - \frac{2\kappa}{3} + \frac{\tau_{xy}\tau_{yz}}{\tau_{xz}}, \tag{4}$$

$$\sigma_z = \sigma - \frac{2\kappa}{3} + \frac{\tau_{xz}\tau_{yz}}{\tau_{xy}},$$

$$\frac{\tau_{xy}\tau_{xz}}{\tau_{yz}} + \frac{\tau_{xy}\tau_{yz}}{\tau_{xz}} + \frac{\tau_{xz}\tau_{yz}}{\tau_{xy}} = 2\kappa. \tag{5}$$

According to (2), relation (5) is equivalent to (3) and can be rewritten in the form

$$(\tau_{xz}^2 + \tau_{yz}^2)\tau_{xy}^2 - 2\kappa(\tau_{xz}\tau_{yz})\tau_{xy} + (\tau_{xz}\tau_{yz})^2 = 0. \tag{6}$$

We put

$$\begin{aligned}
\tau_{xz} &= \kappa\mathbf{T}\cos\varphi, \quad \tau_{yz} = \kappa\mathbf{T}\sin\varphi,\\
\tau_{xz}^2 + \tau_{yz}^2 &= (\kappa\mathbf{T})^2.
\end{aligned} \tag{7}$$

From (6) and (7), we obtain

$$\tau_{xy} = \kappa(1 \pm \sqrt{1 - \mathbf{T}^2})\sin\varphi\cos\varphi. \tag{8}$$

The case of two-dimensional strain takes place for

$$\tau_{xz} = \tau_{yz} = \mathbf{T} = 0. \tag{9}$$

In this case, from (8) and (9), it follows that

$$\tau_{xy} = \kappa(1 \pm 1)\sin\varphi\cos\varphi. \tag{10}$$

Henceforth, we allow for the upper sign in (8) and (10), whereas the lower sign is discarded.

We find from (4), (7), and (8) that

$$\begin{aligned}
\sigma_x &= \sigma - \frac{2\kappa}{3} + \kappa(1 + \sqrt{1 - \mathbf{T}^2})\cos^2\varphi,\\
\sigma_y &= \sigma - \frac{2\kappa}{3} + \kappa(1 + \sqrt{1 - \mathbf{T}^2})\sin^2\varphi,\\
\sigma_z &= \sigma - \frac{2\kappa}{3} + \frac{\kappa\mathbf{T}^2}{1 + \sqrt{1 - \mathbf{T}^2}},\\
\tau_{xy} &= \kappa(1 + \sqrt{1 - \mathbf{T}^2})\sin\varphi\cos\varphi,\\
\tau_{xz} &= \kappa\mathbf{T}\cos\varphi,
\end{aligned} \tag{11}$$

Chuvash State Pedagogical University,
ul. Karla Marksa 38, Cheboksary, 428000 Russia

1028-3358/00/4507-0330$20.00

$$\tau_{yz} = \kappa \mathbf{T} \sin\varphi.$$

According to (8), the absolute value of $\mathbf{T}$ may vary within the limits $|\mathbf{T}| \le 1$. Furthermore, we consider

$$\mathbf{T} = \sin\theta. \tag{12}$$

According to (12), relations (11) take the form

$$\begin{aligned}
\sigma_x &= \sigma - \frac{2\kappa}{3} + \kappa(1+\cos\theta)\cos^2\varphi,\\
\sigma_y &= \sigma - \frac{2\kappa}{3} + \kappa(1+\cos\theta)\sin^2\varphi,\\
\sigma_z &= \sigma - \frac{2\kappa}{3} + \kappa(1-\cos\theta),\\
\tau_{xy} &= \kappa(1+\cos\theta)\sin\varphi\cos\varphi,\\
\tau_{xz} &= \kappa\sin\theta\cos\varphi,\\
\tau_{yz} &= \kappa\sin\theta\sin\varphi.
\end{aligned} \tag{13}$$

We have from (13)

$$(\sigma_x - \sigma_y)^2 + 4\tau_{xy}^2 = \kappa^2(1+\cos\theta)^2. \tag{14}$$

According to (12), in the case of two-dimensional strain (9), the relation $\theta = 0$ holds, and relation (14) takes the form

$$(\sigma_x - \sigma_y)^2 + 4\tau_{xy}^2 = 4\kappa^2. \tag{15}$$

We consider the equations of equilibrium

$$\begin{aligned}
\frac{\partial\sigma_x}{\partial x} + \frac{\partial\tau_{xy}}{\partial y} + \frac{\partial\tau_{xz}}{\partial z} &= 0,\\
\frac{\partial\tau_{xy}}{\partial x} + \frac{\partial\sigma_y}{\partial y} + \frac{\partial\tau_{yz}}{\partial z} &= 0,\\
\frac{\partial\tau_{xz}}{\partial x} + \frac{\partial\tau_{yz}}{\partial y} + \frac{\partial\sigma_z}{\partial z} &= 0.
\end{aligned} \tag{16}$$

We assume that all the stress components (13) depend on the variables x, y and are independent of the z-coordinate:

$$\sigma = \sigma(x,y), \quad \theta = \theta(x,y), \quad \varphi = \varphi(x,y). \tag{17}$$

Substituting relations (13) into equations (16) under assumptions (17), we arrive at the system of three equations with respect to three unknowns σ, φ, and θ:

$$\begin{aligned}
&\frac{\partial\sigma}{\partial x} - \kappa(1+\cos\theta)\sin 2\varphi\frac{\partial\varphi}{\partial x} + \kappa(1+\cos\theta)\cos 2\varphi\frac{\partial\varphi}{\partial y}\\
&\quad - \kappa\sin\theta\cos^2\varphi\frac{\partial\theta}{\partial x} - \frac{\kappa}{2}\sin\theta\sin 2\varphi\frac{\partial\theta}{\partial y} = 0,\\
&\frac{\partial\sigma}{\partial y} + \kappa(1+\cos\theta)\cos 2\varphi\frac{\partial\varphi}{\partial x} + \kappa(1+\cos\theta)\sin 2\varphi\frac{\partial\varphi}{\partial y}\\
&\quad - \frac{\kappa}{2}\sin\theta\sin 2\varphi\frac{\partial\theta}{\partial x} - \kappa\sin\theta\sin^2\varphi\frac{\partial\theta}{\partial y} = 0,\\
&\sin\theta\sin\varphi\frac{\partial\varphi}{\partial x} - \sin\theta\cos\varphi\frac{\partial\varphi}{\partial y}\\
&\quad - \cos\theta\cos\varphi\frac{\partial\theta}{\partial x} - \cos\theta\sin\varphi\frac{\partial\theta}{\partial y} = 0.
\end{aligned} \tag{18}$$

To determine characteristics of the system of equations (18) and relations true along the characteristics, we adjoin the following relations to system (18):

$$\begin{aligned}
\frac{\partial\sigma}{\partial x}dx + \frac{\partial\sigma}{\partial y}dy &= d\sigma,\\
\frac{\partial\varphi}{\partial x}dx + \frac{\partial\varphi}{\partial y}dy &= d\varphi,\\
\frac{\partial\theta}{\partial x}dx + \frac{\partial\theta}{\partial y}dy &= d\theta.
\end{aligned} \tag{19}$$

Considering system of equations (18) and (19) as an algebraic one with respect to the components

$$\frac{\partial\sigma}{\partial x}, \quad \frac{\partial\sigma}{\partial y}, \quad \frac{\partial\varphi}{\partial x}, \quad \frac{\partial\varphi}{\partial y}, \quad \frac{\partial\theta}{\partial x}, \quad \frac{\partial\theta}{\partial y}, \tag{20}$$

we can define

$$\begin{aligned}
&\frac{\partial\sigma}{\partial x} = \frac{\Delta_1}{\Delta}, \quad \frac{\partial\sigma}{\partial y} = \frac{\Delta_2}{\Delta}, \quad \frac{\partial\varphi}{\partial x} = \frac{\Delta_3}{\Delta},\\
&\frac{\partial\varphi}{\partial y} = \frac{\Delta_4}{\Delta}, \quad \frac{\partial\theta}{\partial x} = \frac{\Delta_5}{\Delta}, \quad \frac{\partial\theta}{\partial y} = \frac{\Delta_6}{\Delta}.
\end{aligned} \tag{21}$$

Here, Δ and Δ_i are determined by the Cramer's rule.

In the characteristics, the relations

$$\Delta = \Delta_i = 0, \quad i = 1, 2, \ldots, 6 \tag{22}$$

must be simultaneously fulfilled.

Two characteristic families and relations that are true along them can be found from the conditions $\Delta = \Delta_1 = 0$. The equations for the characteristics are the following:

$$\left(\frac{dy}{dx}\right)_{1,2} = \tan\left[\varphi \pm \left(\frac{\pi}{4} + \mu\right)\right], \quad \tan 2\mu = \frac{1-\cos\theta}{2\sqrt{\cos\theta}}. \tag{23}$$

and the relations (23) true along the characteristics are

$$d\sigma \pm \frac{\kappa(1+\cos\theta)}{\sqrt{\cos\theta}}d\varphi = 0. \tag{24}$$

It is worth noting that in the case of the two-dimensional strain $\theta = 0$, $\cos\theta = 1$, and $\mu = 0$, charac-

teristics (23) become orthogonal, and relations (24) transform into Hencky relationships [1].

In the general case for $\theta \neq 0$, the third characteristic determined from the relation $\Delta = \Delta_6 = 0$ exists, with the equation for it being

$$\frac{dy}{dx} = \tan\varphi. \quad (25)$$

The relation true along characteristic (25) is

$$\left(\frac{\sin\theta}{1+\cos\theta}\right)d\sigma + \kappa\sin\theta\sin 2\varphi d\varphi + \kappa d\theta = 0. \quad (26)$$

Formulas (23)–(26) define the stress for the case of a general two-dimensional problem in the theory of an ideally plastic body. The consideration of other cases brings about no new characteristics.

It should be noted that for a two-dimensional strain, i.e., $\theta = 0$, relation (26) degenerates.

From (13), it follows that

$$\tan 2\varphi = \frac{2\tau_{xy}}{\sigma_x - \sigma_y}, \quad \tan\varphi = \frac{\tau_{yz}}{\tau_{xz}}. \quad (27)$$

According to (27), (23), and (25), the third characteristic (25) is aligned with the bisector of the angle formed by characteristics (23).

REFERENCES

1. A. Yu. Ishlinskiĭ, *Applied Problems in Mechanics* (Nauka, Moscow, 1986), **1**, pp. 62-83.
2. D. D. Ivlev, *Theory of Ideal Plasticity* (Nauka, Moscow, 1966).

Translated by V. Tsarev

Doklady Physics, Vol. 45, No. 7, 2000, pp. 333–335. Translated from Doklady Akademii Nauk, Vol. 373, No. 1, 2000, pp. 42–44.

MECHANICS

The Irwin's and Griffith's Criteria for a Set of Cracks

S. A. Nazarov

Presented by Academician V.P. Myasnikov May 19, 1999

Received July 19, 1999

The usual formulations of the Irwin's and Griffith's criteria allow us to determine the critical load, i.e., the load initiating the growth of cracks. Both of these criteria lead to the same result. The well-known attempts to refine the formulation of these criteria (see [1, 2] for both the force and [3, 4] energy criteria) require the involvement of variational inequalities making it possible to take into account interactions between cracks and to analyze their elongation as a function of the timelike loading parameter. The goal of this paper is to compare predictions concerning the evolution of a set of cracks on the basis of these two criteria.

Let Ω be a two-dimensional isotropic body weakened by the set $M^1, \ldots, M^J$ of segmentlike cracks. We denote the tips of cracks located within Ω as $P^1, \ldots, P^N$ (an edge crack has only one tip, i.e., $N \le 2J$). Having the intention of applying the Irwin's criterion, we assume that the cracks grow along straight lines, their tips correspond to the normal discontinuity, and the shear modes, if any, are negligibly small. Such a stressed state is possible, e.g., for cracks located in the same straight line or for several such rows lying apart from each other. The load $p^\tau = p^0 + \tau p^1$ is applied to the outer surface Γ. Here, $\tau \in [0, \tau_0)$ is the timelike loading parameter (for simplicity, we ignore the bulk forces). We allow polar coordinate system (r_n, φ_n) to correspond with each point P^n, where $r_n = |x - P^n|$ and $|\varphi_n| < \pi$. We denote also stress-intensity coefficients (SICs) at (immovable!) tips P^n generated by forces p^τ as $K_n^\tau = K_n^0 + \tau K_n'$, $n = 1, \ldots, N$. If the load p^τ gives rise to the growth of the crack set $\{M^j(\tau): j = 1, \ldots, J\}$, then the values $K_n(\tau)$ of the SIC corresponding to displaced tips $P^n(\tau)$ differ, in general, from K_n^τ. Assuming that the cracks are open and do not close [in other words, $K_n^0 > 0$ and $h_n(\tau) = |P^n - P^n(\tau)| \ge 0$], we introduce the functions to be determined below:

$$H_n(\tau) = K_n^0 h_n(\tau) > 0, \quad n = 1, \ldots, N. \tag{1}$$

Smirnov Research Institute of Mathematics and Mechanics, St. Petersburg State University, Universitetskaya nab. 7/9, St. Petersburg, 199164 Russia

Further calculations are based on a number of asymptotic relationships for the body's stressed state $\Omega(\tau) = \Omega\backslash\{M^1(\tau) \cup \ldots \cup M^J(\tau)\}$ under an arbitrary (but small) variation of crack lengths. These relationships involve the parameters characteristic of the initial crack positions, which can be used as the aforementioned variational inequalities. Namely, we need to know the coefficients in the expansions of solutions u^0 and u' to the elasticity theory problem for $\Omega(0)$ under the loads p^0 and p', respectively,

$$\begin{aligned} u^0(x) &= l^n(x) + K_n^0 r_n^{1/2}\Phi^1(\varphi_n) + k_n^0 r_n^{3/2}\Phi^3(\varphi_n) + O(r_n^2), \\ u'(x) &= c^{n\prime} + K_n' r_n^{1/2}\Phi^1(\varphi_n) + O(r_n), \quad r_n \longrightarrow 0. \end{aligned} \tag{2}$$

Here, l^n is the linear vector function, $c^{n\prime}$ is a constant, and k_n^0 is the lowest SIC (it does not generate stress singularities, but affects the crack propagation [1, 5]). In addition, we need to know the weight functions ζ^n with singularities in P^n [6, 7], i.e., energy-independent solutions to the uniform problem in $\Omega(0)$, which can be represented as

$$\begin{aligned} \zeta^n(x) &= r_n^{-1/2}\Psi^1(\varphi_n) + c^{nn} + A_{nn} r_n^{1/2}\Phi^1(\varphi_n) + O(r_n), \\ \zeta^n(x) &= c^{mn} + A_{mn} r_m^{1/2}\Phi^1(\varphi_m) + O(r_m), \quad m \ne n. \end{aligned} \tag{3}$$

Here, c^{mn} are constants, and Ψ^1, Φ^1, and Φ^3 are the known angular parts (see, e.g., [8], in which all necessary renormalizations are performed). In (3), coefficients A_{mn} play the role of SICs, and they can be represented in the form of the $N \times N$ matrix A, which turns out to be symmetric [5, 8]. One of the asymptotic formulas mentioned above has the form

$$\begin{aligned} K_n(\tau) &= K_n^0 + \tau K_n' + \frac{1}{2} h_n(\tau) k_n^0 \\ &+ \alpha \sum_{m=1}^{N} A_{nm} H_m(\tau) + O(\tau^2 + h(\tau)^2), \end{aligned} \tag{4}$$

where $\alpha = (\lambda + 2\mu)[2\mu(\lambda + \mu)]^{-1}$, λ and μ are the Lamé constants, and $h(\tau) = \max\{h_1(\tau), \ldots, h_N(\tau)\}$ is the maximum elongation. The three-term asymptotic behavior of the potential energy used by the Griffith's criterion is calculated based on (2) and (3) with the same data set

1028-3358/00/4507-0333$20.00

(see, for example, [8]). Below, we use asymptotic representations similar to (4) omitting the residuals $O(\ldots)$. In other words, we consider small values of the parameter τ and small elongations of cracks.

We now turn to Irwin's criterion, which, in accordance with [1, 2], can be written out in the form

$$\begin{aligned} h_n(\tau) &= 0 \Rightarrow K_n(\tau) \le K_{1c}, \\ h_n(\tau) &> 0 \Rightarrow K_n(\tau) = K_{1c}, \end{aligned} \tag{5}$$

where K_{1c} is the critical value for the SIC. Both relationships in (5) imply that at any time moment τ, we have equilibrium cracks, and the tip propagation is possible only at the critical SIC value. Following the conventional formalism (see, for example, [9]), we find that conditions (5) are transformed into the following variational inequality, allowing us to determine the column $H(\tau) \in (\mathbb{R}_+)^N$ with the components (1):

$$\begin{aligned} \alpha\langle AH(\tau), H(\tau) - X\rangle + \langle BH(\tau), H(\tau) - X\rangle \\ \ge \langle F(\tau), H(\tau) - X\rangle \ \forall X \in (\mathbb{R}_+)^N. \end{aligned} \tag{6}$$

The latter inclusion implies that all components of the column X are nonnegative. Here, B is the diagonal $N \times N$ matrix, symbol $\langle , \rangle$ corresponds to the scalar product in $\mathbb{R}^N$, t denotes the transposition, and

$$\begin{aligned} B &= \mathrm{diag}\{B_1, \ldots, B_N\}, \quad F^I(\tau) = (F_1^I(\tau), \ldots, F_N^I(\tau))^t, \\ B_n &= (2K_n^0)^{-1}k_n^0, \quad F_n^I(\tau) = K_{1c} - K_n^0 - \tau K_n'. \end{aligned} \tag{7}$$

The variational inequality of the same type is equivalent to the minimization problem for the total energy (Griffith's criterion). However, the right-hand part is calculated using a new formula containing surface-energy density γ:

$$\begin{aligned} F^G(\tau) &= (F_1^G(\tau), \ldots, F_N^G(\tau))^t, \\ F_n^G(\tau) &= 2\gamma(\alpha K_n^0)^{-1} - 2^{-1}K_n^0 - \tau K_n'. \end{aligned} \tag{8}$$

Inequalities stemming from the Irwin's and Griffith's criteria are denoted as $(6)_I$ and $(6)_G$, respectively, and their solutions, as $H^I(\tau)$ and $H^G(\tau)$.

If the solution is found, then equalities (1) allow us to reproduce elongations $h_1(\tau), \ldots, h_N(\tau)$ as functions of $\tau \in [0, \tau_0)$. This refutes the opinion of Sih and Leibowitz (see [10], p. 175), who claimed that the Griffith's criterion is insufficient for determining the configuration of the free-surface increment. (The concept of the energy-liberation rate put forward in [10] is a necessary consequence of this criterion but by no means replaces it.)

Statement 1. (i) *If matrix $\alpha A + B$ is negative definite, then there exists a single solution $H(\tau)$ to equation* (6) *and the following estimate holds true*:

$$\begin{aligned} c|H(\tau)|^2 + \langle F(\tau)_+, H(\tau)\rangle \le \langle F(\tau)_-, H(\tau)\rangle \\ \le |F(\tau)_-| \times |H(\tau)|, \end{aligned} \tag{9}$$

the parameter $c > 0$ being independent of $F(\tau)$ and $H(\tau)$; $t_\pm = 2^{-1}(|t| \pm t)$.

(ii) *If matrix $\alpha A + B$ is positive definite, problem* (6) *has no solution.*

Situations (i) and (ii) are interpreted as a stable (quasi-static) and avalanche crack growth (of course, Statement 1 contains only sufficient conditions). It is natural to take the moment $\tau = 0$ as a reference point for which at least one SIC K_n^0 coincides with K_{1c}. We draw attention to the effect caused by the interaction of cracks: Not only nonequilibrium cracks ($K_n^0 = K_{1c}$, $K_n' > 0$) are set in motion but also those with their SICs being close to critical [by virtue of (9), equality $H_n(\tau) = 0$ is valid for certain only in the case when $F_n(\tau)_+ > |F(\tau)_-|$, i.e., at $K_n^1 \ll K_{1c}$]. If $K_1', \ldots, K_N' < 0$, then $H(\tau) = 0$ and the cracks do not move.

Since $\alpha K_{1c}^2 = 2\gamma$ and $0 < K_n^0 \le K_{1c}$, we can find relationships making it possible to compare solutions $H^I(\tau)$ and $H^G(\tau)$:

$$\begin{aligned} F_n^G(\tau) &= (2K_n^0)^{-1}(K_{1c} - K_n^0)^2 + F_n^I(\tau) \ge F_n^I(\tau), \\ n &= 1, \ldots, N. \end{aligned} \tag{10}$$

Statement 2. *Let $\alpha A + B$ be a negative-definite matrix.*

(a) *If off-diagonal elements of the matrix A are nonnegative, then $H_n^I(\tau) \ge H_n^G(\tau)$ for all $n = 1, \ldots, N$.*

(b) *Let $H_n^I(\tau) = H_n^G(\tau)$ for n corresponding to the inequality $K_n^0 < K_{1c}$. Then, we have $H^I(\tau) = H^G(\tau)$.*

Thus, in the formulation used, the force criterion predicts larger elongations of cracks than the energy criterion, and the results undoubtedly coincide only for initially nonequilibrium cracks (this is observed, in particular, for noninteracting cracks). The reason is that we use formulas having the same asymptotic accuracy but different actual errors. The estimate

$$|H^I(\tau) - H^G(\tau)|^2 \le C\max\{(K_{1c} - K_n^0)^2(h_n^I(\tau) - h_n^G(\tau))\}$$

following from (10) and (6) demonstrates that the divergence between the results increases when we predict the propagation of cracks with an SIC K_n^0 that significantly deviates from the critical value. In these problems, bifurcations are especially sensitive to perturbations. Therefore, variational inequalities $(6)_I$ and $(6)_G$ discussed above can lead to qualitatively different patterns for developing sets of cracks in the case of the

unstable quasi-static growth of cracks. For Irwin's criterion, the bifurcation phenomena were studied in [1, 11].

The conditions imposed on A by Statements 2(a) are met for interior cracks located along the same straight line far away from the outer boundary Γ. We now consider the simplest example of an isolated crack with the tips P^1 and P^2. If its length is much shorter than the distance to Γ, then we have, approximately,

$$A = \frac{1}{4\alpha a}\begin{pmatrix} -1 & 2 \\ 2 & -1 \end{pmatrix}.$$

Let forces P^0 and P' be such that at small κ,

$$K_1^0 = K_2^0(1+\kappa) = K_{1c}, \quad k_1^0 = k_2^0(1+\kappa),$$

$$K_1' = K_2', \quad b = 1 - 2ak_n^0(K_n^0)^{-1}.$$

Under condition $b > 2$ ensuring the existence of unique solution to problems $(6)_I$ and $(6)_G$, we have

$$H_1(\tau) = \tau c b^{-1}, \quad H_2(\tau) = 0 \text{ at } \tau \le T,$$

$$H_1(\tau) = \frac{\tau c}{b-2} - \frac{8a\delta}{b^2-4}, \quad H_2(\tau) = \frac{\tau c}{b-2} - \frac{4ba\delta}{b^2-4}$$

$$\text{at } \tau \ge T,$$

$$c = 4aK_1', \quad T = \frac{b\delta}{b+2}(K_1')^{-1},$$

$$\delta_I = \frac{\kappa}{1+\kappa}K_{1c}, \quad \delta_G = \frac{2+\kappa\kappa}{1+\kappa 2}K_{1c}.$$

Until the time moment $\tau = T$, only the P^1 tip propagates. Furthermore, the crack grows at both ends. However, according to the Griffith's criterion, the P^2 tip begins to propagate later than predicted by the Irwin's criterion: $T_G = (1 + \kappa/2)T_I$. Nevertheless, the accuracy on the order of $O(\kappa^2)$ in the calculations of T is in agreement with the accuracy $O(\tau^2)$ of the models under discussion [see (4)]. In both cases, the P^2 tip starts to move at a moment before the hypothetical SIC $K_2^\tau = K_2^0 + \tau K_2'$ has attained the critical value.

ACKNOWLEDGMENTS

The author is grateful to N.F. Morozov and I.I. Argatov for helpful discussions.

This work was supported by the Russian Foundation for Basic Research, project no. 98-01-00974.

REFERENCES

1. S. Nemat-Nasser, Y. Sumi, and L. M. Keer, Int. J. Solids Struct. **16**, 1017 (1980).
2. S. A. Nazarov, Izv. Akad. Nauk SSSR, Mekh. Tverd. Tela, No. 2, 152 (1989).
3. Nguen Quoc Son, C. R. Acad. Sci., Ser. 2 **292**, 817 (1989).
4. S. A. Nazarov and O. R. Polyakova, Izv. Akad. Nauk, Mekh. Tverd. Tela, No. 2, 101 (1992).
5. S. A. Nazarov, Izv. Akad. Nauk, Mekh. Tverd. Tela, No. 3, 124 (1988).
6. H. F. Bueckner, Z. Angew. Math. Mech. **50**, 529 (1970).
7. V. G. Maz'ya and B. A. Plamenevskiĭ, Math. Nachr. **76**, 29 (1977).
8. S. A. Nazarov and O. R. Polyakova, Tr. Mosk. Mat. Ob–va **57**, 16 (1996).
9. J.-L. Lions, *Quelques methods de résolution des problemes aux limites nonlinéares* (Dunod, Paris, 1969; Mir, Moscow, 1972).
10. *Fracture: An Advanced Treatise*, Vol. 2: *Mathematical Fundamentals*, Ed. by H. Liebowitz (Academic, New York, 1969; Mir, Moscow, 1975).
11. L. G. Kolton, Izv. Akad. Nauk SSSR, Mekh. Tverd. Tela, No. 5, 95 (1989).

Translated by K. Kugel

Doklady Physics, Vol. 45, No. 7, 2000, pp. 336–338. Translated from Doklady Akademii Nauk, Vol. 373, No. 1, 2000, pp. 45–47.

MECHANICS

A Hydrophysical Mechanism of the Hurst Phenomenon

V. I. Naĭdenov* and I. A. Kozhevnikova**

Presented by Academician R.F. Ganiev September 14, 1999

Received September 14, 1999

In spite of the fact that the new class of random processes, the so-called fractal Brownian motion, has been successfully used for 30 years in stochastic hydrology, there is no answer to the central problem of the theory: What fundamental laws of nature and, first of all, the conservation laws for momentum, heat, and matter, are responsible for the Hurst phenomenon [1]? In this paper, we construct a simple model of the water percolation in soil illustrating this phenomenon.

1. Fractal Brownian motion. A continuous random process $X = (X_t)_{t \geq 0}$ is referred to as fractal Brownian motion with the Hurst exponent H [2] if it has the following properties:

(1) $X_0 = 0$, $EX_t = 0$ for all $t \geq 0$.

(2) X_t has time-independent increments

$$\mathrm{Law}(X_{t+s} - X_s) = \mathrm{Law}(X_t), \quad s, t \geq 0.$$

(3) X_t is the Gaussian process, $EX_t^2 = |t|^H$, $t \geq 0$, $0 < H \leq 1$.

(4) X_t has continuous trajectories.

If $H = 0.5$, the fractal Brownian motion is simply the conventional Wiener process (as is well known, the increments of the Wiener process form "white noise"); for $0.5 < H < 1$, the increments are also referred to as "black noise."

In physics, these processes correspond to the following types of diffusion. At $H = 0.5$, it is the "normal" Fick diffusion, while all cases with $H \neq 0.5$ can be classed to the Levy diffusion: At $H > 0.5$, we have enhanced diffusion, and at $H < 0.5$, diffusion with geometric constraints.

The aforementioned processes first considered by Kolmogorov in 1940 [3] were called Wiener spirals. In 1968, Mandelbrot and van Ness introduced the term "fractal Brownian motion" [2]. In mid-1960s, Mandelbrot put forward an ingenious interpretation of the Hurst phenomenon, which, in his opinion, can explain not only the phenomenon itself but also two other effects characteristic of many hydrologic processes: exceptionally large outbursts and exceptionally long runs of positive or negative deviations of the process from its average value. For example, the drop in the Caspian Sea level over 48 years (1930–1978) and its rise over the last 20 years are illustrations of these effects. Mandelbrot introduced the term "a process with infinite memory" and, hence, with infinite growth of the spectral density at a frequency tending to zero but without any nonintegrable singularity. The spectral density of such a process is proportional to a fractional power of the frequency, and Mandelbrot called them "fractional noises."

The covariance function and the spectrum of fractal noise have the following form:

$$R_H(n) = \frac{1}{2}(|n+1|^{2H} + |n-1|^{2H} - 2|n|^{2H}),$$

$$f_H(\omega) = \frac{H\Gamma(2H)\sin(H\pi)}{\pi} \times |e^{i\omega} - 1|^2 \sum_{k=-\infty}^{\infty} \frac{1}{|\omega + 2\pi k|^{2H+1}}, \quad |\omega| \leq \pi.$$

In the vicinity of $\omega = 0$, the spectral density can be written as

$$f_H(\omega) = \frac{H\Gamma(2H)\sin(H\pi)}{\pi} \frac{1}{|\omega|^{2H-1}}.$$

Thus, the spectrum of black noise ($0.5 < H < 1$) $f_H(\omega) \longrightarrow \infty$ at $\omega \longrightarrow 0$.

Using a large number of observations concerning the average annual runoff of the Nile during the period of 622–1469 (847 years), Hurst found that $H = 0.7$ [1]. The Hurst exponents are equal to 0.836, 0.662, 0.772, and 0.673 for the Volga, the Dnieper, the Danube, and the Neman, respectively. Here, we construct an example of a hydrological process exhibiting the Hurst phenomenon.

2. Stochastic model of rains. We assume that the number of rains during the time interval $[t_0, t_0 + T]$

* *Water Problems Institute, Russian Academy of Sciences, Novaya Basmannaya ul. 10, Moscow, 107078 Russia*

** *Moscow State University, Vorob'evy gory, Moscow, 119899 Russia*

1028-3358/00/4507-0336$20.00 © 2000 MAIK "Nauka/Interperiodica"

obeys the Poisson law

$$P(k) = \frac{(\lambda T)^k}{k!} e^{-\lambda T}$$

for arbitrary $k = 0, 1, 2, \ldots$, P is the probability of k rainfalls during period T at a given value of λ (an average number of rainfalls per day, which is the characteristic of the meteorological situation for a river basin). The time intervals between rainfalls (sequential events of the Poissonian flow) are independent random variables with the similar exponential distributions characterized by parameter λ. The probability of the event when the drought period $t_{k+1} - t_k = \Delta_k$ is shorter than t is equal to $P\{\Delta_k < t\} = 1 - e^{-\lambda t}$.

In the case when a rainfall duration is much smaller than a drought period, the formation of a precipitation layer can be presented as the pulsed process:

$$p(t) = q \sum_{k=0}^{\infty} \delta(t - t_k),$$

where q is the precipitation layer per rainfall, and $\delta(t)$ is the delta function. The average value of the process is $p(t) = q\lambda$, the correlation function is $R(\tau) = q^2\lambda\delta(\tau)$, and the spectrum is $f(\omega) = 2q^2\lambda$. Thus, the "memory" time for a rainfall process is zero, and the process spectrum is constant in the whole frequency range; i.e., there is no Hurst phenomenon in this process.

3. Dynamics of the moisture content in soil. Following rainfall, the moisture content per unit volume in the soil sharply increases. Owing to the percolation processes, a certain fraction of this moisture moves to the subsoil water level, another evaporates, and the third forms the surface runoff. The percolation factor (the ratio of percolated moisture and the total amount of precipitates) exceeds 0.6 for most drainage basins of main Russian rivers (for example, these coefficients are equal to 0.85, 0.79, and 0.66 for the basins of the Oka, the Moskva, and the Pechora, respectively). Thus, analyzing percolation processes is very important for understanding the mechanisms underlying river runoff.

We now write the equation of water balance for the upper soil layer:

$$\frac{dW}{dt} = q \sum_{k=0}^{\infty} \delta(t - t_k) - Q\left(\frac{W - W_w}{W_p - W_w}\right)^n - \varepsilon Q\left(\frac{W - W_w}{W_p - W_w}\right), \quad (1)$$

where W, W_p, and W_w are the soil moisture content, the porosity, and the moisture content corresponding to the wilting, respectively; Q is the filtration coefficient for water in the moisture-saturated soil; ε is the ratio of evaporation (transpiration) and percolation rates; and n is the power exponent in the substantially nonlinear (power-law) dependence of the moisture conduction coefficient on the moisture content ($n = 3$–5) [4, 5]. The filtration rate substantially depends on the viscosity of water and the porosity of the upper soil layer.

Numerous measurements of the evaporation (transpiration) rate demonstrated its linear dependence on the moisture content (see Fig. 242 in [6], where this dependence is presented for the soddy podzolic loamy soil when sowing winter rye, wheat, and timothy).

The integration of (1) leads to the following pulse process:

$$\theta(t) = \sum_{k=0}^{\infty} \theta_k \varphi(t - t_k), \quad (2)$$

where

$$\varphi(t - t_k) = \frac{\sqrt[m]{\varepsilon}}{\sqrt[m]{(\theta_k^m + \varepsilon)e^{Mm\varepsilon(t - t_k)} - \theta_k^m}}$$

for $t \in [t_k, t_{k+1})$ and $\varphi(t - t_k) = 0$ if $t \notin [t_k, t_{k+1})$ is the function of the pulse shape. The process amplitudes $\theta_k = \lim_{\delta \to 0} \theta(t_k + \delta)$, $\delta > 0$ are found from the solution to the nonlinear discrete stochastic equation

$$\theta_{k+1} = N + \frac{\sqrt[m]{\varepsilon}\theta_k}{\sqrt[m]{(\theta_k^m + \varepsilon)e^{Mm\varepsilon(t_{k+1} - t_k)} - \theta_k^m}},$$

where

$$\theta_k = \frac{W_k - W_w}{W_p - W_w}, \quad M = \frac{Q}{W_p - W_w},$$

$$N = \frac{q}{W_p - W_w}, \quad m = n - 1.$$

If $\varepsilon = 0$ [the percolation rate far exceeds the evaporation (transpiration) rate], the spectral density of process (2) diverges at low frequencies. This phenomenon is explained by a strong power-law dependence of the moisture conduction on moisture content, which is why we have very slow postrainfall relaxation of the moisture content to its equilibrium value with the power-law time dependence. For small ε, there is a fairly wide frequency range where the frequency dependence of the process spectrum has the form $f(\omega) \sim \omega^{-\alpha}$ (for several cases, the calculations yield $\alpha = 0.72$; hence, the Hurst exponent is $H = \frac{\alpha + 1}{2} = 0.86$). In Fig. 1, we show the characteristic realization of random process (2) found by simulating the Poisson distribution. In Fig. 2, we show the histogram of amplitudes for the pulsed process corresponding to the variation of the moisture content in soil, the correlation function is plotted in Fig. 3, and the spectral density for the characteristic realization of random process (2) close to zero is presented in Fig. 4.

Thus, the Hurst phenomenon is explained by a slow (power-law) relaxation characteristic of a viscous fluid in a porous medium. The relaxation takes place from a

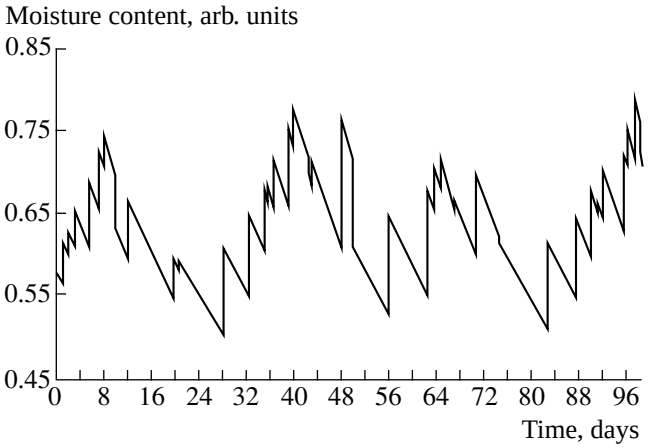

Fig. 1. Realization of the random process of temporal variation in the soil moisture content, which is found by numerical simulations.

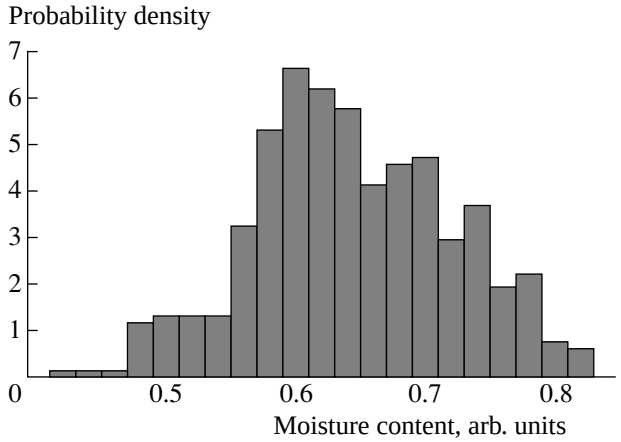

Fig. 2. Probability density for amplitudes of a pulsed process of moisture-content variations in soil, which is constructed according to the characteristic realization.

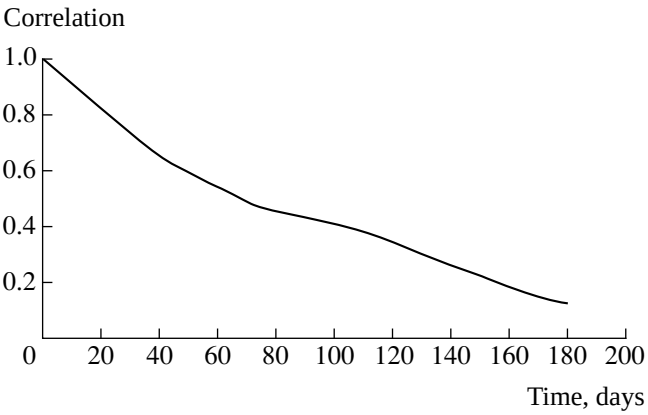

Fig. 3. Correlation function for the random process of the variation of the moisture content in soil.

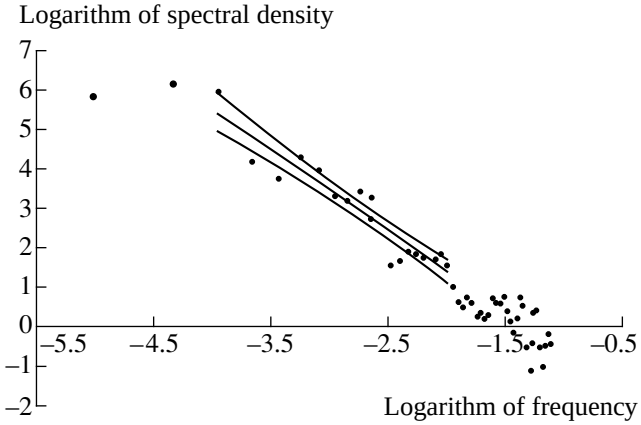

Fig. 4. Approximation of the spectral density at low frequencies by a linear regression and the confidence region of the linear regression at a confidence level of 0.05 for the characteristic realization of variation in the soil moisture content.

state with a high potential energy (at the moment of rainfall) to a state with a lower potential energy (the moment of water reaching the locking section of the river basin).

Note that the importance of the phenomenological approach to the evolution of nonlinear dissipative systems was emphasized in [7].

ACKNOWLEDGMENTS

We are grateful to Corresponding Member of the RAS A.N. Shiryaev for supporting studies in the field of modeling and numerical simulations of the physical processes with a pronounced aftereffect.

This work was supported by the Russian Foundation for Basic Research, project no. 00-01-0743.

REFERENCES

1. H. Hurst, Trans. Amer. Soc. Civ. Eng. **116**, 770 (1951).
2. B. B. Mandelbrot and J. W. van Ness, SIAM Rev. **10**, 422 (1968).
3. A. N. Kolmogorov, Dokl. Akad. Nauk SSSR **26**, 115 (1940).
4. A. M. Globus, *Soil Hydrophysics Background of Mathematical Models in Agricultural Ecology* (Gidrometeoizdat, Leningrad, 1987).
5. P. Ya. Polubarinova-Kochina, *Theory of Soil Water Flows* (Nauka, Moscow, 1977).
6. P. V. Vershinin *et al.*, *Fundamentals of Agricultural Physics*, Ed. by A. P. Ioffe (Fizmatgiz, Moscow, 1959).
7. S. F. Timashev, Ross. Khim. Zh. **42** (3), 18 (1998).

Translated by V. Bukhanov

Doklady Physics, Vol. 45, No. 7, 2000, pp. 339–341. Translated from Doklady Akademii Nauk, Vol. 373, No. 1, 2000, pp. 48–50.

MECHANICS

Determination of Local Mechanical Properties of Materials

S. V. Suknev* and M. D. Novopashin**

Presented by Academician V.P. Larionov October 21, 1999

Received October 29, 1999

Information on the mechanical properties of a material in the region of stress concentration is of fundamental importance for revealing the onset of macroscopic damage (i.e., crack formation) and its subsequent evolution, leading eventually to the decay of load-carrying capacity and to the failure of a structural element. The strength and plasticity criteria used for this purpose are based on finding the correlation between local stresses in the region of their concentration and the mechanical properties of the material. The latter are determined using the results of conventional tests of the samples.

At the same time, a large amount of experimental data [1–8] clearly indicates the significant difference between the mechanical properties of a material in the region of stress concentration and the usual properties determined for a uniform stressed state. In this connection, there exists a problem of evaluating local mechanical properties of the material. The problem is solved in this paper on the basis of the gradient approach to calculating strength. The approach is developed by the authors of [8–11].

According to the conventional approach, the strength is defined by the following condition:

$$\sigma_e < \sigma_0, \tag{1}$$

where $\sigma_e = f(\sigma_{ij})$ and $\sigma_0 = \text{const}$. The equivalent stress σ_e characterizes the internal stressed state of the material and, in the general case, is a function of stress tensor components σ_{ij}. The ultimate stress σ_0 characterizes averaged mechanical properties of the material and is assumed to be a fixed parameter. Since σ_0 characterizes a uniform stressed state, the applicability of the conventional approach is limited to cases where the size of a stress inhomogeneity is large enough to put $\sigma_0 = \text{const}$ there. The essence of the gradient approach as compared to the conventional approach is the following. The mechanical properties are attributed not to the material itself, but to a certain deformed region of finite size. This approach is more consistent with the concept of mechanical strength. Here, the ultimate stress is not a fixed parameter. It depends on the size of the stress inhomogeneity. We denote the characteristic size of the deformed region as L_e; if it is sufficiently large compared to the size of structural components of the material including the possible structural defects (i.e., the conditions of averaging the mechanical properties are certainly met), the value of the local strength differs only slightly from σ_0. On the contrary, if L_e is comparable to the sizes of structural elements, their effect on the local strength becomes noticeable. In this case, the smaller the size L_e with respect to a characteristic size of the material structure L_0, the more pronounced this effect. Thus, the local strength of material should not depend simply on the characteristic size L_e of the deformed region but on the ratio L_0/L_e. Taking this into account, the condition for the local strength can be written as

$$\sigma_e < f(\sigma_0, L_0/L_e). \tag{2}$$

To determine the form of the function $f(\sigma_0, L_0/L_e)$, we need to formulate additional conditions that reflect a specific nature of the problem under study. The requirements for $f(\sigma_0, L_0/L_e)$ for the stress concentration are formulated as follows:

Allowance for stress gradients (gradient hypothesis),

$$\begin{gathered} f(\sigma_0, L_0/L_e) = \sigma_0[1 + f^*(\sigma_{ij}, \sigma_{ij,k})], \\ f^*(\sigma_{ij}, \sigma_{ij,k}) = \text{inv}; \end{gathered} \tag{3}$$

The relation to the traditional criteria

$$f(\sigma_0, 0) = \sigma_0; \tag{4}$$

The constraints on the critical stresses

$$\frac{f(\sigma_0, L_0/L_e)}{K_t} \longrightarrow \text{const}, \quad K_t \longrightarrow \infty. \tag{5}$$

* *Institute of Physical and Technological Problems of the North, Siberian Division, Russian Academy of Sciences, Oktyabr'skaya ul. 1, Yakutsk, 677891 Russia*

** *Mining Institute of the North, Siberian Division, Russian Academy of Sciences, pr. Lenina 43, Yakutsk, 677018 Russia*

1028-3358/00/4507-0339$20.00 © 2000 MAIK "Nauka/Interperiodica"

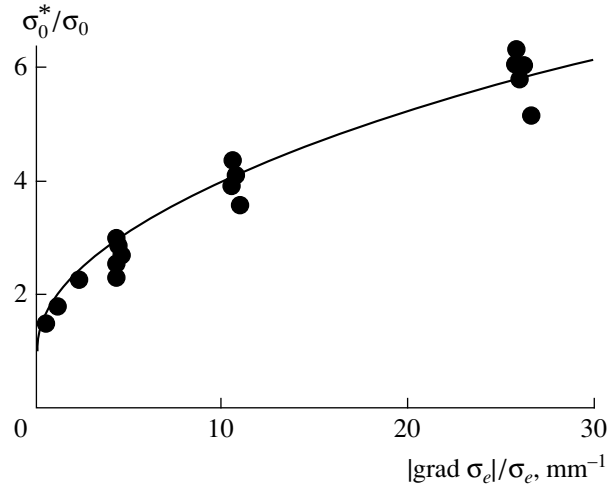

Fig. 1. Local strength of epoxy fiber glass as a function of the relative gradient of equivalent stress under tension.

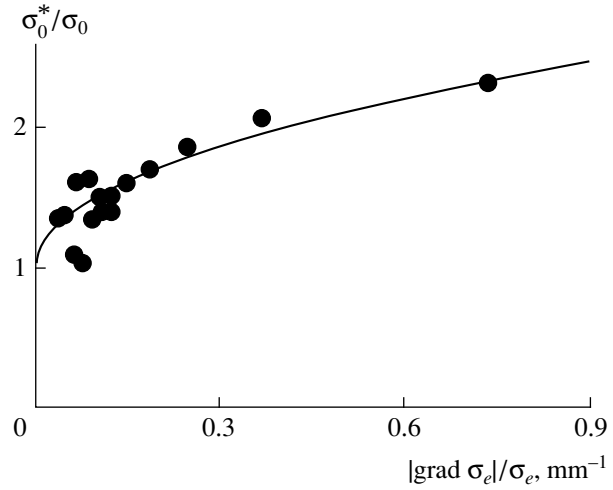

Fig. 2. Local strength of gypsum as a function of the relative gradient of equivalent stress under compression.

Here, $f^*(\sigma_{ij}, \sigma_{ij,k})$ is a dimensionless function of the stress-tensor components and of the stress-gradient tensor, this function being invariant with respect to transformations of the coordinate system; K_t is the coefficient characterizing the stress concentration.

Requirement (3) has the following implications. Under conditions of stress concentration, the characteristic size of the deformed region is determined by the size of the stress inhomogeneity rather than of the body as a whole. This size depends on the features of the stress distribution; therefore, according to the gradient hypothesis, the onset of the limiting state is caused by both the values of the stress itself and its gradients at the point under study.

Requirement (4) provides the transformation of gradient criterion (2) into the conventional criterion (1) in the case of the uniform stressed state.

Requirement (5) reflects a well-known experimental fact: At any sharpness of a notch and the value of the theoretical coefficient for the stress concentration, the fracture of a material occurs under a finite load [12]. For sharp concentrators, its value depends only on the notch length. Requirement (5), in fact, provides the relation of the gradient criterion (2) to the linear mechanics of fracture.

Taking into account requirements (3)–(5), the function of the local strength has the form [8, 9]

$$f\left(\sigma_0, \frac{L_0}{L_e}\right) = \sigma_0\left(1 + \sqrt{\frac{L_0}{L_e}}\right), \tag{6}$$

$$L_e = \frac{\sigma_e}{|\text{grad}\sigma_e|}. \tag{7}$$

It is shown in [11] that function (6) meeting requirements (3)–(5) also provides for physically consistent behavior of the critical defect size as a function of the stress concentration coefficient if the latter can be presented in the form $K_t = 1 + \alpha\sqrt{a/\rho}$, where α is a numerical coefficient dependent on the body dimensions, a is the defect (concentrator) size, and ρ is the radius of curvature for the concentrator at a dangerous point.

We now consider several examples of using expression (6) in estimating the local mechanical properties of various materials.

Local strength of a plate with side notches under tension. The experimental data on the local strength σ_0^* of plates made of epoxy fiber glass with side U-shaped notches are reported in [7]. The plates were tested for uniaxial tension. Both the depth of the notch and the curvature radius of the notch tip were varied. All the samples were brittle-broken by a rupture at the minimum cross section. The experimental data (dots) in Fig. 1 are fitted by function (6) of the local strength (solid curve). The stress σ_0 is the tensile strength of a smooth sample. The size L_e was determined based on (7), and the largest normal stress was considered as the equivalent one. The calculated curve agrees well with the experimental data.

The local strength under compression for a plate with a central hole. The experimental data on the shear fracture in the region of the compressing stress concentration in plates made of gypsum with central circular and elliptic holes, which were subjected to uniaxial compression, are reported in [2]. The diameter of a circular hole or the size of an elliptic hole at a dangerous cross section was varied. At the moment of the crack formation, the applied pressure was fixed. In Fig. 2, experimental data (points) are fitted by function (6) (solid curve). The material was assumed to obey the Coulomb strength condition, and, in this case, σ_0 is the material shear strength. The calculated curve also agrees well with the experimental data.

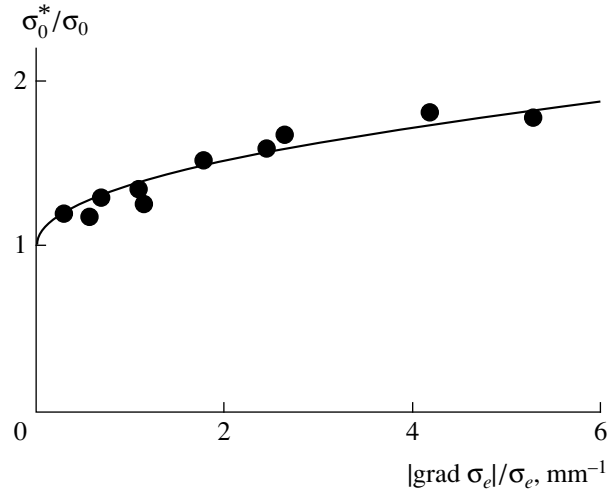

Fig. 3. Local yield stress of low-carbon steel versus relative gradient of equivalent stress under tension.

Local yield under tension of a plate with a central hole. Plates made of a low-carbon steel with central circular and elliptical holes were subjected to uniaxial tension [8]. The size of the hole and curvature radius in its top were varied. The moment of the onset of the local yield was revealed on the basis of the holographic interferometry by means of analyzing the interference pattern in the regions of tensile-stress concentration. The experimental data (dots) are approximated by function (6) (solid curve) (Fig. 3). It was assumed that the material obeyed the Mises plasticity condition, and in this case, σ_0 is the yield stress of the material. Similar to the previous examples, the calculated curve agrees well with the experimental data.

Thus, the mechanical properties of a material in the stress concentration region that characterize the formation of macroscopic damage in the form of a crack or of a local region of plasticity depend on the inhomogeneity of the stress field and can be determined according to (6) using the gradient approach. The examples presented above show that the regularities revealed have a rather general nature and are inherent to various materials differing in chemical composition, structure, and preparation technology. Despite the different physical mechanisms underlying the deformation processes and the damage accumulation in these materials, the onset of the ultimate state at the macromechanical level obeys the same scaling law that describes variations in the mechanical properties of the material.

ACKNOWLEDGMENTS

This work was supported by the Russian Foundation for Basic Research, projects nos. 93-013-16526 and 98-05-65656.

REFERENCES

1. E. Z. Lajtai, Int. J. Rock Mech. Min. Sci. **9**, 569 (1972).
2. V. Nesetova and E. Z. Lajtai, Int. J. Rock Mech. Min. Sci. **10**, 265 (1973).
3. A. Bascoul and J. C. Maso, J. Mec. Appl. **4**, 197 (1980).
4. A. Bascoul and J. C. Maso, J. Mec. Appl. **5**, 375 (1981).
5. H. Nisitani and H. Noguchi, Trans. Jpn. Soc. Mech. Eng., Ser. A **52** (477), 1286 (1986).
6. M. D. Novopashin, L. I. Bochkarev, and S. V. Suknev, Probl. Prochn., No. 1, 75 (1988); No. 1, 122 (1988).
7. H. Hyakutake, T. Hagio, and H. Nisitani, Int. J. Pressure Vessels Piping **44**, 277 (1990).
8. M. D. Novopashin, S. V. Suknev, and A. M. Ivanov, *Viscoelastic Strains and the Limiting State of the Structural Elements with the Stress Concentrators* (Nauka, Novosibirsk, 1995).
9. M. D. Novopashin and S. V. Suknev, Model. Mekh. **1(18)** (3), 131 (1987).
10. S. V. Suknev and M. D. Novopashin, Fiz.-Tekh. Probl. Razrab. Polez. Iskop., No. 4, 54 (1999).
11. S. V. Suknev, Prikl. Mekh. Tekh. Fiz. **40** (4), 222 (1999).
12. V. V. Panasyuk, *Mechanics of the Quasi-Brittle Fracture of Materials* (Naukova Dumka, Kiev, 1991).

Translated by T. Galkina

Doklady Physics, Vol. 45, No. 7, 2000, pp. 342–344. Translated from Doklady Akademii Nauk, Vol. 373, No. 2, 2000, pp. 191–193.

MECHANICS

Bodies with Heterogeneities: The Case of Sets of Cracks

Academician V. A. Babeshko

Received February 17, 2000

We consider the problem of the localization of a vibration process by a set of plane parallel cavities (cracks) described by the Griffith theory [1]. These types of heterogeneities are the most widespread objects accompanying stratified inhomogeneous geological structures including an imitator of breaks. They are widespread imperfections in materials with defects and also the main precursors of strength loss in structures, thus determining the onset of their brittle rupture.

In this study, we have found the general relationships providing the localization of a wave process in an elastic medium by objects of such a type.

These investigations open up possibilities for a principally new method of vibrational excitation of zones containing heterogeneities on the energy-preserving resonance basis when directional seismic antennas are submitted to supplementary requirements dictated by the conditions of localization [2].

We attempt to improve the classification of such objects, previously called vibration-strength *viruses*. The basis of this classification is the potentialities of the mathematical formalism developed and used to investigate these viruses [3, 4].

Studies in this field of mechanics were initiated by the original theoretical investigations of Academician Vorovich [5, 6] and, on the other hand, by theoretical and experimental investigations of mathematicians and geophysicists from the Siberian Division of the Russian Academy of Sciences.

The discovered high-frequency resonance in semibounded deformable media with heterogeneities [7] made it possible to approach from an unexpected side the investigation of wave processes in complex media as opposed to linear-acoustic ones. As is well known, there is no concept of static strains in linearly acoustical media, and the objects localizing the wave processes are termed open cavities. To avoid, by this and other reasons, calling our objects open cavities, we used the term vibration-strength viruses, which have been explained in more detail in [4].

Kuban State University,
ul. Karla Libknekhta 9, Krasnodar, 350640 Russia

1. We consider an elastic space divided by parallel horizontal cross sections into $L + 1$ layers, the upper and lower of them being half-spaces.

Aligning the x_1Ox_2 plane in parallel to the plane of heterogeneities, we arrive at a problem in which in the cross section $x_3 = h_l$ inside the elastic space, there are cavities (cracks) with carriers S_l, $l = 1, 2, \ldots, L$. The set representing an association of carriers in the cross section $x_3 = h_l$ can be that of simply connected or multiply connected domains.

According to the notation of [4], such a set of heterogeneities was called a virus and denoted as

$$V(S_l), \quad l < L.$$

We refine this notation as applied to the problem under investigation.

We introduce the following definition:

Definition. *A virus composed of L parallel cracks in an elastic space is called a class-2 virus or an L-level virus of the S-type, denoted as*

$$V(2/h_1; S_1/\ldots/h_L; S_L). \tag{1}$$

If a certain S_k is an unbounded plane, it is denoted in formulas by the sign ∞.

This definition presumes that, for a certain $l = k$, the set S_k can be the entire plane. In this case, we use the sign ∞ instead of S_k in the denotation of virus (1); i.e., the space is divided into two parts by this set. Thus, for describing the upper or lower half-spaces with one horizontal crack, it is necessary to use the respective notation

$$V(2/0; \infty/h_1; S_1), \ \ h_1 > 0 \text{ or } h_1 < 0.$$

This is a two-level virus.

If we take a layer with one crack instead of a half-space, this is a three-level virus, which can be written out in the following form:

$$V(2/0; \infty/h_1; S_1/h_2; \infty), \ \ h_1 > 0.$$

The definition presumes that the description of the set S_l in the cross sections h_l or the requirements for the regions of the medium in which they are sought must be given additionally.

It should be noted that the vibration-strength virus formed by rigid planar inclusions belongs to class 1 and is denoted in a similar manner.

1028-3358/00/4507-0342$20.00

We now formulate two types of problems in the theory of vibration-strength viruses. Below, the medium-vibration frequency ω $(0 \le \omega < \infty)$ (the static case is also included), mechanical, and physical characteristics of the medium, as well as external actions on the system, are referred to the concept of the problem parameters.

Direct problem. A vibration-strength virus of a certain class with fixed sets h_l and S_l is given. It is necessary to find the values of the remaining problem parameters including also the external actions that provide the localization of the wave process by the virus.

First inverse problem. For a virus of a certain class with a given h_l and other problem parameters including also the external actions, it is necessary to find the sets S_l for which the wave process is localized by the virus.

Second inverse problem. For a virus of a certain class with given problem parameters including also the external actions, it is necessary to find the sets h_l and S_l for which the wave process is localized by the virus.

The case of a static problem and an increase in strains within a certain zone are appreciated as a zero-frequency wave process and as the localization, respectively.

We demonstrate here one of the results of investigating the direct problem in the theory of vibration-strength viruses.

Below, we consider an elastic layer with L cracks, i.e., the case when the $(L + 2)$-level virus of the class 2 is given:

$$V(2/0; \infty/h_1; S_1/\ldots/h_L; S_L/h_{L+1}; \infty), \quad h_1 > 0. \qquad (2)$$

The problem consists in clarifying conditions which the problem parameters must obey in order for the virus to localize a wave process in its neighborhood.

2. To investigate our problem, we use the method developed in [2, chapter XI] preserving the notation accepted in this study.

We will consider the stresses with amplitudes w_{ls}; l, $s = 1, 2, 3$ and with a frequency ω acting at crack boundaries. We denote the Fourier two-dimensional transform by capital letters and assume that

$$Q_{ls}(\alpha_1, \alpha_2) = \iint\limits_{S_l} q_{ls}(\xi_1, \xi_2) e^{i(\alpha_1\xi_1 + \alpha_2\xi_2)} d\xi_1 d\xi_2,$$

where α_k and $k = 1, 2, 3$ are the parameters of the Fourier transform.

Repeating the manipulations of [2], we arrive at a set of integral equations and consider a widespread case of the type

$$\sum_{l=1}^{L}\sum_{s=1}^{3} \iint\limits_{\Gamma_1\Gamma_2} e^{-i(\alpha_1 x_1 + \alpha_2 x_2)} P_{ls}^{-1}(\alpha_1, \alpha_2) D^{-1}(u) \times K_{ls}(\alpha_1, \alpha_2) P_{ls}(\alpha_1, \alpha_2) Q_{ls} d\alpha_1 d\alpha_2 = w_{pn}(x_1, x_2), \qquad (3)$$

$$u^2 = \alpha_1^2 + \alpha_2^2,$$

$$x_1, x_2 \subset S_p, \quad n = 1, 2, 3, \quad p = 1, 2, \ldots, L.$$

Here, we take the following notation:

$$u_{ls}^{+} - u_{l+1s}^{-} = q_{ls}. \qquad (4)$$

Passing to the vector representation in equation (3), we can write out the set of equations in the operator form:

$$K\mathbf{Q}(\alpha_1, \alpha_2) = \iint\limits_{\Gamma_1\Gamma_2} e^{-i(\alpha_1 x_1 + \alpha_2 x_2)} P^{-1}(\alpha_1, \alpha_2) D^{-1}(u),$$

$$K(u) P(\alpha_1, \alpha_2) \mathbf{Q}(\alpha_1, \alpha_2) d\alpha_1 d\alpha_2 = \mathbf{f}(x_1, x_2), \qquad (5)$$

$$x_1, x_2 \subset S.$$

Here, $D(u)$ is the integral function. $K(u)$ is the matrix-valued function, whose elements are $K_{ls}(\alpha_1, \alpha_2)$ blocks. Elements of the matrix-valued function are integral functions, the following asymptotic estimates being valid for the main ones: $u[1 + O(u^{-1})]D(u)$. $\mathbf{Q}(\alpha_1, \alpha_2)$ is the multidimensional vector, whose components are the elements Q_{ls} arranged in a certain sequence. In the same sequence, the vector $\mathbf{f}(x_1, x_2)$ composed of the components w_{nq} is formed.

Furthermore, we introduce the vector space $\mathbf{Q} = \{q_l \subset H_0^1\}$, which is the direct sum of the Sobolev spaces [8], assuming that the boundaries of the domains S_l satisfy the necessary conditions of smoothness:

$$\{q_l\} \subset H_0^1 = \sum_{l=1}^{L} \oplus H_0^1(S_l).$$

We determine (5) as an operator acting from H_0^1 in L_2.

The following theorem is valid.

Theorem 1. *Operator equation* (5) *is equivalent to the equation of the second kind with an entirely continuous operator in* H_0^1.

3. For a given frequency ω, we denote real zeros of the functions $D(u)$ and $\mathrm{Det}K(u)$ as ζ_m and z_m, respectively, $m = 1, 2, \ldots, M$. In the case of discrepancy in the number of real zeros, we add up to the number M the complex zeros nearest to the real axis.

We construct the function

$$D_1(u) = \prod_{m=1}^{N} (u - \zeta_m), \quad D_0(u) = D(u) D_1^{-1}(u). \qquad (6)$$

For the matrix-valued function $K(u)$, we construct the representation

$$K(u) = K_0(u) K_1(u). \qquad (7)$$

Here, the matrix-valued function $K_1(u)$ is polynomial, and, for zeros, its determinant has the values z_m, $m = 1, 2, \ldots, M$.

The elements of the matrix-valued function $K_0(u)$ are the integral functions, and their determinant has no real zeros.

Various methods for constructing representation (7) are described in [9, 10] and in the references cited in these studies.

The matrix-valued function $P(\alpha_1, \alpha_2)$ is a polynomial with a constant determinant.

We now consider the set of integral equations of type (5) in which $K(u)$ and $D(u)$are replaced by $K_0(u)$ and $D_0(u)$, and a new unknown quantity $\mathbf{Q}_0(\alpha_1, \alpha_2)$ is also introduced. The set is denoted in the form

$$K_0\mathbf{Q}_0(\alpha_1, \alpha_2) = \mathbf{f}(x_1, x_2). \quad (8)$$

The set of integral equations (8) is similar to integral equations of mixed static problems in the elasticity theory. For investigating this set, it is possible to use methods developed in [2, 9, 10] and other studies in which the static mixed problems are analyzed.

In the case when the complex zeros are also taken as ζ_m and z_m along with the real ones, i.e., M is high, set (8) can be solved by the asymptotic methods and an approximate solution can be constructed.

Having constructed the inverse operator K_0^{-1}, we can write out the solution to the operator equation in the form

$$\mathbf{Q}_0(\alpha_1, \alpha_2) = K_0^{-1}\mathbf{f}(x_1, x_2).$$

The key result of this investigation, which can be found by analogy with the case of one heterogeneity, is given by the following theorem.

Theorem 2. *Let the sizes for the domains S, the mechanical and physical characteristics of elastic layer, and the parameters h_k for the chosen frequency $\omega \geq 0$ be such that the following equality takes place*:

$$\mathbf{Q}_0(\alpha_1, \alpha_2) = 0, \quad \sqrt{\alpha_1^2 + \alpha_2^2} = z_m, \quad m = 1, 2, \ldots, M.$$

In this case, the virus localizes the wave process in its neighborhood.

The cases of solving certain inverse problems of this theory are given in [8].

ACKNOWLEDGMENTS

The author devotes this paper to the 80-year jubilee of his teacher Academician I.I. Vorovich, who stood near the source of this field of science.

This work was supported by the Federal Purposeful Program “Integration,” project no. 368; by the Russian Foundation for Basic Research, projects nos. 98-01-04091, 98-05-03980, 99-01-00787, and r2000Yug; by the Ministry of Education, project no. 990848; by the US Foundation for Civil Research and Development of Independent States of the Former Soviet Union, project no. REC-004. The opinion of the Foundation may disagree with the conclusions of this paper.

REFERENCES

1. V. M. Aleksandrov, B. I. Smetanin, and B. V. Sobol’, *Thin Stress Concentrators in Elastic Bodies* (Nauka, Moscow, 1993).
2. V. A. Babeshko, E. V. Glushkov, and Zh. F. Zinchenko, *Dynamics of Inhomogeneous Linearly Elastic Bodies* (Nauka, Moscow, 1989).
3. V. A. Babeshko, Izv. Sev.-Kavk. Nauchn. Tsentra Vyssh. Shk., Spec. Issue, p. 90 (1994).
4. V. A. Babeshko, Izv. Vyssh. Uchebn. Zaved. Sev.-Kavk. Region., Estestv. Nauki, No. 1, 24 (1998).
5. I. I. Vorovich, Dokl. Akad. Nauk SSSR **245**, 817 (1979) [Sov. Phys.–Dokl. **24**, 302 (1979)].
6. I. I. Vorovich, Dokl. Akad. Nauk SSSR **245**, 1076 (1979) [Sov. Phys.–Dokl. **24**, 304 (1979)].
7. V. A. Babeshko, I. I. Vorovich, and I. F. Obraztsov, Izv. Akad. Nauk SSSR, Mekh. Tverd. Tela, No. 3, 74 (1990).
8. J.-L. Lions and E. Magenes, *Problemes aux limites non homogénes et applications* (Dunod, Paris, 1968; Mir, Moscow, 1971).
9. I. I. Vorovich, V. A. Babeshko, and O. D. Pryakhina, *Dynamics of Massive Bodies and Resonant Phenomena in Deformable Media* (Nauchnyĭ Mir, Moscow, 1999).
10. I. I. Vorovich and V. A. Babeshko, *Dynamic Mixed Problems of Elasticity Theory for Non-Classic Regions* (Nauka, Moscow, 1979).

Translated by V. Bukhanov

Doklady Physics, Vol. 45, No. 7, 2000, pp. 345–349. Translated from Doklady Akademii Nauk, Vol. 373, No. 2, 2000, pp. 194–198.

MECHANICS

A Nonlinear Game Problem on the Reorientation of an Asymmetric Body with Poorly Determined Parameters under the Effect of Uncontrolled Perturbations

V. I. Vorotnikov

Presented by Academician V.V. Rumyantsev October 5, 1999

Received October 5, 1999

We consider a nonlinear game problem of reorienting an asymmetric body under uncontrolled perturbations, when the moments of inertia are inaccurately specified and only their estimates are given. A given "geometric" constraint is imposed on the possible control. We develop a method for solving this problem on the basis of the "equivalent" linearization of nonlinear systems with conflicting control factors [1–6] and methods of the linear theory of games [7]. This approach is related to the concepts of decomposition [8] in nonlinear controlled systems and employs the control methods [9] based on solving auxiliary problems of control with respect to part of variables [9, 10].

We find direct estimates of the admissible range for perturbations. The estimates are found taking into account the constraints imposed on the control, initial positions of the body, and tolerances for the principal central moments of inertia. Within the limits of these estimates, we develop a constructive method allowing us to determine the positional controls and an upper estimate for the time of guaranteed reorientation.

1. The formulation of the problem. We consider the Euler dynamic equations

$$A_1\dot{x}_1 = (A_2 - A_3)x_2x_3 + u_1 + \nu_1 \quad (123), \qquad (1.1)$$

governing the angular motion of a body with respect to its center of mass. (Here, only one of three equations is written; two others are obtained by cyclical permutations of subscripts 1, 2, 3.)

In (1.1), x_i and u_i are the components of angular velocity and the controlling moment along the principal central axes of inertia, respectively, and A_i are the principal central moments of inertia. The moments ν_i characterize external forces and uncontrolled perturbations. Hereafter, $i = 1, 2$, and 3, and the summation over i from 1 to 3 is implied. We denote as **x**, **u**, and **v** the vectors involving x_i, u_i, and ν_i, respectively.

Ural State Technical University,
Nizhniĭ Tagil Branch, Krasnogvardeĭskaya ul. 59,
Nizhniĭ Tagil, 622006 Russia

The moments of inertia are constant and are specified by the estimates

$$A_i^- \le A_i \le A_i^+, \qquad (1.2)$$

where A_i^- and A_i^+ are given numbers. The values of $\Delta A_i = A_i^+ - A_i^-$ are not assumed to be small; hence, A_i can vary within a wide range.

In addition to (1.1), we consider the kinematic equations with the Rodrigue–Hamilton variables governing the body orientation:

$$\begin{aligned} 2\dot{\lambda}_0 &= -\sum(x_i\lambda_i), \\ 2\dot{\lambda}_1 &= x_1\lambda_0 + x_3\lambda_2 - x_2\lambda_3 \quad (123). \end{aligned} \qquad (1.3)$$

Variables λ_0, λ_i forming vector $\boldsymbol{\lambda}$ obey the relationship

$$\lambda_0^2 + \sum\lambda_i^2 = 1. \qquad (1.4)$$

We choose control $\mathbf{u} \in K$ belonging to the class of piecewise functions $\mathbf{u} = \mathbf{u}(\mathbf{x}, \boldsymbol{\lambda}, \mathbf{x}^0, \boldsymbol{\lambda}^0)$ ($\mathbf{x}^0$ and $\boldsymbol{\lambda}^0$ are initial values of **x** and $\boldsymbol{\lambda}$, respectively), such that

$$\left\{\sum[u_i(A_i^-)^{-1}]^2\right\}^{1/2} \le \alpha = \text{const} > 0. \qquad (1.5)$$

Inequality (1.5) defines an ellipsoidal range for admissible controls.

The perturbations $\mathbf{v} \in K_1$ can have the form of arbitrary piecewise functions $\mathbf{v}[t]$ satisfying the constraint

$$\left\{\sum[\nu_i(A_i^-)^{-1}]^2\right\}^{1/2} \le \beta = \text{const} > 0. \qquad (1.6)$$

Problem 1. The problem is to find for arbitrary $\mathbf{v} \in K_1$ and arbitrary A_i satisfying conditions (1.2) the controls $\mathbf{u} \in K$ that transfer the body from the initial state $\boldsymbol{\lambda}(t_0) = \boldsymbol{\lambda}^0$ to the given state $\boldsymbol{\lambda}(t_1) = \boldsymbol{\lambda}^1$ during a finite

1028-3358/00/4507-0345$20.00

time. Both these states are states of rest: $\mathbf{x}(t_0) = \mathbf{x}^0 = \mathbf{x}(t_1) = \mathbf{x}^1 = \mathbf{0}$. The time instant $t_1 > t_0$ is not fixed.

Without any loss of generality, we assume below that $\boldsymbol{\lambda}^1 = (1, 0, 0, 0)$.

Remarks. (1) Problem 1 is related to control problems for a set of systems (but not for a single system) in which a desired result is guaranteed at any, even most adverse, perturbations. Such a formulation of the problem is typical of the game theory. (2) Other problems and methods of control over mechanical systems under poorly determined conditions were considered, for example, in [8, 11–15].

2. An auxiliary linear system with conflicting control parameters. Following [2–4], we differentiate with respect to time both sides of the equations for $\dot{\lambda}_i$ in (1.3), substituting $\dot{x}_i$ by their expressions from (1.1). After some transformations, we obtain the equalities

$$\ddot{\lambda}_i = f_i(\boldsymbol{\lambda}, \mathbf{u}) + \varphi_i(\boldsymbol{\lambda}, \mathbf{v}, \mathbf{x}),$$

$$f_1 = \frac{1}{2}(\lambda_0 u_1 A_1^{-1} + \lambda_2 u_3 A_3^{-1} - \lambda_3 u_2 A_2^{-1}),$$

$$\varphi_1 = \frac{1}{2}[\lambda_0(v_1 + M_1)A_1^{-1} + \lambda_2(v_3 + M_3)A_3^{-1} - \lambda_3(v_2 + M_2)A_2^{-1}] - \frac{1}{4}\lambda_1 \sum x_i^2, \quad (2.1)$$

$$M_1 = (A_2 - A_3)x_2 x_3 \quad (123).$$

Quantities f_i and φ_i were treated in [2–4] as auxiliary controls and perturbations, respectively. In such an approach, the "initial" controls u_i depend explicitly on A_i. In the case of (1.2), this approach leads to ill-defined u_i.

Within the framework of the equivalent linearization method, this difficulty can be settled in the following manner.

According to (1.2), we have $A_i = A_i^- + \delta_i A_i^-$, where δ_i is an arbitrary number in the given range $\delta_i \in [0, \delta_i^+]$, with $\delta_i^+ = (A_i^+)(A_i^-)^{-1} - 1$. In many technical problems, δ_i ranges between 0.1 and 0.4, so that the tolerances for A_i are about 10–40%.

Using the equalities (which can be easily verified)

$$A_i^{-1} = [A_i^-(1 + \delta_i)]^{-1} = (A_i^-)^{-1}(1 - \delta_i^*),$$

$$\delta_i^* = \delta_i(1 + \delta_i)^{-1},$$

we rewrite expressions (2.1) in the form

$$\ddot{\lambda}_i = f_i^*(\boldsymbol{\lambda}, \mathbf{u}) + \varphi_i^*(\boldsymbol{\lambda}, \mathbf{u}, \mathbf{v}, \mathbf{x}), \quad (2.2)$$

where

$$\varphi_1^* = \varphi_1 - \frac{1}{2}[\lambda_0 \delta_1^* u_1 (A_1^-)^{-1} + \lambda_2 \delta_3^* u_3 (A_3^-)^{-1} - \lambda_3 \delta_2^* u_2 (A_2^-)^{-1}] \quad (123),$$

and the expressions for f_i^* are derived from those for φ_i^* with $\varphi_i = 0$ and $\delta_1^* = \delta_2^* = \delta_3^* = 1$.

We will treat f_i^* and φ_i^* as the auxiliary controls u_i^* and perturbations v_i^*, respectively. As a result, expressions (2.2) can describe the system with conflicting control parameters

$$\ddot{\lambda}_i = u_i^* + v_i^*. \quad (2.3)$$

In this case, the "initial" controls u_i take the form

$$u_1 = \frac{2A_1^-}{\lambda_0}[(\lambda_0^2 + \lambda_1^2)u_1^* + (\lambda_1\lambda_2 + \lambda_0\lambda_3)u_2^* + (\lambda_1\lambda_3 - \lambda_0\lambda_2)u_3^*] \quad (123). \quad (2.4)$$

To estimate the auxiliary perturbations v_i^*, we put forward the principle of assignment and subsequent confirmation of their upper bounds on the set of states for linear system (2.3).

We will solve initial nonlinear Problem 1 on the basis of the corresponding game problems for linear system (2.3). As a result, equation (2.4) can be treated as a general form of the controls in Problem 1. Parameters of this form, namely, the auxiliary controls u_i^*, are determined by solving the corresponding linear game problems.

3. An auxiliary linear game problem and algorithm for solving Problem 1. We now solve a problem on the fastest transfer of system (2.3) to the position

$$\lambda_i = \dot{\lambda}_i = 0 \quad (3.1)$$

for any admissible v_i^*.

We treat this problem as a differential game. For this problem to be solvable, admissible upper bounds of u_i^* have to be higher than those of v_i^*. We assume that the corresponding constraints take the form

$$|u_i^*| \le \alpha_i^*, \quad |v_i^*| \le \beta_i^* = \rho_i \alpha_i^*, \quad 0 < \rho_i < 1.$$

In contrast to the constraints imposed on u_i, the form of those imposed on u_i^* and v_i^* is due to purely mathematical features of the item; namely, the most acceptable solution to Problem 1 is to be sought within the framework of the approach under consideration.

For given α_i^* and β_i^* (such that $\alpha_i^* > \beta_i^*$), the game problem described above for system (2.3) is reduced (see [7]) to the problem on the optimum fast response for the system

$$\ddot{\lambda}_i = (1-\rho_i)u_i^*, \quad |u_i^*| \le \alpha_i^*. \tag{3.2}$$

The boundary conditions are the same as those for system (2.3). System (3.2) is reduced to (2.3) if $v_i^* = -\rho_i u_i^*$. These "worst" v_i^* are the optimum controls for an "enemy."

The problem of finding the response rate for system (3.2) has the following solution [8]:

$$u_i^*(\lambda_i, \dot{\lambda}_i) = \begin{cases} \alpha_i^* \operatorname{sgn}\psi_i(\lambda_i, \dot{\lambda}_i), & \psi_i \ne 0 \\ \alpha_i^* \operatorname{sgn}\lambda_i = -\alpha_i^* \operatorname{sgn}\dot{\lambda}_i, & \psi_i = 0. \end{cases} \tag{3.3}$$

Here, $\psi_i = -\dot{\lambda}_i - [2\alpha_i^*(1-\rho_i)]^{-1}\lambda_i|\lambda_i|$ are the switching functions.

Owing to the conditions $\dot{\lambda}_i^0 = \dot{\lambda}_i^1 = 0$ (they follow from the equalities $\mathbf{x}^0 = \mathbf{x}^1 = \mathbf{0}$), the quantity

$$\tau = \max(\tau_i), \quad \tau_i = 2\left\{\left|\lambda_i^0\right|[\alpha_i^*(1-\rho_i)]^{-1}\right\}^{1/2} \tag{3.4}$$

is the minimum guaranteed time of control in the linear game problem for system (2.3). In this case, the quantity τ gives the guaranteed time of reorientation in Problem 1.

The iteration method of solving Problem 1 involves the following stages [2–4]:

(1) Assignment of β_i^* and preliminary choice of $\tau = \tau_i$. This procedure predetermines the values of α_i^* and ρ_i in (3.3).

(2) Check of actual validity for the inequalities $|v_i^*| \le \beta_i^*$ and constraint (1.5) on the set S of states for system (2.3) and (3.3).

This algorithm will be specified in Section 5.

Remarks. (1) Controls taking form (2.4) lead formally to the "singularity" $\lambda_0 = 0$. However, in the course of the control, $\lambda_0 \in [\lambda_0^0, 1]$. (2) If $\boldsymbol{\lambda}^1 \ne (1, 0, 0, 0)$ or λ_0^0 is small, it is sufficient to consider controls (2.4) with permuted indices.

4. Estimation of the admissible range for uncontrolled perturbations. We find a sufficient condition for α, β, λ_0^0, and δ_i that ensures the possibility of solving Problem 1 on the basis of the proposed approach. Let $\delta^* = \max(\delta_i^*)$.

Theorem 1. *Let the admissible range for the perturbations v_i be estimated by the inequality*

$$\beta < \left(\frac{\sqrt{3}}{3}|\lambda_0^0| - \delta^*\right)\alpha. \tag{4.1}$$

Then, Problem 1 *can be solved by controls* (2.4) *and* (3.3) *satisfying given constraint* (1.5).

We prove Theorem 1 in three stages.

(i) We obtain estimates for u_i on the set S with the help of the equalities

$$\sum [u_i(A_i^-)^{-1}]^2 = 4\left\{\lambda_0^{-2}\left[\sum \lambda_i u_i^*\right]^2 + \sum u_i^{*2}\right\}. \tag{4.2}$$

On the set S, the relationship $\lambda_0^2 \ge (\lambda_0^0)^2$ holds [1–4].

Therefore, using (4.2) and the Cauchy–Bunyakovskiĭ inequality, we have

$$\frac{1}{4}\sum [u_i(A_i^-)^{-1}]^2 \le \lambda_0^{-2}\sum \lambda_i^2 \sum u_i^{*2} + \sum u_i^{*2} \tag{4.3}$$
$$= \left(\lambda_0^{-2}\sum \lambda_i^2 + 1\right)\sum u_i^{*2} = \lambda_0^{-2}\sum u_i^{*2} \le (\lambda_0^0)^{-2}\sum u_i^{*2}.$$

(ii) We then estimate v_i^* on the set S. Using the Cauchy–Bunyakovskiĭ inequality and $|x_1 x_2| \le \frac{1}{2}\sum x_i^2$ (123), we can estimate expressions (2.2) for v_i^* as

$$|v_1^*| \le \beta^* + \frac{1}{2}\delta^*\left\{\sum [u_i(A_i^-)^{-1}]^2\right\}^{1/2}$$
$$+ \frac{1}{4}|\lambda_0 r_1 + \lambda_2 r_3 - \lambda_3 r_2 - \lambda_1|\sum x_i^2$$
$$\le \beta^* + \delta^*|\lambda_0^0|^{-1}\left[\sum u_i^{*2}\right]^{1/2} + \frac{1}{4}L\sum x_i^2,$$
$$\beta^* = \frac{1}{2}\beta, \quad L = \left(1 + \sum r_i^2\right)^{1/2},$$
$$r_1 = (A_1^+ - A_3^-)(A_2^-)^{-1} \quad (123).$$

To estimate $\sum x_i^2$, we solve the set of equations for $\dot{\lambda}_i$ in (1.3) as algebraic equations in x_i. As a result, we obtain the relationships

$$x_1 = 2\lambda_0^{-1}[(\lambda_0^2 + \lambda_1^2)\dot{\lambda}_1 + (\lambda_1\lambda_2 + \lambda_0\lambda_3)\dot{\lambda}_2 \tag{4.4}$$
$$+ (\lambda_1\lambda_3 - \lambda_0\lambda_2)\dot{\lambda}_3] \quad (123).$$

Using (4.4), we obtain the inequality

$$\frac{1}{4}\sum x_i^2 \le \lambda_0^{-2}\sum \dot{\lambda}_i^2.$$

The estimates for $\dot{\lambda}_i^2$ on the set S take the form [5]

$$\dot{\lambda}_i^2 \le (\dot{\lambda}_i^+)^2 = |\lambda_i^0|(\alpha_i^*)^{-1}\left[(\alpha_i^*)^2 - (\beta^*)^2\right].$$

As a result, we have

$$|v_i^*| \le \varphi,$$
$$\varphi = \beta^* + \delta^*|\lambda_0^0|^{-1}\left[\sum \alpha_i^{*2}\right]^{1/2} \tag{4.5}$$
$$+ (\lambda_0^0)^{-2} L \sum\left\{|\lambda_i^0|(\alpha_i^*)^{-1}\left[(\alpha_i^*)^2 - (\beta_i^*)^2\right]\right\}.$$

(iii) Finally, we use estimates (4.3) and (4.5) to prove the theorem. We prove that, provided that condition (4.1) is satisfied, there exist numbers α_i^* and β_i^* such that $\alpha_i^* > \beta_i^*$ and inequalities

$$|v_i^*| \le \beta_i^*, \tag{4.6}$$

confirming the assigned upper bounds β_i^* of the auxiliary perturbations v_i^*, and (1.5) hold on set S.

Taking (4.1) into account, we assume that

$$\beta^* = \frac{1}{2}\left(\frac{\sqrt{3}}{3}|\lambda_0^0| - \delta^*\right)\alpha - \varepsilon,$$
$$\alpha_i^* = \alpha^* = \frac{\sqrt{3}}{6}|\lambda_0^0|\alpha, \quad \beta_i^* = \frac{\sqrt{3}}{6}|\lambda_0^0|\alpha - \varepsilon_1, \tag{4.7}$$

where $\varepsilon > \varepsilon_1 > 0$ are arbitrarily small numbers.

For (4.7), we have $\alpha_i^* > \beta_i^*$ at an arbitrarily small positive fixed number $\varepsilon > 0$. Hence, the auxiliary game problem for linear system (2.3) is solvable [7].

We now prove that, for sufficiently small $\varepsilon > 0$, inequalities (4.6) are satisfied on the set S. Indeed, in this case, the values of φ in (4.5) differ arbitrarily little from $\frac{\sqrt{3}}{6}|\lambda_0^0|\alpha$. Taking (4.7) into account, we hence have $|v_i^*| \le \beta_i^*$ on the set S.

We then prove that, for sufficiently small $\varepsilon > 0$, constraint (1.5) holds on the set S. Indeed, taking (4.3) and (4.7) into account, we have

$$\sum [u_i(A_i^-)^{-1}]^2 \le 4(\lambda_0^0)^{-2}\sum \alpha_i^{*2}$$
$$= 12(\lambda_0^0)^{-2}\left[\frac{\sqrt{3}}{6}|\lambda_0^0|\alpha\right]^2 = \alpha^2.$$

Thus, by choosing a sufficiently small $\varepsilon > 0$, we can ensure that, provided condition (4.1) holds on the set S, the assigned upper bounds of v_i^* are confirmed and estimate (1.5) for controls (2.4) and (3.3) is valid. The theorem is proved.

Remarks. (I) Inequality (4.1) is a sufficient condition because it was derived with the use of more restrictive inequalities.

(II) Condition (4.1) makes it possible to solve Problem 1 with the use of controls (2.3) and (3.3) for a sufficiently large (although finite) value of τ. If condition (4.1) is confidently satisfied, the algorithm given in Section 3, which will be described more accurately in Section 5, can be employed to find the guaranteed time τ of reorientation.

(III) Inequality (4.1) is applicable if $\sqrt{3}|\lambda_0^0| - 3\delta^* > 0$. Without any loss of generality, we can assume that $|\lambda_0^0| \ge 1/2$; hence, the values of δ_i vary within the range $0 \le \delta_i < \sqrt{3}(6 - \sqrt{3})^{-1} = 0.4051$ and can exceed unity if $1 > |\lambda_0^0| > 1/2$.

(IV) When $\delta_i = 0$, condition (4.1) is reduced to the estimate that was previously obtained [6] for the tolerance range for perturbations, provided A_i are exactly known.

(V) Taking into account the results of [5], an estimate similar to (4.1) can be obtained in the case of constraints imposed on each component u_i.

5. Algorithm of solving Problem 1 and evaluation of the guaranteed reorientation time. Let the values of α and δ_i be given and estimate (4.1) be satisfied for certain, i.e.,

$$\beta = \left(\frac{\sqrt{3}}{3}|\lambda_0^0| - \delta^*\right)\alpha - \Delta, \tag{5.1}$$

where $\Delta > 0$ is a given number. In this case, we can use the following iteration method to find τ:

(a) According to (4.7), we set $\alpha_i^* = \alpha^*$ to ensure the validity of inequality (1.5).

(b) We then choose a test value τ of τ_i in order to predetermine, by virtue of (3.4), the values of β_i^*.

(c) Finally, using estimates (4.5), we check the validity of the inequalities $|v_i^*| \le \beta_i^*$. If these inequalities are not satisfied (or satisfied for certain), the value of τ should be increased or decreased, respectively.

It is possible to estimate directly the upper bound of τ.

Theorem 2. *If equality* (5.1) *holds, then*

$$\tau \le \tau^* = 2\lambda^*\sqrt{2\Delta^{-1}},$$
$$\lambda^* = \left\{\max\left|\lambda_i^0\right| + 2L[(\lambda_0^0)^{-2} - 1]\right\}^{1/2}. \quad (5.2)$$

6. Example. We consider the reorientation of a body (space vehicle) from the position $\mathbf{x}^0 = \mathbf{0}$ and $\boldsymbol{\lambda}^0 = (0.701, 0.353, 0.434, 0.432)$ to the position $\mathbf{x}^1 = \mathbf{0}$ and $\boldsymbol{\lambda}^1 = (1, 0, 0, 0)$, with A_1^-, A_2^-, and A_3^- equal to 4×10^4, 8×10^4, and 5×10^4 kgm^2, respectively.

Let $\alpha = 11.2 \times 10^{-3}$ s^{-2} and $\delta_i = 0.1$. Estimate (4.1) takes the form $\beta < 3.5147 \times 10^{-3}$ s^{-2}. Assuming that $\Delta = 2 \times 10^{-3}$ s^{-2}, we find from (5.1) that $\beta = 1.5147 \times 10^{-3}$ s^{-2}.

In accordance with (4.7), we set $\alpha_i^* = \alpha^*$. Employing the algorithm described in Section 5, we find that $\tau = 117.45$ s, provided the reorientation is due to controls (2.4) and (3.3) in which $\alpha_i^* = 2.2661 \times 10^{-3}$ s^{-2}, $\rho_1 = 0.9548$, $\rho_2 = 0.9444$, and $\rho_3 = 0.9447$. In this case, constraint (1.5) is satisfied.

Note, for comparison, that direct estimate (5.1) yields $\tau^* = 119.75$ s.

ACKNOWLEDGMENTS

This work was supported in part by the Russian Foundation for Basic Research, project no. 99-01-00965, and the Russian Ministry of Education.

REFERENCES

1. V. I. Vorotnikov, Prikl. Mat. Mekh. **58**, 82 (1994).
2. V. I. Vorotnikov, Dokl. Akad. Nauk **343**, 630 (1995) [Phys.–Dokl. **40**, 146 (1995)].
3. V. I. Vorotnikov, Prikl. Mat. Mekh. **61**, 63 (1997).
4. V. I. Vorotnikov, *Partial Stability and Control* (Birkhauser, Boston, 1998).
5. V. I. Vorotnikov, Izv. Akad. Nauk, Teoriya Sist. Upravlen., No. 3, 53 (1999).
6. V. I. Vorotnikov, Dokl. Akad. Nauk **367**, 764 (1999) [Dokl. Phys. **44**, 577 (1999)].
7. N. N. Krasovskiĭ, *Game Problems for Motion Meeting* (Nauka, Moscow, 1970).
8. F. L. Chernous'ko, Izv. Akad. Nauk, Tekh. Kibern., No. 1, 209 (1993).
9. V. I. Vorotnikov, *Stability of Dynamic Systems with Respect to a Part of Variables* (Nauka, Moscow, 1991).
10. V. V. Rumyantsev and A. S. Oziraner, *Stability and Motion Stabilization with Respect to Part of the Variables* (Nauka, Moscow, 1987).
11. E. S. Pyatnitskiĭ, Prikl. Mat. Mekh. **60**, 707 (1996).
12. I. M. Anan'evskiĭ, Prikl. Mat. Mekh. **61**, 52 (1997).
13. A. Miele, T. Wang, and W. W. Melvin, J. Optim. Theory Appl. **49**, 1 (1986).
14. G. Leitmann and S. Pandey, J. Optim. Theory Appl. **70**, 25 (1991).
15. N. D. Botkin, M. A. Zarh, W. M. Kein, *et al.*, Izv. Akad. Nauk, Tekh. Kibern., No. 1, 68 (1993).

Translated by V. Chechin

Doklady Physics, Vol. 45, No. 7, 2000, pp. 350–352. Translated from Doklady Akademii Nauk, Vol. 373, No. 3, 2000, pp. 329–331.

MECHANICS

Filtration-Flow Effects and Variants of Constructing Nonlinear Filtration Laws in the Case of Violation of the Darcy Rule with Isotropic Filtration Properties

N. M. Dmitriev and V. M. Maksimov

Presented by Academician A.N. Dmitrievskiĭ August 28, 1999

Received September 14, 1999

Numerous experimental investigations have established not only the possibility of using the Darcy rule but also limits of its applicability [1, 2]. In the process of these investigations, the Darcy rule was shown to be valid for both isotropic and anisotropic media, but it is fulfilled merely within a certain range of filtration rates. Thus, the upper and lower boundaries for the applicability of the Darcy rule can be indicated. The upper boundary is caused by the manifestation of inertial forces at high filtration rates, while the lower one, by physicochemical effects for interaction of a fluid with a solid skeleton and by non-Newtonian rheological properties of the fluid. In this study, we consider the generalizations of the Darcy rule with isotropic filtration properties at high filtration rates.

A number of papers [3, 4] are devoted to constructing nonlinear constitutive equations of the filtration theory at high filtration rates. However, in these investigations, methods of the theory of nonlinear tensor functions and those of crystal physics [5, 6] were hardly used. Using the theories indicated makes it possible not only to develop general methods of constructing nonlinear constitutive equations but also to find possible effects. Analysis of nonlinear filtration laws generalizing the Darcy rule with isotropic filtration properties showed that nonlinear filtration properties can be anisotropic and, moreover, manifest asymmetry; i.e., they have different filtration properties in the case of flow along the same straight line in different directions.

The basic law of the filtration theory (Darcy rule) represents the linear relation between two effective vector fields, namely, the filtration-pressure gradient $\nabla_i p$ and the filtration rate w_i. The presence of this relation is experimental fact. On the other hand, the Darcy rule can be derived by averaging the Navier–Stokes equations for the case of the fluid flow in a periodic lattice [7]. Thus, the Darcy rule represents the differential form of the momentum-conservation law for a specific continuous medium that represents a composite material consisting of solid skeleton and a fluid. Therefore, in the Darcy rule, both fluid properties and void-space properties of the solid skeleton are given and specified. In the case of filtration of a Newtonian viscous fluid, it turns out that these properties can be separated. The fluid properties are specified only by the viscosity coefficient μ, while the void-space properties are determined by its symmetry and can be given by the penetrability-coefficient tensor k_{ij} or by the tensor r_{ij} for the filtration-resistance coefficients. The last argument makes the Darcy rule similar to constitutive relationships like Ohm's or Fick's laws. This is associated with the fact that one more property of the fluid motion is introduced by the Darcy rule.

In the context of constitutive relationships, the principal equation of the filtration theory postulates, in the general case, a relation of the form

$$\nabla_i p = f_i(w_i, \rho, \mu, \chi_\alpha, T_\alpha), \tag{1}$$

where ρ is the fluid density, χ_α are the invariant scalar parameters describing a porous medium and possibly the fluid, and T_α are the material tensors specifying and setting the properties of the void space for the solid skeleton. Assumption of the linearity for relation (1) leads to the Darcy rule. The simplest variant for generalizing the Darcy rule, which corresponds to equation (1), implies the subsequent expansion of the function f_i into the Taylor series in terms of powers of w_i:

$$\frac{1}{\mu}\nabla_i p = -r_{ij}w_j - r_{ijk}w_i w_k - r_{ijkl}w_j w_k w_l. \tag{2}$$

Here, r_{ij}, r_{ijk}, and r_{ijkl} are the material tensors setting the filtration resistance. In equality (2) and below, we consider the problem in the Cartesian coordinate system and assume, for simplicity, that the summation is carried out with respect to the repeated subscripts. The explicit forms of the tensors r_{ij}, r_{ijk}, and r_{ijkl} depend on the class (group) of symmetry of the void space [5, 6].

Institute of Oil and Gas Problems, Russian Academy of Sciences, ul. Gubkina 3, Moscow, 117296 Russia

1028-3358/00/4507-0350$20.00

For an isotropic porous medium, relationship (2) yields the filtration law in the form

$$\frac{1}{\mu}\nabla_i p = -r_1 w_i - r_2 w^2 w_i, \quad (3)$$

where r_i are the scalar coefficients and w is the modulus of the filtration-rate vector. Relationship (3) differs from the Forchheimer law [4], commonly used in underground hydromechanics, in which the nonlinearity is given by a term of the form $r_2 w w_i$. It is necessary to note that the result presented by relationship (3) was found previously in [8] as the solution to the Ozeen and Navier–Stokes equations. To substantiate the Forchheimer formula and obtain a more general representation for relations (1), it is necessary to use the more rigorous results of [9, 10]. According to these studies, relations (1) can be represented in the form of the expansion in terms of the basis tensors and their combinations [10], whose multipliers are functions of the invariants (the generalized Hamilton–Cayley formulas). In this case, the representation of the most general form of the nonlinear filtration law for isotropic porous media is given by the relationship [9]

$$\frac{1}{\mu}\nabla_i p = f g_{ij} w_j, \quad (4)$$

where f is the function of w and g_{ij} is the metric tensor. The construction of filtration law (4), i.e., the definition of the explicit form of $f(w)$ for a particular isotropic porous medium can be realized by processing only one experimental curve representing the dependence of the gradient-pressure modulus on the modulus of the filtration-rate vector. Indeed, it follows from relationship (4) that $f(w) = \nabla p/\mu w$. Thus, the approximation of the experimental dependence of ∇p on w determines the form of $f(w)$ and, therefore, the nonlinear filtration law. In the framework of a similar approach, the one-term and two-term representations of the nonlinear filtration law [4] differ only by the choice of the class of functions used for the approximation. However, the isotropic filtration properties in the Darcy rule are manifested also by anisotropic porous media with the cubic symmetry of the effective void space [6]. Porous media with a cubic symmetry of the effective void space have the following generalized representations for the nonlinear laws accurate to the cubic terms in the filtration-rate expansion [10]:

$$\frac{1}{\mu}\nabla_i p = -f_1 g_{ij} w_j - f_2 O_{(h)ijkl} w_j w_k w_l, \quad (5)$$

$$\frac{1}{\mu}\nabla_i p = -\varphi_1 g_{ij} w_j - \varphi_2 T_{(d)ijk} w_j w_k - \varphi_3 O_{(h)ijkl} w_j w_k w_l, \quad (6)$$

where f_i and φ_i are the functions of the principal vector invariants formed by convolutions of basis tensors with the filtration-rate vector, g_{ij}, $T_{(d)ijk}$, and $O_{(h)ijkl}$ are the basis tensors [10]. Equality (5) yields the filtration law for the groups (classes) of symmetry $\bar{6}/4$, $\bar{3}/4$, $\bar{6}/2$, and equality (6), $3/\bar{4}$ and $3/2$ (the notation for the symmetry groups is given according to Shubnikov). The analysis of relationships (4)–(6) shows that they all represent the Darcy rule with isotropic filtration properties in the case when f, f_1, and φ_1 are constant and $f_2 = 0$, $\varphi_2 = 0$, and $\varphi_3 = 0$. However, while passing to the nonlinear filtration law, the filtration properties substantially differ. The nonlinear filtration resistances specified by the relationship $r(n_i) = -\nabla_i p n_i/\mu w$ have the following form for filtration laws (4), (5), and (6), respectively:

$$r = f(w), \quad r = f_1 + f_2(n_1^4 + n_2^4 + n_3^4)w^2,$$
$$r = \varphi_1 + 6\varphi_2 n_1 n_2 n_3 w + \varphi_3(n_1^4 + n_2^4 + n_3^4)w^2, \quad (7)$$

where n_i are the components of the basis vector determining the direction of the filtration-rate vector with respect to the crystallographic axes [10]. Analysis of expressions (7) shows that the filtration properties in laws (5) and (6) are direction-dependent and, moreover, they manifest an asymmetry in law (6) along the direction for which $n_1 n_2 n_3 \neq 0$. Thus, a change in the symmetry of filtration properties is possible while passing from the linear to the nonlinear filtration law. It is necessary to take this fact into account in the experimental determination of these laws. Therefore, when constructing the nonlinear filtration laws, we need to carry out complex experimental investigations even for media manifesting isotropic properties in the Darcy rule.

The procedure of experimentally determining nonlinear filtration properties for actual rocks containing hydrocarbon row material must include determination of both the effective symmetry of the void space and the explicit form of the functions f_i and φ_i. One variant for complex investigations can involve determination of elastic and hydrodynamic effective properties. Using the elastic characteristics of a core, it is possible to determine the symmetry of elastic properties, which coincides with the symmetry of the fourth-rank tensor in representations (2), (5), and (6), and to establish the directions of crystallographic axes [11, 12]. After the elastic symmetry and positions of principal axes have been determined, it is necessary to cut several smaller cores from the primary one for subsequent hydrodynamic studies. In the case of cubic symmetry, the minimum number of cores can be two for relationships (5) and three for relationships (6). However, since the elastic symmetry of cubic crystals is given by the tensor $O_{(h)ijkl}$ for all symmetry groups, it is impossible to determine the type of the nonlinear filtration law after establishing only elastic symmetry. Therefore, it is necessary

to prepare three cores. The optimum directions of the core symmetry axes are the following:

$$n_i^{(1)} = (1, 0, 0), \quad n_i^{(2)} = \left(\frac{\sqrt{2}}{2}, \frac{\sqrt{2}}{2}, 0\right),$$

$$n_i^{(3)} = \left(\frac{\sqrt{3}}{3}, \frac{\sqrt{3}}{3}, \frac{\sqrt{3}}{3}\right).$$

As is easy to establish for the directions found, the vectors w_i and $\nabla_i p$ are located on one straight line and, as a result of experimental investigations, the plots of the dependences $\Delta p/L = F(w, n_i^{(\alpha)})$ are obtained, where Δp is the difference of pressures or the Leibenzon functions on the core in the course of the fluid and gas filtration, respectively. Furthermore, L is the core length, and w is the filtration rate for the fluid filtration or the mass-flow rate for the gas filtration. Expressing experimental data in the form

$$\frac{\Delta p}{\mu w L} = \frac{F(w, n_i^{(\alpha)})}{\mu w},$$

we find the values of the filtration resistances $r(n_i^{(\alpha)})$ along the corresponding directions. As has been noted, in the general case, the desired expressions for f_i and φ_i are the functions of the invariants formed by convolutions of the rate vector with the basis tensors. However, the assumption that f_2, φ_2, and φ_3 depend on the invariants increases the exponent for the rate in the representation of the filtration resistances (7). This considerably complicates the representation for these dependences, whereas all the known experimental data are well processed using two or three constants in the polynomial representation of the filtration law. Therefore, remaining within the framework of the classical representation of the nonlinear filtration law, we can assume that $f_1 = \varphi_1 = a + bw$, $\varphi_2 = c$, $f_2 = \varphi_3 = d$, where a, b, c, and d are certain constants to be found experimentally. In this case, the linear combinations of the filtration resistances $r(n_i^{(\alpha)})$ for the directions $n_i^{(1)}$ and $n_i^{(2)}$ make it possible to determine d

$$r(n_i^{(1)}) - r(n_i^{(2)}) = 0.5dw^2, \tag{8}$$

and $a + bw$,

$$2r(n_i^{(2)}) - r(n_i^{(1)}) = a + bw. \tag{9}$$

The representation of the constant c in filtration law (6) is obtained from the measurements for the third core along the positive $+n_i^{(3)}$ and the negative $-n_i^{(3)}$ directions:

$$r(+n_i^{(3)}) - r(-n_i^{(3)}) = \frac{4\sqrt{3}}{3}c. \tag{10}$$

Carrying out the experimental investigations according to the scheme proposed and processing the experimental data on the basis of relationships (8)–(10) make it possible to find the nonlinear filtration law generalizing the Darcy rule with isotropic filtration properties. In this case, feasible effects associated with manifestation of the anisotropy and asymmetry in filtration properties are taken into account.

The analysis of constructing nonlinear filtration laws for media manifesting transversal-isotropic and orthotropic filtration properties in the Darcy rule is related to even greater "structuring" of both the filtration properties and filtration laws and presents an object for additional study.

ACKNOWLEDGMENTS

This work was supported by the Russian Foundation for Basic Research, project no. 98-01-00915.

REFERENCES

1. A. G. Ar'e, *Physical Principles for Filtration of Underground Water* (Nedra, Moscow, 1984).
2. A. E. Scheidegger, *The Physics of Flow Though Porous Media* (Univ. of Toronto Press, Toronto, 1974).
3. S. V. Belov, *Porous Substances in Industry* (Mashinostroenie, Moscow, 1981).
4. K. S. Basniev, I. N. Kochina, and V. M. Maksimov, *Underground Hydromechanics* (Nedra, Moscow, 1993).
5. Yu. I. Sirotin and M. P. Shaskol'skaya, *Principles of Crystal Physics* (Nauka, Moscow, 1975).
6. V. V. Lokhin and L. I. Sedov, Prikl. Mat. Mekh. **27** (3), 293 (1963).
7. N. S. Bakhvalov and G. P. Panasenko, *Averaging of Processes in Periodic Media* (Nauka, Moscow, 1984).
8. Yu. P. Korotaev and M. B. Panfilov, *Development of Methods for Determining Parameters of Porous Media according to the Data of Its Microstructure* (IRTs Gazprom, Moscow, 1993).
9. Yu. I. Sirotin, Prikl. Mat. Mekh. **28**, 653 (1964).
10. Yu. I. Sirotin and V. F. Pleshakov, Prikl. Mat. Mekh. **30**, 243 (1966).
11. A. M. Kuznetsov, A. G. Kovalev, D. I. Sal'nikov, *et al.*, Neft. Khoz., No. 7, 44 (1997).
12. T. N. Krechetova and E. S. Romm, Izv. Akad. Nauk SSSR, Mekh. Zhidk. Gaza, No. 1, 181 (1983).

Translated by V. Bukhanov

Doklady Physics, Vol. 45, No. 7, 2000, pp. 353–357. Translated from Doklady Akademii Nauk, Vol. 373, No. 3, 2000, pp. 332–336.

MECHANICS

Numerical Simulation of the Transition between the Regular and Mach Reflection of Shock Waves under the Action of Local Perturbations

M. S. Ivanov, A. N. Kudryavtsev, and D. V. Khotyanovskiĭ

Presented by Academician G.G. Chernyĭ October 25, 1999

Received October 11, 1999

1. INTRODUCTION

The hysteresis in transition between the regular and Mach reflections of steady-state shock waves, which was recently revealed by numerical [1] and experimental [2] methods, stimulated widespread interest in this classical problem of gas dynamics. As is known [3], for strong shock waves (when the incident-flow Mach number $M > M_* \approx 2.2$ and the adiabatic index of the gas $\gamma = 1.4$), theory predicts the range of angles of incidence $\alpha_N < \alpha < \alpha_d$ in which both regular and Mach reflections are possible. Here, α_N is the angle determined from the so-called Neumann criterion and giving a theoretical lower boundary for the existence of the Mach reflection. Angle α_d corresponds to the criterion of the maximum flow deflection, according to which, at angles exceeding α_d, regular shock-wave reflection is impossible. Existence of this double solution range (with an angular width equal to 6.5° at $M = 4$ and exceeding 10° at $M = 6$) suggests that the smooth variation of the angle of incidence can be accompanied by hysteresis behavior in the change of the reflection type. Namely, it was supposed [4] that regular reflection must be observed up to $\alpha = \alpha_d$. After that, the jumplike transition to the Mach configuration with a finite height of the Mach pedestal should occur. According to the same conjecture, the subsequent smooth decrease in the angle retains the Mach configuration throughout the entire double-solution range, where the height of the Mach pedestal should gradually decrease and eventually vanish at $\alpha = \alpha_N$. This is the picture of transition actually revealed by recent numerical calculations [1, 5, 6].

The experimental results are less definite. In the experiments carried out in closed-jet wind tunnels [7, 8], both transitions (direct and reverse) occur at practically the same values of the angle very close to α_N. At the same time, studies using the free-jet facilities [2, 9] confirm the existence of hysteresis. However, the angle of transition to the Mach reflection observed there does not agree with the theoretical predictions. In these experiments, the transition to the Mach reflection occurs within the double-solution range. For nearly two-dimensional flows, the angles of the transition are by 3°–4° larger than α_N but much smaller than α_d. The reverse transition was again observed at $\alpha = \alpha_N$.

We argue that the following hypothesis can explain all these results. In the double-solution range, both regular and Mach configurations are steady-state and, thus, are stable with respect to small perturbations. Finite-amplitude perturbations can cause transition between these states. We note that the possibility of nonunique solutions to the time-independent Euler equations is well known [10]. Moreover, in the double-solution range, the stability of the regular reflection with respect to infinitely small perturbations of the incident flow was proved by analytical methods [11].

It seems rather plausible that the threshold amplitude of perturbation initiating the transition to the Mach reflection should decrease with the growth of the incidence angle and vanish at $\alpha = \alpha_d$. On the contrary, amplitude of perturbation causing the reverse transition must fall with decreasing α and tend to zero as $\alpha \longrightarrow \alpha_N$. Then, the above results can be explained by the fact that, in free-jet wind tunnels, perturbations initiating the transition are less intense than those arising in closed-jet wind tunnels, while the numerical calculations completely ignore these perturbations. Note that the difference between the aforementioned types of wind tunnels can be associated with the existence of acoustic waves in those with closed jet. The waves are generated by a turbulent boundary layer formed at the walls of the working chamber.

To confirm or refute the stated hypothesis, investigations of the effect produced by perturbations of different nature on the transition are needed. Numerical simulations of the effect of short-time but intense perturbations of the incident flow considerably increasing or decreasing its velocity during a certain time interval were carried out in [12, 13]. It was shown that such perturbations could cause transitions between regular and

Institute of Theoretical and Applied Mechanics, Siberian Division, Russian Academy of Sciences, Institutskaya ul. 4/1, Novosibirsk, 630090 Russia

1028-3358/00/4507-0353$20.00

Mach reflections in both directions. Nevertheless, it was rather difficult to analyze them, because they gave rise to a system of three moving gas-dynamic discontinuities that interacted with the steady-state shock-wave configuration in a rather complicated manner. In this paper, we study the effect of local perturbations introduced as density variations in a gas stream flowing toward the point of shockwave reflection at fixed values of velocity and pressure. An advantage of these perturbations is related to the fact that the region with changed density is separated from the surrounding gas by a contact discontinuity and is simply carried away by the flow, while the major part of the flow remains unperturbed. At the same time, we believe that such perturbations are not the main cause of the earlier transition to the Mach reflection in wind tunnels compared to that predicted by the numerical calculations. This point calls for further detailed analysis.

In this paper, using these perturbations as a convenient tool, we want to show that in the problem under consideration, two steady states actually arise in the system and the transition between them can be caused by finite-amplitude perturbations. Moreover, our purpose is to investigate how the feasibility of such a transition depends on the amplitude of the imposed perturbation.

2. FORMULATION OF THE PROBLEM AND METHOD FOR SOLVING IT

The effect of local density perturbations on the change of the types of reflection of a steady-state shock-wave was studied by numerical solution of the two-dimensional time-dependent Euler equations describing the flow of the ideal gas with a constant specific heat and adiabatic index $\gamma = 1.4$. We used the high-order total variation diminishing scheme. To calculate flows on the faces of the calculation cells, we solved approximately the problem of the decay of a discontinuity that separates states occurring at both sides of a face, by the Harten–Lax–van Leer–Einfeldt (HLLE) method. This method is highly reliable for flows with strong shock waves and/or low-density regions. Except for the cells situated both near gas-dynamic discontinuities and points of local extremum of the solution, the parameters at the faces were reconstructed from their averages over the cell volume by using formulas accurate to the fourth order. Other details of the numerical method are presented in [14].

A wedge acting as a shock-wave generator was placed inside a rectangular calculation region. Similarly to experiments [8], it had the shape of a right triangle with a front-edge angle equal to 15°. Variation in the angle of the generated wave was performed by rotation of the wedge about the trailing edge (Figs. 1 and 2). A distance between this edge of the wedge and the lower boundary of the calculation region was $g = 0.56w$, where w is the length of the wedge hypotenuse. A supersonic influent stream was specified at the left boundary of the region. The lower boundary was treated as a symmetry line. This corresponds to the actual geometry of the experiment, where the interaction of two shock waves generated by symmetric wedges is usually studied. This is done to eliminate the effect of the boundary layer that would occur in the case of wave reflection from a rigid wall. The right boundary was situated sufficiently far from both the wedge and the point of shockwave reflection in order to ensure the flow to be supersonic everywhere within the cell. We used a multiblock structured computational net with the total number of cells equal to 84000.

The calculations were carried out in a way described below. First, for a certain α belonging to the double-solution range, we calculated a steady-state shockwave configuration by the method of temporal relaxation. Then, perturbation was introduced at the left boundary of the region. For this purpose, we varied the density of the stream inflowing through it by $\Delta\rho$. Such variation of boundary conditions was performed in several cells, being the closest to the lower boundary. The changed boundary conditions were kept constant for a certain time T. Then, the perturbation was switched off; and the unperturbed density ρ_∞ was again specified in all of the cells at the left boundary.

3. RESULTS OF THE CALCULATIONS

In all calculations, the Mach number of the unperturbed incident flow was $M = 4$. For this value of the Mach number, we had the angle $\alpha_N = 33.4°$ and $\alpha_d = 39.2°$.

Figure 1 illustrates the transition from the regular reflection to the Mach configuration under the effect of local density variations. The angle $\alpha = 36°$ of the wave incidence corresponded approximately to the middle of the double-solution range. The density was decreased by 25% in the lower ten calculation cells belonging to the left boundary of the region. The duration of the perturbation was $T = 0.6w/a_\infty$, where a_∞ is the sound velocity in the unperturbed incident flow. A steady-state regular configuration represented the initial conditions for the calculations. Figure 1 shows a flow field (density isolines) at the time point $t = 0.7w/a_\infty$ after the perturbation has been introduced. By this time, which corresponds to beginning of formation of the Mach pedestal in the flow, the perturbation has already been switched off. A region of the reduced density is clearly seen in the plot as a narrow strip belonging to the lower part of the calculation region. Further on, the height of the Mach pedestal continued to grow until the eventual formation of the steady-state Mach configuration shown in Fig. 1 was formed at the time moment $t = 6.0w/a_\infty$.

The results concerning the simulation of the reverse transition (from the Mach reflection to the regular configuration) are presented in Fig. 2. The calculation was carried out for the same angle of the wave incidence $\alpha = 36°$. To place the triple point of the Mach configu-

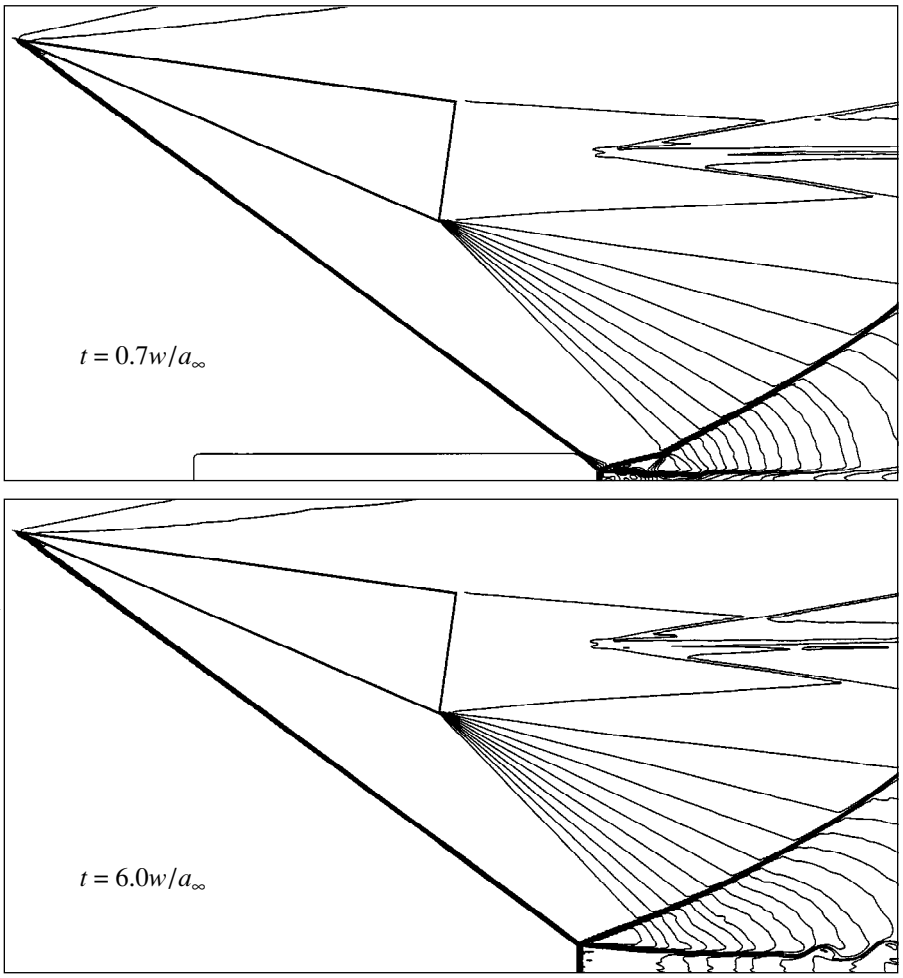

Fig. 1. Transition from the regular reflection to the Mach one under the action of a local density perturbation.

ration inside a zone of increased density, the density was enhanced in calculations by 50% in 20 calculation cells. As compared to the first case, the duration of perturbation was much longer: $T = 2.5w/a_\infty$.

When the perturbation and the triple shock-wave configuration began to interact, the height of the Mach pedestal decreased, and finally, at the time point $t = 2.6w/a_\infty$, the pedestal disappeared (Fig. 2). If we switch off the perturbation after that, the formed regular reflection survives. At $t = 6.0w/a_\infty$, the calculated final regular configuration is also shown in Fig. 2.

In the both cases, the mechanism underlying the change of the reflection type is the same. Entering a zone with the changed density, the incident shock-wave is refracted. As a result, it reaches the lower boundary or the triple point at the angle different from that corresponding to the perturbation-free conditions. At a certain decrease in the density, this angle becomes larger than the critical angle α_d calculated for parameters of the perturbed incident flow. This makes the transition to the Mach reflection inevitable. Similarly, at a certain increase in the density, the angle under which the incident shockwave reaches the triple point becomes smaller than α_N. As a result, transition to regular reflection occurs.

The angle of the refracted shockwave α_{rs} can be calculated by using a self-similar solution to the classical problem, which considers interaction of a shock wave with a contact discontinuity [10]. For the three values of the angle of incidence $\alpha = 34°$, 36°, and 38°, the results of these calculations are shown in Fig. 3.

The plot presented allows us to easily estimate the threshold perturbation amplitude changing the type of the reflection. For example, to cause the transition to the Mach configuration at the wave incidence angle $\alpha = 36°$, it is necessary to decrease the density approximately by 21%. At $\alpha = 38°$, the same result is attained at the density decrease by 8.5%. The numerical simulation completely confirms the results of this simple theoretical analysis.

There are two reasons according to which the transition from the regular reflection to the Mach one

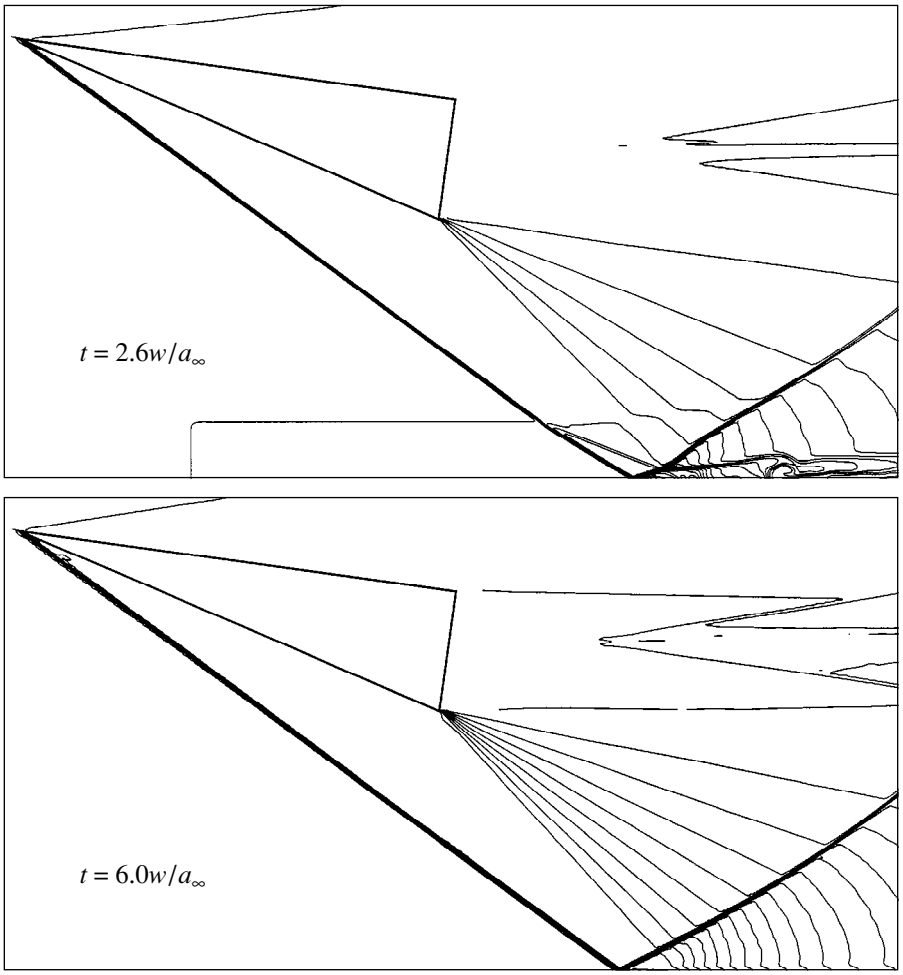

Fig. 2. Transition from the Mach reflection to the regular one under the action of a local density perturbation.

occurs much easier than the reverse transition. Firstly, varying the flux density, we change the Mach number as well, which, in turn, causes variation of both α_N and α_d. This produces only a slight effect on the transition to the Mach reflection, because α_d depends weakly on the Mach number. At the same time, α_N can be essentially decreased by an increase in the Mach number. As a result, the threshold amplitude of the perturbation causing the transition to the regular reflection grows considerably.

Secondly, even a perturbation localized within a very small region can cause transition to the Mach reflection. To initiate transition to regular reflection, the perturbation must be much longer than the former in both space and time. Its spatial dimension must exceed a height of the Mach pedestal, and its duration must be such that the rather slow process of decreasing the height of the Mach pedestal would have time to be completed. According to these reasons, in the double-solution range, the Mach shock-wave configuration, in a certain sense, is more stable than that of the regular reflection. This conclusion agrees completely with experimental results, because the transition to regular reflection is always observed at angles rather close to α_N and slightly exceeding it.

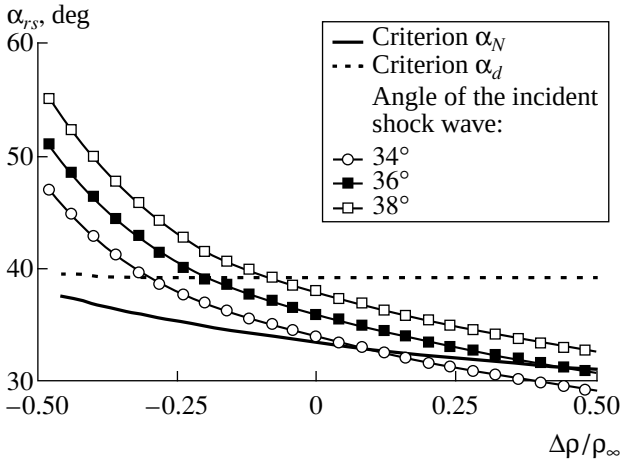

Fig. 3. Angles of refraction of a shock wave and the criteria for the transition α_N and α_d as functions of an amplitude of the density perturbation.

4. CONCLUSIONS

By means of numerical simulation, we have shown that in the case when the angle of incidence of a shock wave lies within the double-solution range, local variations in the density of the incident flow can cause transition between regular and Mach shock-wave configurations. The threshold amplitude of the perturbations causing such a transition can be determined by means of simple theoretical analysis. As compared to the reverse transition, the transition to the Mach reflection can be initiated much more easily. As a result, in the double-solution range, the Mach configuration can be considered to be more stable than that of the regular reflection. This fact is in complete agreement with available experimental data.

ACKNOWLEDGMENTS

The authors are grateful to Academician G.G. Chernyĭ for advising us to consider in this problem the effect of local density perturbations introduced in the incident flow.

This work was supported by the Russian Foundation for Basic Research (project no. 98-01-00677) and INTAS (project no. 96-2356).

REFERENCES

1. M. S. Ivanov, S. F. Gimelshein, and A. E. Beylich, Phys. Fluids **7**, 685 (1995).
2. A. Chpoun, D. Passerel, H. Li, and G. Ben-Dor, J. Fluid Mech. **301**, 19 (1995).
3. H. G. Hornung, Annu. Rev. Fluid Mech. **18**, 33 (1986).
4. H. G. Hornung, H. Oertel, and R. J. Sandeman, J. Fluid Mech. **90**, 541 (1979).
5. M. S. Ivanov, D. Zeitoun, J. Vuillon, *et al.*, Shock Waves **5**, 341 (1996).
6. M. S. Ivanov, G. N. Markelov, A. N. Kudryavtsev, and S. F. Gimelshein, AIAA J. **36**, 2079 (1998).
7. H. G. Hornung and M. L. Robinson, J. Fluid Mech. **123**, 155 (1982).
8. M. S. Ivanov, G. P. Klemenkov, A. N. Kudryavtsev, *et al.*, Dokl. Akad. Nauk **357**, 623 (1997) [Phys.–Dokl. **42**, 691 (1997)].
9. M. S. Ivanov, G. P. Klemenkov, A. N. Kudryavtsev, *et al.*, in *Proceedings of the XXI International Symposium on Shock Waves, Great Keppel Island, Australia, 1997*, Vol. 2, pp. 819–824.
10. G. G. Chernyĭ, *Gas Dynamics* (Nauka, Moscow, 1988).
11. V. M. Teshukov, Prikl. Mekh. Tekh. Fiz., No. 2, 26 (1989).
12. M. S. Ivanov, A. N. Kudryavtsev, G. N. Markelov, and S. F. Gimelshein, AIAA Pap. 97-2511 (1997).
13. M. S. Ivanov, S. F. Gimelshein, and G. N. Markelov, Comput. Math. Appl. **35** (1/2), 113 (1998).
14. M. S. Ivanov, A. N. Kudryavtsev, S. F. Gimelshein, *et al.*, in *Proceedings of the IV ECCOMAS CFD Conference, Athens, 1998*, Vol. 1, Part 2, pp. 869–874.

Translated by Yu. Verevochkin